DUBLIN CITY UNIVERSITY
School of Physical Sciences

A thesis for the degree of Master of Science

Novel blood platelet diagnostic platform

Supervisor: Prof. Colette McDonagh

by Aurora Panzera, M.Sc.
Student number: 58127020

September, 2011

Contents

Abstract

This project involves the design and implementation of a platform to investigate the activation state of platelets. The final aim is to develop an assay to be used for diagnostic purposes.

Blood platelets play a key role in the cardiovascular system. When the endothelium of the vessel wall is damaged platelets adhere and become activated, leading to platelet aggregation to maintain physiological haemostasis. Any abnormality in platelet functionality induces thrombus or atherosclerotic plaques leading to life-threatening consequences such as stroke. Recent reports suggest that the detection of activated platelets in the blood may be a useful indicator of the onset of stroke and other cardiovascular abnormalities. Hence, the detection of the functional state of platelets is of huge clinical importance.

A luminescence-based platelet bio-assay which uses high brightness silica nanoparticles (NPs) as super-bright labels is an innovative and promising tool for diagnostics. Compared to assays carried out using conventional single molecule dye labels, the usage of NPs makes it possible to enhance the detection efficiency of the assay and to achieve a reduced limit-of-detection. In this work NPs doped with a near infra-red dye are synthesized and their interactions with the platelets are characterized. Protocols of conjugation of antibodies towards platelet surface antigens to NPs are tested.

The second part of the work studies the activation state and the morphology of platelets in different environments by using single molecule dye label assays and with AFM. The confinement of platelets in micrometer sized area using a protein patterning technique makes the analysis innovative and potentially very useful.

Chapter 1

Introduction and background

1.1 Nanoparticles as fluorescent probes

The application of fluorescence is central to many fields. The nanoscale world is ideally investigated with fluorescent materials. Fluorescence analysis has in fact high signal-to-noise ratios, a good spatial resolution which is just limited by the diffraction of the light, and an excellent temporal resolution on the scale of the fluorescence processes (typically nanoseconds).

The progress of science with its applications requires the development of new robust and bright materials. Fluorescent emitters/probes being in use nowadays belong to different classes of materials, examples of these are shown in figure 1.1. The

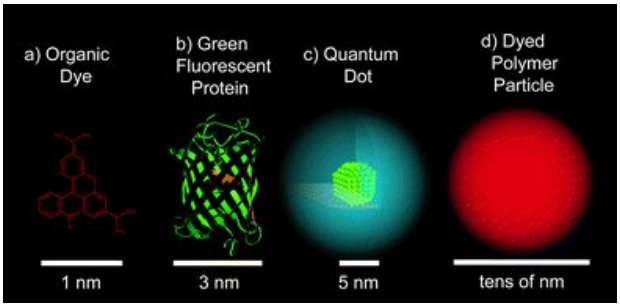

Figure 1.1: Common fluorescent probes in the nanoscale range. Ref: [1].

smallest probes are single dye molecules (≈1 nm). Different dyes can be synthesized with different absorption and emission proprieties, with emissions spanning from UV to near infra-red. They are widely used in the biological applications because of their small size and consequent hypothetical minimal interaction with the

system. However, the small size of single molecules affects the labelling efficiency with relative high background signals arising from non-specific labelling due to the easy diffusion of the dye away from its target [1]. Moreover single dyes molecules are not protected from the surrounding environment and can undergo quenching upon interactions or collisions with other molecules like solvent molecules, oxygen and ions [2]. The fluorescent emitters of this category are generally not very bright.

Nanoparticles (NPs) are more robust and stable emitters/probes. NPs enclose thousands of dye molecules in a matrix, therefore protecting the dye from external interactions with the solvent [3]. When dye molecules are encapsulated inside a chemically and mechanically stable vehicle, the dye has an increased photostability [4]. By embedding fluorescent molecules inside a matrix, because of thousands of dye molecules encapsulated within each NP,a high signal amplification is achieved. Compared to the use of a single molecule label fluorescence signal is enhanced and signal-to-noise ratio is reduced [5].

A particle is defined as NP if its diameter is $\leq$100 nm. For objects in this scale the number of atoms at the surface is significant relative to the total number of atoms of the material. In fact, size-dependent properties happen on the nano-scale, e.g. surface plasmon resonance for some metal NPs or supermagnetism for magnetics NPs [6].
Additionally, NPs can be suspended in a solvent with no sedimentation or floating due to the strong interaction of the NP surface with the solvent.

1.1.1 Use of nanoparticles in bioassays

NPs can be used in many biological and biomedical fields, such as sensors, fluorescent markers for *in vitro* and *in vivo* analysis, clinical diagnostic tools, drug delivery, and MRI contrast agents. The synthesis materials and methods are chosen according to the target application.

To cite just some of the interesting examples that can be found in the literature, superparamagnetic ferrite NPs can be used to remotely control neurons. Herein, a specific surface modification allows to target the cells of interest, and the use of a radio-frequency magnetic field heats the NPs, thermally activating the ion channels [7]. Magnetic NPs can be used also as drug carriers against tumor cells. A tumoral drug is bound to the NP surface, and the NPs are kept in the tumor region by the use of a magnetic field [8]. Semiconductor nanocrystals (quantum dots) can be used for tissue microscopy. These are bright and photostable fluorophores

having the property of quantum confinement. Quantum dots have a broad excitation spectrum but a narrow Gaussian emission at wavelengths controllable by the size of the material. Larson and others have shown how they can be used in multiphoton imaging of the blood stream instead of the common fluorophores used in angiography, simply with an appropriate surface functionalization with water-soluble ligands [9]. Noble metal NPs, gold especially, also plays an important role in current research, because of their unique optical properties arising from localized surface plasmon resonance. Plasmon waves create strong enhancement and spatial confinement of the electromagnetic field around the metallic NPs that plays a key role in surface-enhanced Raman spectroscopy and metal enhanced fluorescence [10]. El-Sayed and others have shown that gold NPs can be used in oral cancer diagnostics by conjugating them with a specific antibody [11].

Silica NPs are extensively used for biological applications due to their biocompatibility and low toxicity [12]. Moreover the surface of silica can be easily functionalized with well known chemistry techniques. Chemically modifying the silica surface with the addition of functional groups makes it possible to covalently conjugate the NPs to an antibody, allowing the targeting of a specific type of cell, as shown by Zhao and others in an assay for quantification of pathogenic bacteria [13]. Silica NPs are also widely used for intercellular targeting, sensing and drug delivery. A few examples include the labelling of a variety of different cells using mesoporous silica fluorescent NPs, from Lin and others [14], and the delivery of genetic material in tumoral cells using silica NPs conjugated with DNA fragments, that get released into the cytoplasm and consequently migrate into the nucleus with consequent protein expression [15]. Cellular uptake of NPs is primarily size dependent. NPs smaller that 100 nm can cross the cellular membrane through endocytosis, a mechanism in which the nanomaterial is engulfed in vesicles [16]. The group of Xia and others have shown that this process is highly dependent on the molecules present on the NP surface. They show how gold NPs coated with a shell of alternating hydrophobic and hydrophilic ligands behave differently crossing the cell membrane compared to randomly ordered coated NPs [17]. From the research work of Dawson et al., it is known that NP uptake into cells is dependent on the presence of proteins adsorbed on the NP surface [16]. Proteins get adsorbed when the NPs are inserted in an environment, like in the blood stream, or get adsorbed during the synthesis and handling of the NPs, even working in the most clean conditions [18, 19].

From all these examples, the importance of surface chemistry when dealing with biological materials is apparent.

1.1.2 Silica nanoparticle synthesis methods

Silica particles are prepared in a mixture of water, alcohol, and ammonia by hydrolysis and condensation of alkoxysilanes. Alcohol is normally used as a homogenizing agent since alkoxysilanes and water are immiscible. The catalyst for the hydrolysis and condensation can be a base or a acid. The hydrolysis takes places by a nucleophilic mechanism. In a basic environment, water dissociates to produce nucleophilic hydroxyl anions (OH^-) in a rapid reaction, and then the hydroxyl group attacks the silicon atom. A decrease in the electron density of the silicon atom happens when the hydroxyl anion replaces an alkoxide group (OR), accelerating therefore the hydrolysis rate of other alkoxide groups. Once an alkoxide group is hydrolyzed, the others will be hydrolyzed rapidly, followed by the condensation of $Si(OH)_4$, resulting in the creation of monodisperse silica spheres [20]. The chemical reactions describing the hydrolysis and condensation of alkoxysilanes can be briefly written as follows [21]:

$$Si(OR)_4 + 4H_2O = Si(OH)_4 + 4ROH \tag{1.1}$$

$$nSi(OH)_4 = nSiO_2 + 2nH_2O \tag{1.2}$$

The main alkoxysilane used in NP synthesis is tetraethyl orthosilicate (TEOS), with the formula $Si(OC_2H_5)_4$. This molecule consists of four ethyl groups attached to ${SiO_4}^{4-}$ ion, which is called orthosilicate.

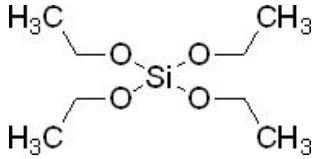

Figure 1.2: Chemical structure of tetraethyl ortosilicate (TEOS).

Spherical silica NPs are generally made by one of two chemical approaches, reverse microemulsion or Stöber sol-gel synthesis. Stöber and co-workers in the

late 1960s, developed a protocol based on the sol-gel chemistry of silicon alkoxides [22]. Stöber's method involves the hydrolysis and condensation of TEOS in ethanol solution in the presence of water with ammonia as a catalyst to create monodisperse, spherical, electrostatically-stabilized particles.

In the reverse microemulsion techniques, the hydrolysis and condensation of TEOS happen inside tiny droplets of water enclosed in surfactants shells [23]. A microemulsion is a thermodynamically stable distribution in a continuous oil medium of water droplets with size range of tens to hundreds of nanometers. The surfactant molecules create reverse micelles around the water droplets with the non-polar tails towards the oil phase, thus resulting in a confined environment or nano-reactor in which the NP synthesis take place [24]. The micelles collide with each other by Brownian motion and occasionally fuse together. When two droplets containing different reactants collide and undergo fusion, the chemical reactions takes place. The kinetics and dynamics of the microemulsion are regulated by the dynamic character of the micelles [25]. A NP is formed inside the droplet when the atoms of the insoluble reaction product being free in the micelle come together to produce a thermodynamically stable cluster, in a process called nucleation. The cluster goes on growing if the critical size is exceeded, otherwise spontaneous deaggregation can occur [26].

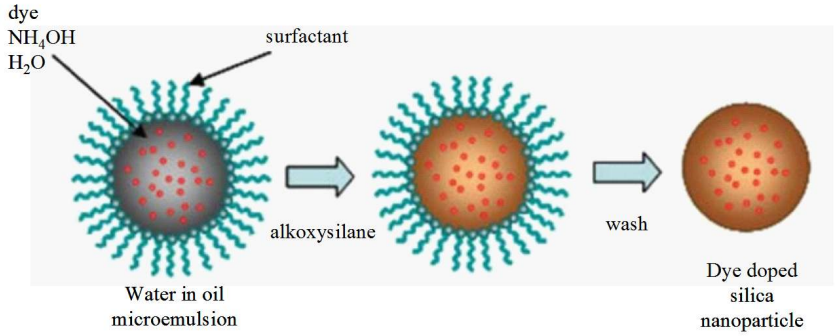

Figure 1.3: Schema of microemulsion synthesis of a dye doped silica nanoparticle. Ref: adapted from [27]

The confined nanoreactor environment within the surfactant shell yields highly monodisperse NPs with narrower size distributions than those obtained in the

Stöber synthesis. Moreover microemulsion-based synthesis aids the incorporation of non-polar fluorophores, which are often difficult to integrate into the hydrophilic silica matrix [28]. However, as the dye molecules are not covalently attached to the silica matrix, over time the fluorophores can leach out of the NPs, consequently decreasing NPs brightness, increasing background signal and releasing the dye molecules in the environment. To prevent dye leaching, a step can be added before the microemulsion synthesis in which the dye molecules are covalently conjugated with a silane coupling agent [29]. Another aspect of the microemulsion method is that these syntheses often have low yields and that the use of surfactants necessitates several washing cycling before the NPs can be used in any biological applications. If some surfactant molecules are left on the NP surface, lysis or disruption of cell membranes can occur [30].

1.1.3 Short overview of surface modification of silica

Surface modification of silica NPs can be done by coupling organosilanes or organic molecules with the functional groups present on the NP silica surface. On the NP surface there are two types of functional groups, siloxane (Si-O-Si) and silanol (Si-OH). The reaction with the silanol group constitutes the principal modification pathway [31]. When the surface -OH groups are treated with organofunctionalized silanes a Si-O-Si bond is created. Organosilanes in common use are trialkoxysilanes, which react with the silanol groups releasing the corresponding alcohol. Different trialkoxysilanes can be employed in the silica surface modification. The methoxy- and ethoxy-silanes are the most effective due to their greater reactivity. The reaction of the organosilane can happen via one, two or all three alkoxy groups (see figure 1.4). As a consequence there can be some degree of polymerization of the organosilane on the NP surface [31].

An example of surface modification is the addition of amino-groups on the NP surface, also called amination. In this case the used silane coupling agent is aminopropyltriethoxysilane (APTES), in which the R chain of figure 1.4 corresponds to NH_2-CH_2-CH_2-CH_2, thus creating pendant amino groups on the silica surface.

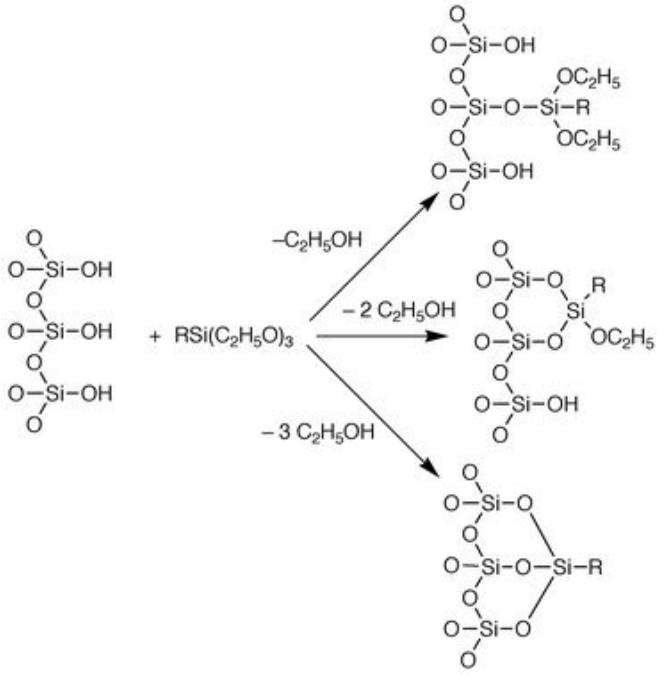

Figure 1.4: Modification of silica using triethoxysilane [31].

1.2 Importance of blood platelets

Platelets are small pseudocells in the blood that help control bleeding. They plug small holes in blood vessels and assist in the clotting process. Platelets are shaped like a disk with a diameter of about 2-3 μm. They cannot be considered as true cells since they do not have a nucleus. The average lifespan of a platelet is in average 10 days [32].

Platelets play a pivotal role in haemostasis because when an injury occurs they are activated and mobilized quickly to create a haemostatic plug [33]. When the subendothelial matrix is exposed upon vascular injury normal haemostasis takes place [34] (see figure 1.5).

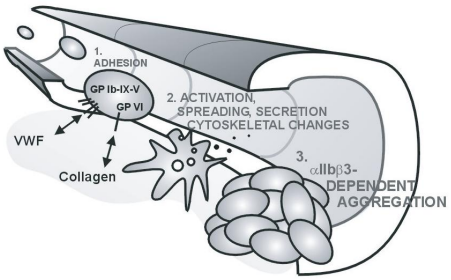

Figure 1.5: Normal haemostasis after vascular injury. Ref: [34].

Platelets are critically involved in atherothrombosis (the hardening and narrowing of the body's arteries) and thromboembolism (formation of a clot that breaks loose and is carried by the blood stream to plug another vessel) [35, 36]. The rupture of an atherosclerotic plaque or thrombosis can cause acute ischaemic events like stroke (i.e. when the heart tissue is starved of nutrients like oxygen) [37]. In these events platelet adhesion happens quickly, followed by activation and aggregation [38]. The result is a thrombus that can obturate the vessel or that can be carried away with the blood stream to create an embolus in a distal artery. Thrombus formation can be induced by the rupture of an atherosclerotic plaque and the consequent exposure of the matrix underlying in the vessel wall, as shown in figure 1.6, or by pathological turbulent shear stress [36, 34]. It has been

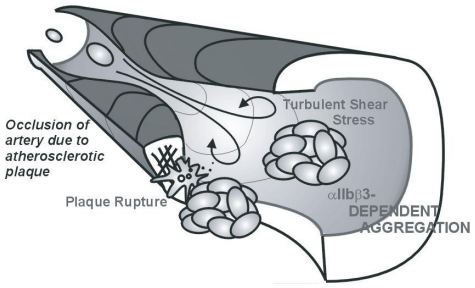

Figure 1.6: Thrombus formation in response to atherosclerotic plaque rupture. Platelets are activated upon exposure of the underlying lipid core, in particular von Willebrand factor (vWF) and collagen. Ref:[34].

suggested that platelet reactivity increases in the event of an ischaemic stroke, as underlined by the increase of products derived from platelet activation processes [39]. Thus, studying the activation state of the platelets can be a tool for predicting atherothrombotic events [40].

Because of the crucial role of platelets in atherothrombosis, the study of them is vital for the early diagnosis of life-threatening diseases.

1.2.1 Platelet activation and role of receptors

Platelets circulating in the blood are activated when collagen fibrils and thrombin are exposed. Collagen, that is present in the outermost layer of a blood vessel, is exposed after damage in the vein wall, and thrombin is locally produced at sites of vascular injury. Platelets adhere to the vessel walls employing von Willebrand factor (vWF) as a cofactor. They change their shape spreading out on the wall surface, and form a monolayer on the damaged area [41]. More platelets are then recruited through the continued action of thrombin and the secretion of soluble molecules such as ADP and P-selectin. As more platelets become activated, they stick to each other (cohesion) increasing the height of the haemostatic plug. A schematic of platelet adhesion and cohesion on a vein wall is shown in figure 1.7. Plug stability is sustained by the continued signaling within platelets. Fibrinogen, von Willebrand factor and other ligands bind to activated integrins which are present on the platelet surface, ensuring therefore stable contacts between platelets. Platelet-platelet contacts allow the binding of ligands on the surface with receptors on the surface of nearby platelets. Molecules secreted by activated platelets are accumulated in the gaps between platelets [42].

Several functional receptors are present on the surface of a platelet. These receptors are involved in the adhesion process between platelet and platelet and between platelet and the extracellular matrix. These receptors are also involved in the activation process and in the recruiting of additional platelets. When platelet receptors bind to ligands or to counter-receptors they transmit intracellular signals, modulating changes in the receptors profile, and activating signalling pathways [34]. The most important platelet receptors are glycoprotein (GP) Ib-IX-V, GPVI, and the integrin αIIbβ3. After the engagement of primary platelet adhesive receptors such as GPIb-IX-V or GPVI, fast activation of platelet integrins like of αIIbβ3 takes place. When the platelet is activated, the integrin αIIbβ3 goes through a conformational change like in a "switch-blade" mechanism (Fig. 1.8). Once αIIbβ3 is in the extended conformation, it binds to fibrinogen or to vWF. The binding of αIIbβ3 to the von Willebrand factor after Ca^{2+}-dependent activation is critically involved in thrombus formation at high shear stress [34].

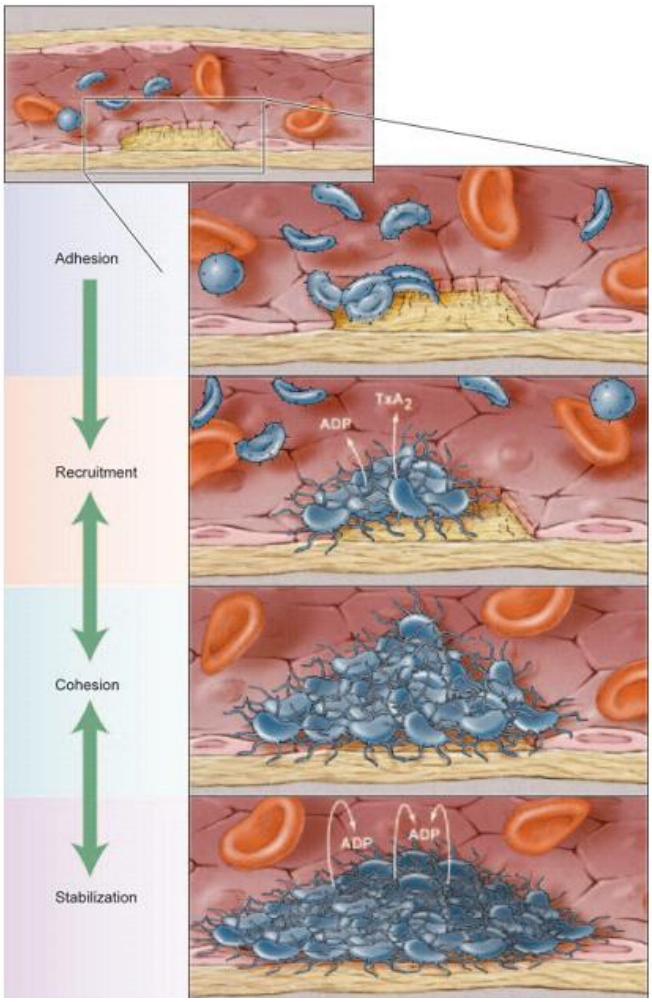

Figure 1.7: Platelet adhesion and cohesion after exposure of the vessel underlying matrix. Ref: [42].

An activated platelet can therefore be distinguished from a resting platelet by looking at the conformation status of its integrins αIIbβ3. A peculiarity of the activation process is also the surface exposition of insoluble molecules, like of P-selectin. P-selectin is a protein found in the storage granule membrane of unstimulated platelets which becomes translocated to the surface of activated platelets [43]. This work involves labelling of activated platelets only or using specific antibodies which can bind just to the activated form of αIIbβ3, or using antibody towards the secreted P-selectin.

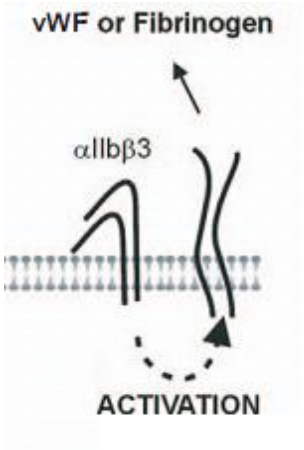

Figure 1.8: Activation through conformational change of the integrin αIIbβ3 that binds vWF or fibrinogen and mediates platelet aggregation. Ref: [34].

1.3 Basics of Fluorescence Spectroscopy

The emission of light that occurs from electronically excited states is called luminescence [44]. When light arises from the relaxation of a singlet excited state, it is called fluorescence, and when it arises from a triplet excited state it is called phosphorescence. From a spectroscopic point of view these processes are easily separable because of their different characteristic life-times.
The life-time, τ, is the average time that a molecule spends in the excited state before de-exciting to the ground state and τ is the temporal parameter that describes the luminescence process kinetics, given by

$$N(t) = N_0 \exp^{-\frac{t}{\tau}} \tag{1.3}$$

where $N(t)$ is the number of photons observed at a time t after an excitation pulse has illuminated an ensemble of fluorophores and N_0 is the number of photons detected at time $t = 0$.

The absorption and emission of light can be described in terms of the Jablonsky diagram (fig. 1.9). The ground state, the first and second excited singlet and the first and second excited triplet states are indicated respectively as S_0, S_1, S_2, and T_1, T_2. For each state there exist several vibrational states. At room temperature the energy gap between S_0 and S_1 is too large for thermal population of S_1, so a light source is necessary to induce fluorescence. After the absorption of light, which

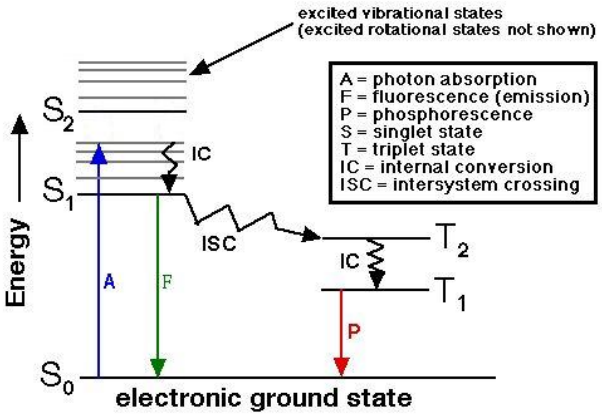

Figure 1.9: Jablonski diagram.

occurs in about 10^{-16} s, several processes take place. A fluorophore can be excited to a higher vibrational state of either S_1 or S_2, after which the molecule relaxes rapidly to the lower vibrational level of S_1. This process is called *internal conversion* and takes place in $\approx 10^{-12}$ s. Alternatively the fluorophore can undergo a spin conversion to T_1, in a process called *intersystem crossing*. The transition $T_1 \rightarrow S_0$ is forbidden as the electron in T_1 has the same spin orientation as the electron in S_0. This forbidden transition rule reflects on the rate of the phosphorescence process. Phosphorescence life-times for these transitions span from milliseconds to seconds. However the decay from S_1 to an excited vibrational state of S_0, which gives fluorescence emission, occurs on the nanosecond time scale and is followed by a picosecond transition to the ground vibrational state of S_0. This is an allowed transition because the electron in the excited orbital is paired to a second electron of opposite spin in the ground state [44].

The emission spectrum which is a plot of fluorescence intensity versus wavelength at fixed λ_{exc}, is a characteristic of a particular fluorophore, because it depends upon the chemical structure of the fluorophore and shows the structure due to the individual vibrational energy levels of the ground and the excited state (see fig. 1.10). The absorption or excitation spectrum is a plot of the wavelength dependence of the absorbed light. By plotting fluorescence data as excitation and emission spectra it is easy to see two other features: the *Stokes's shift* and *Kasha's rule*.
Referring to the Jablonsky diagram (figure 1.9) it is clear that between absorption

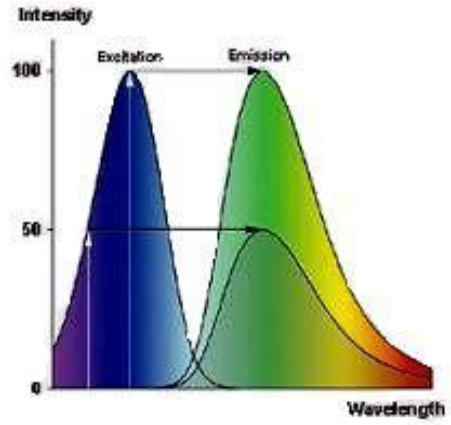

Figure 1.10: Sketch of normalized excitation and emission spectra for a fluorophore. The separation between the two is due to Stokes's shift. Kasha's rule is shown by the arrows.

and fluorescence emission there is loss of energy due to the relaxation to the lower vibrational level of S_1 by internal conversion. Moreover the transition $S_1 \rightarrow S_0$ involves higher vibrational levels of S_0 that rapidly raise the equilibrium resulting in a further loss of energy. As a result, the emission of light takes place at lower energy (higher wavelengths) with respect to excitation. This phenomenon is called the *Stokes's shift*, since it was first observed by Sir George Gabriel Stokes in 1852. Kasha's rule states that the emission spectra are independent of excitation wavelength. This is because after absorption the fluorophores rapidly relax to the lowest vibrational state of S_1 from which any transition to S_0 begins. The relaxation is probably the result of overlapping among numerous states of nearly the same energy.

A fundamental parameter that characterizes fluorescence emission is the quantum yield, ϕ_F. It is the emitted/absorbed photons ratio and is defined as [44]:

$$\phi_F = \frac{\Gamma}{\Gamma + k_{nr}} \tag{1.4}$$

where Γ is the emission rate of the fluorophore and k_{nr} the rate of the non-radiative decay processes to S_0. ϕ_F is always < 1 due to the Stokes losses of energy and becomes close to unity when $k_{nr} << \Gamma$. Because τ_f is defined as the time a molecule spends in the excited state before relaxing to S_0, it is determined by the

rate of all the processes that depopulate S_1:

$$\tau_f = \frac{1}{\Gamma + k_{nr}} \tag{1.5}$$

Due to the fact that fluorescence is a random process, only a fraction of the molecules relax exactly at $t = \tau_f$, therefore τ_f is an average value of the time spent in S_1. For a single exponential decay, 63% of the molecules relax at $t < \tau_f$ and 37% at $t > \tau_f$.

1.4 Fluorescence Imaging

Imaging of a sample can be achieved by collecting the fluorescence light emitted upon light excitation. In the process of one photon absorption, the rate of absorption is linear with respect to input intensity of light. A laser focused by an objective is assumed to have a Gaussian shape both in the object plane and in the optical path direction [45], with therefore a non-zero intensity in the out-of-focus planes. The consequence is that the excitation volume is not confined in the focal plane, and also the planes above and below the focus get excited in an hourglass shape as shown in figure 1.11.

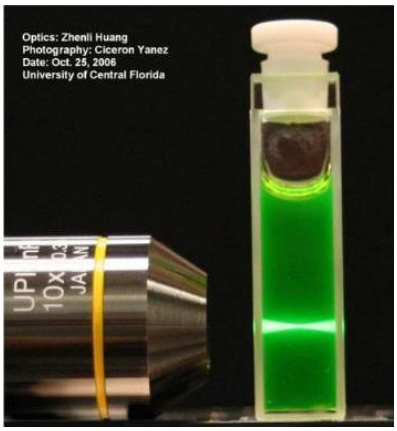

Figure 1.11: Excited volumes by one-photon laser source $\lambda = 380$ nm in fluorescein solution.

Ref: adapted from http://belfield.cos.ucf.edu/one%20vs%20two-photon%20excitation.html

One-photon excitation does not allow optical sectioning. Optical sectioning is obtained by spatial filtering the emission in front of the detector. Nowadays one

photon fluorescence imaging is mainly performed under confocal detection (see section 2.1.1).

One drawback of using a lamp source when imaging a point into the specimen is that there are fewer emitted photons to collect at any given instant. Thus, to avoid building a noisy image, each point must be illuminated for a long time to collect enough light to make an accurate measurement. In turn, this increases the length of time needed to create a point-by-point image. The solution is to use a light source of very high intensity. The modern choice is a laser light source, which has the additional benefit of being available in a wide range of wavelengths [46].

Unfortunately, fluorescence emission has not an infinite duration as molecules can undergo photobleaching. The phenomenon of *photobleaching* occurs when a fluorophore permanently loses the ability to fluoresce due to photon-induced chemical damage and covalent modification. Upon transition from an excited singlet state to the excited triplet state, fluorophores may interact with another molecule or with light to produce irreversible covalent modifications. The triplet state is relatively long-lived with respect to the singlet state, thus allowing excited molecules more time to undergo chemical reactions with components in the environment. The average number of excitation and emission cycles that occur for a particular fluorophore before photobleaching is dependent upon the molecular structure and the local environment.
The excitation power released per plane is independent of the focusing plane position along the optical axis. Thus, the main drawback of techniques like confocal microscopy is the photobleaching of molecules in out of focus planes which leads to degradation of the image.

1.5 Main objectives of the work

To design and implement a platform to investigate the activation state of platelets.

Key elements of the work are:

- Nanoparticle synthesis and characterization
- Nanoparticle-platelet interactions

- Platelet immobilization on surfaces
- Morphology and fluorescence signal of platelets

Chapter 2

Materials, methods and instrumentation

2.1 Instruments

2.1.1 Laser scanning confocal microscope

One photon fluorescence imaging, whose principles has been described in section 1.4, is nowadays extensively performed under confocal detection. The confocal microscope incorporates the ideas of point-by-point raster scanning of the specimen and rejection of out-of-focus light. The rejection of out of focus light is achieved by placing a screen with a pinhole in front of the detector. The focal point of the objective lens forms an image onto the pinhole screen. The specimen plane and the pinhole screen are conjugate planes (and hence the name "confocal"). By using a laser scanning confocal microscope two- and three-dimensions pictures of the specimen can be obtained, as well as a temporal series of 2D images. The description of how an image is created is as follows: a laser beam passes a light source aperture and is then focused by an objective lens into a small focal volume within a fluorescent specimen. A mixture of emitted fluorescent light as well as reflected laser light from the illuminated spot is then recollected by the objective lens. A beam splitter separates the light mixture by allowing only the laser light to pass through and reflecting the fluorescent light into the detection apparatus (fig. 2.1). After passing the pinhole the fluorescent light is detected by a photodetector, for example a photomultiplier tube (PMT) or avalanche photodiode, transforming the light signal into an electrical one which is recorded by a computer. The detector

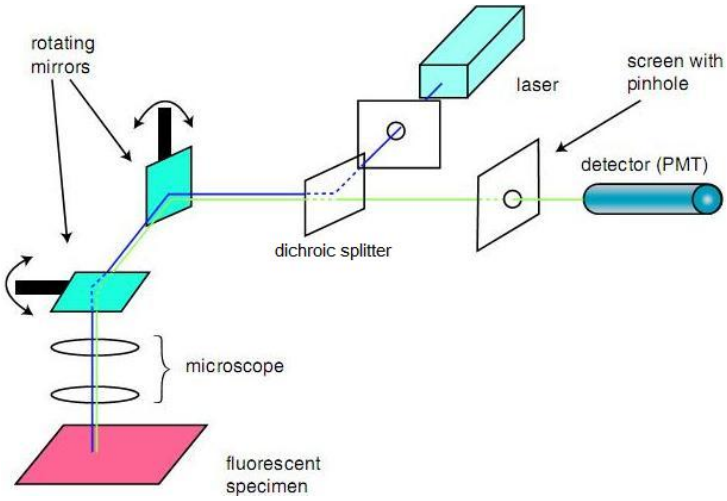

Figure 2.1: Basic setup of a confocal microscope. Light from the laser (blue) is scanned across the specimen by the scanning mirrors. Excitation light and fluorescence emission (green) are separated by a dichroic splitter. Optical sectioning occurs as the fluorescence light passes through a pinhole on its way to the detector.

aperture obstructs the light that is not coming from the focal point, as shown in figure 2.2. The out-of-focus points are thus suppressed. Most of the returning light is blocked by the pinhole. This results in sharper images compared to conventional fluorescence microscopy techniques and permits one to obtain images of various z axis planes (z-stacks) of the sample.

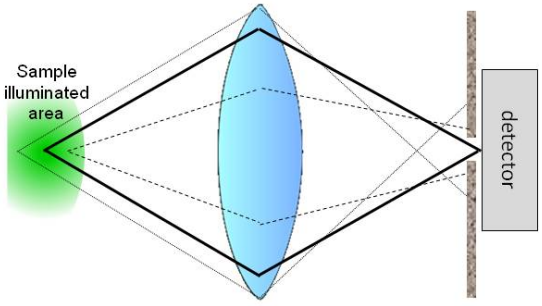

Figure 2.2: Schematic of how a pinhole aperture placed in front of the detector rejects the out of focus light. The light coming from the in-focus plane (solid line) passes through the pinhole, while the light coming from the planes under it (fine dotted line) and over it (dashed line) are blocked.

The detected light originating from an illuminated volume element within the specimen represents one pixel in the resulting image. As the laser scans over the plane of interest a whole image is obtained pixel by pixel and line by line, while the brightness of the resulting image pixel corresponds to the relative intensity of detected fluorescence light. The beam is scanned across the sample in the horizontal plane using one or more (servo-controlled) oscillating mirrors. The scan speed can be varied. Slower scans provide a better signal to noise ratio resulting in better contrast and higher resolution. Information can be collected from different focal planes by raising or lowering the microscope stage.
The ability of a confocal microscope to create sharp optical sections makes it possible to build 3D profiles of the specimen [47].

2.1.2 Dynamic light scattering

Dynamic light scattering (DLS) measures the time-dependent fluctuations in the intensity signal of the scattered light. From this measurement it can be determined the translational diffusion coefficient, which is related to the hydrodynamic diameter of the particles in solution. The rate of intensity fluctuation is dependent upon particle size. The intensity fluctuations for smaller particles have a higher frequency than for larger particles (see figure 2.3). The scattering intensity sig-

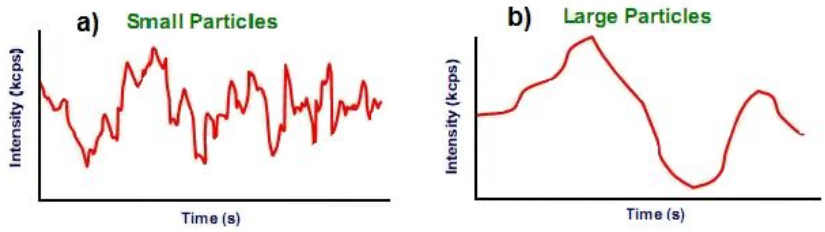

Figure 2.3: Scattering intensity fluctuations for a sample of a) small particles, and b) larger particles.

nal is passed into a digital correlator which multiplies and integrates short time scale fluctuations in the signal measured over a delay time τ, as shown in figure 2.4. The output is the correlation function for the sample. The correlation function describes how much a signal is similar to itself over a sample time τ, chosen appropriately according to the time characteristics of the signal. It is calculated

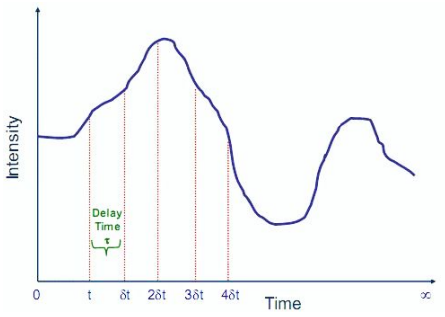

Figure 2.4: Scattering intensity is recorded every t and $t+\tau$, and is mathematically processed by the correlator which gives as output the correlation function.

as

$$G(\tau) = \int_{\infty}^{0} I(t)\, I(t+\tau)\, dt \tag{2.1}$$

and, for samples containing monodisperse particles, it is a single exponential decay

$$G(\tau) = A[1 + B \cdot exp^{(-2\Gamma\tau)}] \tag{2.2}$$

where A is the baseline and B the intercept of the correlation function, $\Gamma = Dq^2$ where D is the translational diffusion coefficient and $q = (4\pi n/\lambda) \cdot sin(\vartheta/2)$, with n refractive index of solution, λ is the wavelength of the laser, and ϑ the scattering angle.
For polydisperse particles the correlation function is

$$G(\tau) = A[1 + B \cdot g_1(\tau)^2] \tag{2.3}$$

where $g_1(\tau)$ is the sum of all exponential decays contained in the correlation function.

The diffusion coefficients are extracted by fitting the correlation function with a suitable algorithm, and the resulting diffusion coefficient distribution can be converted into a particle size distribution using the Stokes-Einstein equation, as shown in figure 2.5. The Stokes-Einstein equation (2.4) relates the particle hydrodiameter d to the diffusion coefficient D

$$d = \frac{k_b T}{3\pi\eta D} \tag{2.4}$$

where k_B is the Boltzman constant, T the temperature, η the sample viscosity.

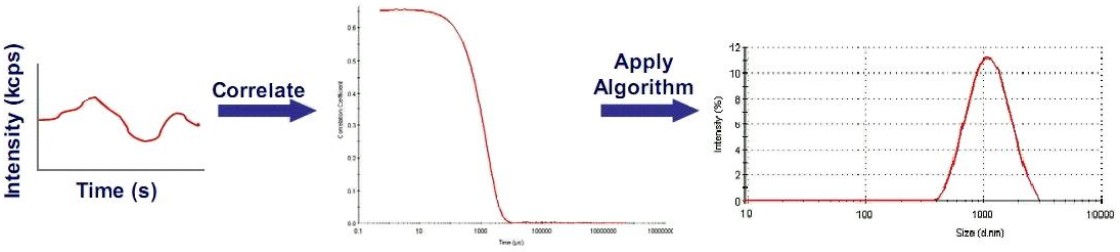

Figure 2.5: Intensity of scattering versus time pass through a correlator, which plots a correlation function that is fitted to obtain the size distribution of the sample.

To obtain the size distribution from the correlation function, the function is plotted on a semi-log plot (note: if the distribution is polydisperse, the semi-log plot is curved), and then it is fitted with a third order polynomial

$$Ln[G] = a + b\tau + c\tau^2 \tag{2.5}$$

from which the value b gives the z-average diffusion coefficient, which then gives the mean diameter of the particles. The ratio $2c/b^2$ is the polydispersity index, PDI, which describes the width of the distribution of the sizes. PDI can vary from 0 to 1 values, with 0 being a 100% monodisperse sample. Generally values of PDI lower than 0.1 are almost monodisperse samples and samples with PDI lower than 0.3 are accepted to be good monodisperse samples. Samples with PDI higher than 0.7 indicate a very polydisperse sample, and care should be taken in interpreting results as the sample may not be suitable for the technique, e.g. a sedimenting high size tail may be present.

2.1.3 Freeze-dryer

Freeze drying is used to dry nanoparticles after synthesis to obtain the mass of the sample. A typical freeze-dryer consists of one or more freeze-drying chambers attached to heating units, a freezing coil connected to a refrigerator compressor, and a vacuum pump (fig. 2.6). The material is placed in the chamber when it is still at room temperature. When the chamber is sealed and the process begins, the instrument activates the compressors which lower the temperature. The material is frozen solid, separating the water from the molecules surrounding it. The vacuum

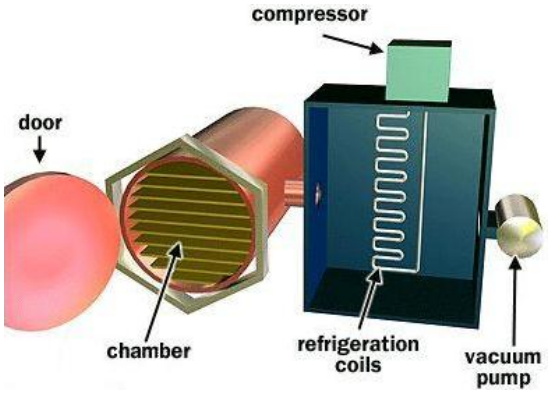

Figure 2.6: Schematic of a freeze dryer. There is usually a chamber with usually shelves, or a manifold with the possibility to attach several flasks controlled by separate valves.

pump is then run to lower the atmospheric pressure below 0.06 ATM by forcing air out of the chamber. The change of phase of water happens when the heating units apply a small amount of heat to the chamber. Since the pressure is so low, the ice turns directly into water vapor in a process known as sublimation. This continues for many hours while the material gradually dries out. Once the material is dried sufficiently, the chamber is brought back to ambient pressure, and the material removed.

2.1.4 Aggregometer

An aggregometer is an instrument designed to measure platelet aggregation in platelet rich plasma (PRP). An aggregometer is a specialized photometer for plasma which relates the relative transmitted light through a plasma sample to its aggregation status. A measurement is generally performed placing the PRP in an incubation well which heats the sample to 37° C for 10 minutes before testing. PRP is then transferred to the reaction well, where the samples are stirred and data are recorded. The stirring device turns the stir bar in the cuvette from 800 to 1200 rpm, keeping the platelets in suspension. The transmitted light is sent to a photomultiplier and a recorder. As the PRP is stirred, the recorder first stabilizes to form the baseline, which is close to 0% transmission. After a few seconds, an aggregating agonist is pipetted forcibly into the specimen to start the reaction. In a normal specimen, after the agonist is added, the platelets'

shape changes from discoid to spherical. The intensity of the transmitted light increases slightly in proportion to the degree of shape change. The transmittance is monitored continuosly and recorded into a time-plot. As platelet aggregates form, more light passes through the PRP, and the recorder begin to move towards 100% light transmission. Aggregation is complete in 6 to 10 minutes. Abnormalities are reflected in diminished or absent shape change and diminished aggregation [48].

2.1.5 Flow cytometry

Flow cytometry uses the principles of light scattering, light excitation, and emission of fluorochrome molecules to generate specific multi-parameter data from particles and cells in the size range of 0.5 μm to 40 μm diameter. Cells, suspended in a medium like PBS or HEPES buffer, are placed in a cuvette in the instrument. The instrument takes an amount of liquid, and passes the fluid in a sheath in a hydro-dynamically focused stream. The flow is reduced in diameter, forcing the cells into the center of the stream, and then the flow intercepts an optimally focused laser light source. Cells pass the laser light one cell at a time. As the cells or particles of interest intercept the light source they scatter/emit fluorescence, which is sent to different detectors (generally photomultiplier tube (PMT)) by using optical filters (see figure 2.7).

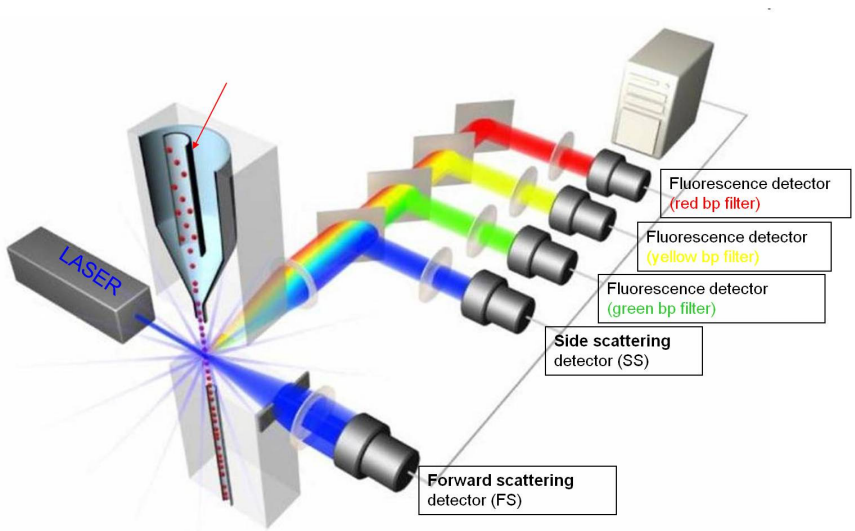

Figure 2.7: Schematic of a flow cytometry instrument.

Forward scattering (FS) is the amount of light that scatters in the forward direction as laser light strikes the cell. From the analysis of the forward scattering, obtained from a detector placed directly in the path of the laser, is obtained information about the size of the cell, as shown in figure 2.8. A cell traveling through

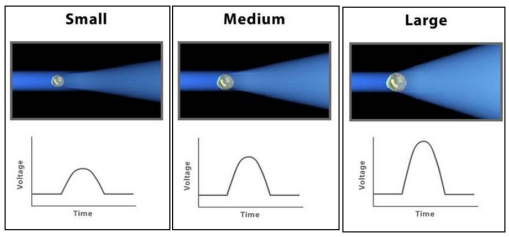

Figure 2.8: A smaller cell scatters the light differently from a larger cell, therefore the electric pulse recorded is weaker in amplitude compared to a larger one.

the laser beam scatters light at all angles. Side scatter is caused by granularity and structural complexity inside the cell. The side scattering (SS) is collected by a detector placed at 90° from the laser path.
Fluorescence light arising from fluorophores which are excited is separated by optical filters and recorded into different channels, normally labelled as FL1, FL2 and FL3.

Histogram files can be in the form of one-parameter or two-parameter files. A one-parameter histogram is a graph of cell count on the y-axis and the measurement parameter on the x-axis (like FL1). A two-parameter histogram is a graph representing two measurement parameters (like FS and SS), on the x- and y-axes, and cell count height on a density gradient. Particle counts are shown by dot density or by contour plot.

2.1.6 Atomic Force Microscopy

Atomic force microscopy (AFM) is a high-resolution type of scanning probe microscopy. There are some significant advantages of AFM as an imaging tool in biology and physics when compared with other techniques. AFM achieves molecular resolution and can also be performed in fluids permitting samples to be imaged in near native conditions. The fluid may be exchanged or modified during imaging and therefore there is the potential for observing biological processes [49].

To acquire an image the microscope raster-scans a mechanical probe/tip over the sample while measuring the local environment in question. Unlike traditional optical microscopes, scanned-probe systems do not use optical radiations and lenses. Resolution is therefore limited only by the size of the probe, rather than diffraction effects like in optical microscopes [50]. AFM operates by measuring attractive or repulsive forces between a tip and the sample. When the tip is driven close to a sample surface, a deflection of the cantilever occurs because of forces between the tip and the sample as described by the Hooke's law

$$\Delta z = \frac{\Delta F}{k_c} \tag{2.6}$$

where the deflection Δz is given by the acting force ΔF and the spring constant of the tip k_c.

The different imaging modes of AFM make it an instrument suitable for different applications. Imaging modes can be static(also called contact modes) or dynamic (or non-contact modes) where the cantilever is oscillated.

In contact mode the tip is raster-scanned across the 3D surface. The cantilever is bent as it moves over the surface profile and its deflection is measured by the detection apparatus. By looking at the cantilever deflection the local sample height can be measured. The deflection is measured with picometer resolution by an optical lever, which operates by reflecting a laser beam off the cantilever. The reflected laser beam hits a detector composed of two or more side-by-side photodiodes, as shown in figure 2.9. The difference between the signals of the photodiodes indicates the position of the laser spot on the detector and thus the deflection of the cantilever. When the tip is scanned over the sample surface then the deflection of the cantilever can be recorded as an image which represents the three dimensional shape of the sample surface (deflection image).

In constant force mode, the deflection is maintained constant by continuously adjusting the tip. To avoid collisions between the tip and the surface and a possible consequent damage of the sample, the tip is not driven at a constant z-height. The tip-to-sample distance is regulated by a feedback mechanism by keeping fixed the force between the tip and the surface. The faster the feedback loop can react to the cantilever deflections, the faster the AFM can acquire images. The ability to track the surface in this manner is limited by the feedback circuit only.

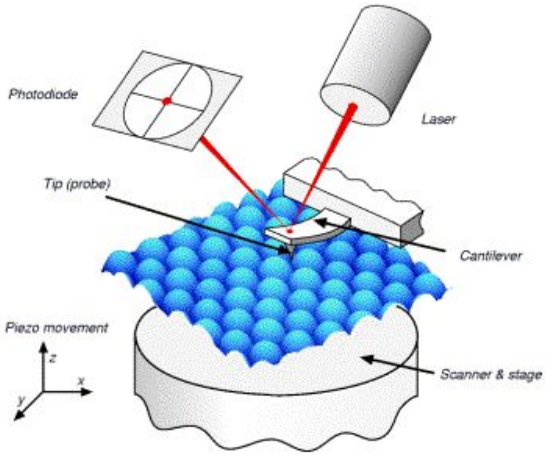

Figure 2.9: Concept of AFM and the optical lever. The laser spot is focussed on the back of the cantilever and the angle of the reflected laser is detected by a photodiode.

Soft samples like biological samples provide a more difficult surface to image because the forces exerted by the tip during imaging can cause deformation of the sample. Operating the AFM in tapping mode improves lateral resolution on soft samples. Instead of maintaining a constant tip-sample distance, the cantilever is oscillated in a direction normal to the sample. The contact with the surface is therefore only intermittent, reducing the lateral forces applied on the sample as the tip is raster-scanned. The lateral forces such as drag, which could be cause of damage, are therefore virtually eliminated [50].

In tapping mode the cantilever is oscillated with a frequency close to the tip's resonance frequency or to one of its harmonics. The amplitude of the oscillation is typically a few nanometers (<10 nm). The oscillation amplitude, phase and resonance frequency are modified by tip-sample interaction forces. During its oscillation the tip reaches the region where repulsive forces arise. The long range forces such as van der Waals, which are dominant from 1 nm to 10 nm above the surface, decrease the resonance frequency of the cantilever. The decrease in the resonance frequency is combined with the feedback loop system to maintain a constant oscillation amplitude or frequency by adjusting the average tip-to-sample distance. Measuring the tip-to-sample distance at each (x,y) data point allows the scanning software to construct a topographic image of the sample surface [51].

For ideal samples and conditions the AFM is capable of better than 1 nm lateral

resolution and of 0.01 nm resolution in height measurement [49].

2.2 Biological buffers and fixatives

2.2.1 Buffers

Why use a buffer

In the preparation of biological samples, buffers are used to suspend or wash the cells. Biological samples have a certain pH and a certain intracellular ion concentration. Many chemical reactions occurring in a cell are affected by the acidity of the surrounding medium. Changing the pH of the reaction solution can inhibit a particular reaction or change its reaction rate. Moreover biochemical reactions are especially sensitive to pH since many molecules contain atoms that may be charged or neutral depending on pH. A change in the charge of these atoms has significant consequences on the biological activity of the molecule. It is therefore important to control the pH by using buffer solutions.

Buffers always consist of an acid mixed with its corresponding base. The pH of this kind of solution can be written with the Henderson-Hasselbalch equation

$$pH = pK_a + log\frac{[A^-]}{[HA]} \tag{2.7}$$

where $[A^-]$ is the concentration of the conjugate base, [AH] is the concentration of the acid and pK_a is the acid dissociation constant

$$K_a = \frac{[H^+][A^-]}{[HA]}. \tag{2.8}$$

When the concentration of base equals the concentration of acid, the ratio of equation 2.7 is one and the pH equals the pK_a. A change in the pH of -1/+1 happens when the ratio decrease/increase of as much as a factor of ten. Therefore solutions having pH value close to their pK_a value have the property of maintaining the pH relatively constant when neutralizing added acids and bases (in the so called "buffering region").

The use of the correct buffer assures that the cells are kept alive and unaltered in their main functionalities.

PBS preparation

Phosphate buffered saline (PBS) is a water-based salt solution containing sodium chloride, sodium phosphate, potassium chloride and potassium phosphate. The buffer helps to maintain a constant pH. It is a buffer largely used with biological samples since it is isotonic (ion concentration of the solution is the same as in the human body), has physiological osmolarity and it is non-toxic to cells.
In this project PBS is prepared by diluting 137mM NaCl, 2.7mM KCl, 1mM Na_2HPO_4 and 1.76mM KH_2PO_4 in purified and deionized water (Milli-Q). The pH of the buffer is adjusted to pH 7.4 with the addition of 1M NaOH. PBS was stored at room temperature.

HEPES preparation

In this work, HEPES buffer has been used for washing the platelets before fixation occurs, or as a diluting solution for plasma. HEPES (4-(2-hydroxyethyl)-1-piperazineethanesulfonic acid) is a buffering agent containing both positive and negative ionizable groups. HEPES buffer is widely used in cell culture, largely because, compared to other buffers commonly used in cell culture, it is better at preserving physiological pH when changes in carbon dioxide concentration occur.
It is prepared with salts and sugar: in a clean flask are added 137 mM NaCl, 2.7 mM KCl, 1 mM $MgCl_2$, 5.6 mM glucose and 20 mM HEPES diluted in purified and deionized water (Milli-Q). The solution is then brought to pH 7.4 with the addition of 1M NaOH. The buffer so prepared has to be stored in a fridge and used within a week, or it can be aliquoted and frozen and thawed when needed.

2.2.2 Fixatives

Fixation process

Fixation is a step in the preparation of biological samples performed to preserve cells and tissue constituents in a state as similar as possible to the live-state and to prepare them for the further preparative procedures. Fixation stops autolysis and bacterial decomposition and stabilizes the cellular and tissue constituents. Aldehydes are crosslinking fixatives that act by creating covalent chemical bonds

between proteins in tissue. These extra bonds anchor proteins which otherwise would be soluble to the cytoskeleton and increase the rigidity of the tissue.

PFA preparation

Paraformaldehyde (PFA) is one of the most common crosslinking fixatives. Paraformaldehyde is the condensation reaction product of formaldehyde consisting of connected formaldehyde molecules. The units of the paraformaldehyde polymer are $–CH_2O–$; at one extreme of the polymer chain there is an OH group and at the other a hydrogen atom: $H0–(CH_2O)_nH$, where n can vary between 8-100. When

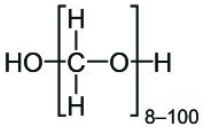

Figure 2.10: Paraformaldehyde chemical structure.

used on cells, the aldehyde group can bind to nitrogen and some other atoms of proteins forming a methylene bridge. Formaldehyde acts as a fixative entirely through its reactions with proteins. Other substances, like carbohydrates, lipids and nucleic acids, remain trapped in a matrix of cross-linked proteins but are not chemically changed unless fixation is protracted for several days [52].
In this work PFA solution 3.7% (w/v) is used to fix platelets for light microscopy analysis. The protocol used to prepare the solution is the following: 1.85 grams of PFA are mixed with 3.5 ml of Milli-Q water and 50 μl of NaOH 2N. To be able to dissolve the powder, the flask is heated in a hot water bath. The obtained solution is then diluted 1:10 in phosphate buffered saline and stored in the dark.

Glutaraldehyde preparation

An other crosslinking fixative used in cell preparation is glutaraldehyde. Glutaraldehyde is composed of small units separated by 3 methylene bridges. The glutaraldehyde chemical formula is $HCO\text{-}(CH_2)_3\text{-}CHO$, from which can be seen that each of the units have two aldehyde groups. This translates in an increased potential for cross-linking than with paraformaldehyde because the cross linking

reactions can occur through both the -CHO groups and over variable distances [52]. The free aldehyde groups are protruding from the side of each units of the polymer chain and from both of the extremes. All these -CHO groups will combine with any nitrogens present in the close environment, therefore there is a big potential for cross-linking with proteins (see figure 2.11). Glutaraldheyde solution does not

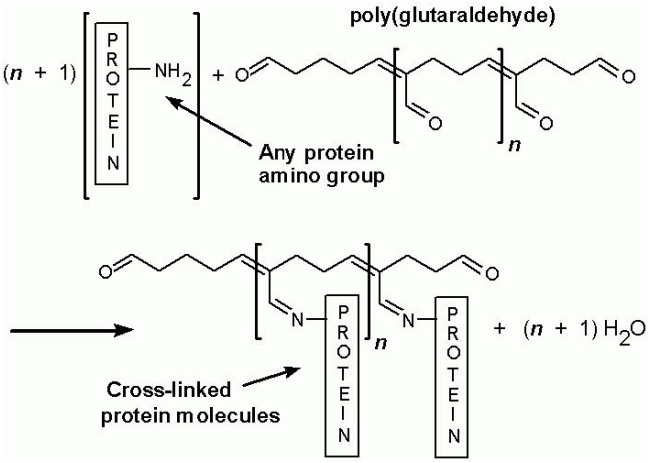

Figure 2.11: Reaction of poly(glutaraldehyde) with amino groups of proteins.

emit fluorescence, but after glutaraldehyde reacts with the sample, enhancement of cells' autofluorescence occurs [53].
In this project, for platelet fixation, glutaraldheyde is used in a dilution of 1% (w/v) in Milli-Q water.

2.3 Blood handling protocol

Blood is obtained from healthy volunteers. Fresh blood is drawn by a syringe containing a volume of sodium citrate (3.8% (w/v) in water), in a volume ratio 1:10 of blood, to prevent blood coagulation.
Platelet rich plasma (PRP) is obtained by centrifuging the blood at 170 RCF for 10 minutes. Upon centrifugation, the clear supernatant, that is the platelet rich plasma, is removed by pipetting. The remaining denser sample is centrifuged again at 720 RCF for 10 minutes to obtain the platelet poor plasma (PPP), which is the yellowish supernatant over the thick dark red solution.

Samples to be disposed of are neutralized with a disinfectant against viruses and bacteria, Virkon®.

Blood samples are handled only in a specific biohazard fume hood. The biohazard designated area has been independently assessed by a HEA inspector. All protocols and handling for the safe practice of using live biological samples from human origin have been liaised with the DCU Biological Safety Committee, with the advice of Dr. Robert O'Connor (The University Biological Safety Advisor).

Chapter 3

Nanoparticle synthesis and functionalization

3.1 Introduction

This chapter describes the experiments involving:

- nanoparticle synthesis and characterization
- nanoparticle surface modification
- antibody conjugation to nanoparticles.

3.2 Nanoparticle synthesis and charactherization

3.2.1 Introduction

The goal is to synthesize dye doped silica NPs and to conjugate them to an antibody towards a platelet receptor, in order to use the NPs as labels for activated platelets only.
We chose silica as an encapsulation material for the reasons already explained in section 1.1.1. The criteria for selecting the dye is that it must absorb in the red or near infra-red region of the spectrum. Haemoglobin in the blood absorbs all over the visible spectrum up to 600 nm, as shown in figure 3.1. Therefore, when using NPs in bioassays, a dye absorbing in the near infra-red region assures a minimal absorption from haemoglobin.

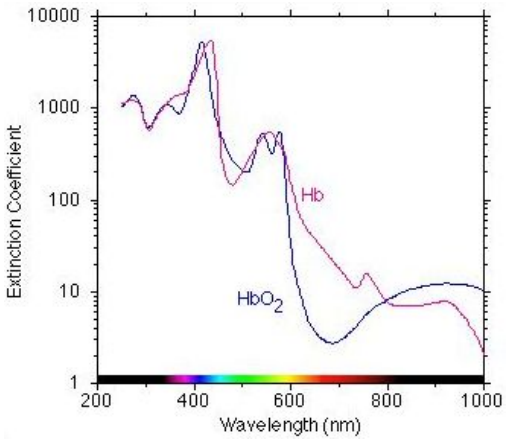

Figure 3.1: Absorption of oxy-haemoglobin ($Hb0_2$) and deoxy-haemoglobin (Hb).
Ref: http://www.indiana.edu/ sexlab/ei-vp-uvaprobe.html

The dye chosen was 4,5-Benzo-5'-(iodoacetaminomethyl)-1',3,3,3',3'-pentamethyl-1-(4-sulfobutyl)indodicarbocyanine, commonly referred as NIR664-iodoacetamide, with formula $C_{37}H_{42}IN_3O_4S$. This dye has already been successfully encapsulated into silica NPs "in house", showing a good stability and a good fluorescence yield. It is soluble in methanol, with absorption maximum at λ =664 nm, and fluorescence emission maximum at λ =689 nm, ensuring minimal absorption from the blood components.

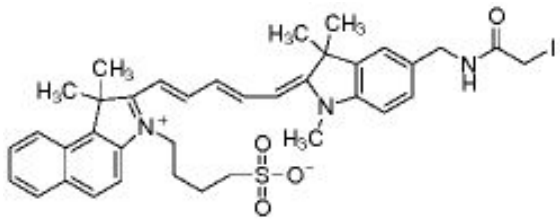

Figure 3.2: Chemical structure of NIR664-iodoacetamide.

The required NP diameter has to be in the range of 60-150 nm. As explained in section 1.1.1, NPs with diameters of the order of tens of nanometers tend to be taken up in the cell; instead our aim is to use the NPs as an external probe for the platelets, targeting chosen receptors on the platelet surface. On the one hand a larger size not only avoids the NPs being uptaken non-specifically, but also allows for the possibility of more dye molecules being embedded in the silica matrix, hav-

ing therefore a brighter label and lowering the limit of detection (LOD). On the other hand, a NP which is too large can also cause problems. It can occupy too much space on the platelet surface, leading to a small number of NPs labelling the platelet. It can also have too many antibodies attached on its surface, promoting repulsion or clustering between the NPs themselves.

3.2.2 Synthesis by the microemulsion process

To synthesize NPs doped with NIR664, we followed a protocol established in-house [29].
The first step involves the conjugation of the dye to a silane, in order to increase the affinity of the dye with the TEOS. Since NIR664 has a iodoacetamide group (see fig. 3.2), it is suitable for the derivatization of thiols. Therefore it can be conjugated to any molecule having a pendant SH group, like, for our purposes, to (3-Mercaptopropyl)triethoxysilane (MPTES) (figure 3.3).
For dye conjugation the dye is first dissolved in hexanol for a final concentration

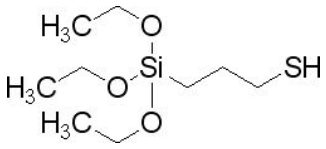

Figure 3.3: Chemical structure of MPTES, containing the end SH group.

of $\approx 10^{-3}$ molar. Addition of MPTES, in a molar ratio 2:1 with the dye, takes place in a glove box. The dye solution is then left inside the glove box, constantly under stirring, for about 3-4 hours protected from the light.
A key point in the dye conjugation process is the importance of working in a sealed protection atmosphere. The mercaptosilane is largely sensitive to humidity present in the air and it can hydrolyze before being conjugated to the NIR664 dye. In early experiments performed outside of the glove box, the products obtained after the microemulsion synthesis were a whitish sediment, which translates to an unsatisfactory inclusion of the dye into the silica matrix. The most significant failures in dye inclusion were obtained under high humidity conditions, supporting the thesis of incomplete dye conjugation because of hydrolysis of the mercaptosilane.
Another important parameter is the incubation time. In experiments with in-

cubation time longer than 5 hours, the product obtained was a solid compact sediment impossible to re-disperse. Large clusters are still present in solution even after a long time of ultrasonication and they are not dispersable even after mechanical crushing. For an optimal incubation time of the dye with the mercaptosilane one molecule of NIR664-iodoacetamide is conjugated with one molecule of MPTES. Longer incubation times can lead to the formation of clusters of 3 or more molecules, affecting therefore the silica condensation process during NP synthesis. It is also important that the reaction takes place in the dark, to prevent damage to the dye from photobleaching.

The second step is the microemulsion synthesis. In a flask are added, in order, 3.8 g of Triton-X as a surfactant, 15 mL of cyclohexane as the main oil phase, 2 mL of dye-conjugated solution plus 1.6 mL of hexanol, and 960 μl of deionized water. The solution is then sonicated for a short while and left stirring for about 5 minutes in order to have a uniform distribution of water nanocompartments. Afterwards 200 μl of TEOS are added. Molecules of TEOS and of dye conjugated to MPTES migrate into the droplets and the reaction of hydrolysis of the alkoxysilanes slowly takes place due to the presence of the reactant (water). After 30 minutes stirring, 80 μl of ammonium hydroxide solution (28% in water), which acts as a catalyst, is added to speed up the hydrolysis and the condensation process of silica. The solution is then left stirring for 24 hours at room temperature.

In the third step, the NP surface is modified by the addition of amino groups. The protocol involves the introduction of the desired functional group(s) on the surface of the primary dye-doped silica NPs by condensation of TEOS and organosilane reagents containing the active functional groups. Amino groups are introduced using (3-aminopropyl)-trimethoxysilane (APTMS), and methylphosphonate groups are introduced by 3-trihydroxysilyl)propyl methylphosphonate (THPMP), a water-dispersible silane reagent, as can be seen in figure 3.4.
For the surface modification, in the same flask where the synthesis is still taking place, are added 100 μl of TEOS, 30 minutes later are introduced 80 μl of THPMP and five minutes later 20 μl of APTMS are added, constantly under stirring.

As described by Bagwe and others [54], APTMS condenses together with TEOS, creating amino groups on the NP surface, and THPMP, which introduces

Figure 3.4: Chemical structure of A) APTMS, B) THPMP. APTMS is used to add amino groups -NH_2 on NP surface.

methylphosphonate groups on the NP surface, is used as a stabilizer against aggregation. The stability of NPs in solution is primarily measured by the zeta potential of the sample. The zeta potential of undoped and unmodified silica NPs is in the range of -40 mV $\sim$ -30 mV, hence agglomeration of NPs is forbidden by electrostatic repulsion. Since the pKa value of the amine groups is 9.0, when high concentrations of amine groups are added to the surface at physiological pH, the positively charged amino group can bond to negative surface silanol groups. The overall charge on the surface is so reduced, with a zeta potential value close to zero, thus reducing the electrostatic repulsion between the NPs and therefore increasing NP agglomeration. As the amount of inert functional group methyl phosphonate is added to the surface, due to its low pKa value of 2.0, the zeta potential value of NPs become more highly negative. Most of the amino groups on the silica surface interact with methylphosphonate groups preventing back-bonding and strong electrostatic repulsion forces arise between NPs, as shown in figure 3.5.

The time interval between the addition of TEOS and the organosilane reagents is important because, if kept too short, most of the active functional groups would be buried inside the particles, as the condensation reaction of the organosilane is faster than that of tetraethylorthosilicate.

The last step in NP synthesis is extraction and washing of NPs. To stop the synthesis, an equal volume of acetone is added to the reaction flask. Acetone addition causes a flocculation process in which NPs accumulate and slowly precipitate. Complete precipitation is achieved after centrifugation at 3200 RCF for 5 minutes. The supernatant containing all the unreacted products and the dissolved reagents are discarded. NPs are confined in the solid colored sediment. Several washes in ethanol and then in water are performed in order to completely remove any adsorbed molecules on the NP surface. NPs are dispersed in ethanol or water after $\approx$

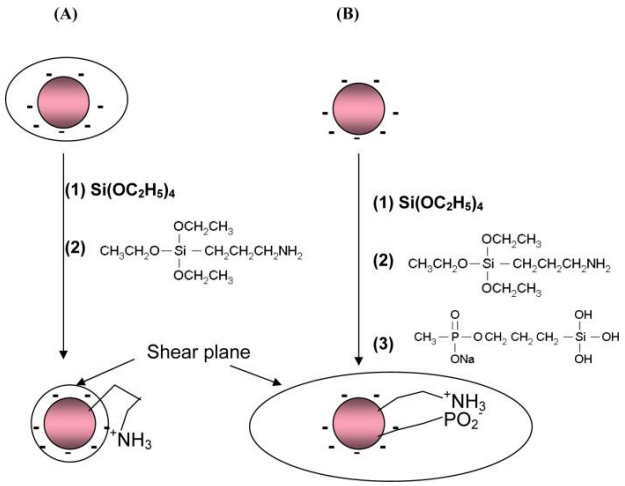

Figure 3.5: Schematic diagram showing the mechanism by which the back-bonding of amine-modified silica NPs is reduced by the addition of methyl phosphonate groups on the silica NP surface (B), compared to silica NPs functionalized just with amino groups (A). Ref: [54].

10 minutes sonication, and then are spun down with centrifugation at 13000 RCF for 15 minutes.

3.2.3 Characterization of NIR664 doped NPs

NIR664 doped silica NPs are synthesized by the microemulsion method and surface modified with the addition of amino and phosphonate groups, as described above (paragraph 3.2). The main characterization methods being used are dynamic light scattering (DLS), transmission electron microscopy (TEM), and spectroscopic techniques.

Dynamic light scattering and transmission electron microscopy characterization

The NP synthesis protocol was improved over time until the NPs samples matched the requested criteria. To characterize the uniformity of the synthesized sample, the average diameter and the morphology, two main analysis techniques were used. A DLS instrument, whose principles have been described in 2.1.2, measures the average hydrodynamic diameter of the NPs considered as spherical, the size distribution of the sample and the zeta potential of the NPs solution. TEM is

a microscope that employs electrons as a imaging beam in place of light, which is used in conventional microscopes (like transmission light microscopes, fluorescence microscopes, and so on). A TEM instrument has a resolution much higher than light based microscopes, being able to image the nanometer scale. Therefore it shows the actual shapes and dimensions of the NPs samples.

The NPs synthesized with the optimal protocol (already described in section 3.2.2) have an average diameter of 90 ± 15 nm, with a polydispersity index (PDI) spanning from 0.13 to 0.23 according to DLS analysis. The NP size achieved is suitable for the project aims, and the low PDI values underline the low polydispersity of the samples. The zeta potential is also measured using DLS. The zeta potential describes the amount of charge present on the surface of the scattering particles. The further the charge is from zero, either positively or negatively, the more stable will be the NP. A highly charged surface ensures the repulsion of the particles between themselves, therefore assuring stability of the particles dispersion and low degree of clustering. The NP samples have an average zeta potential in distilled water of -30 ± 7 mV. A typical DLS size distribution for a sample of NIR664 doped NPs is shown in figure 3.6.

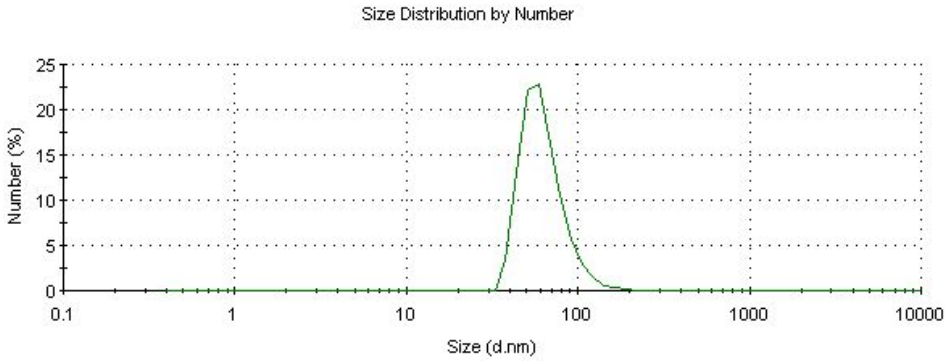

Figure 3.6: DLS analysis of a sample of NIR664 doped silica NPs, surface modified with APTMS and THPMP, in water. The zeta average diameter size is 101 nm, the peak number distribution is at 74 nm and the intensity distribution has a peak at 112 nm with a width of 47.3 nm. The PDI is 0.143 and the zeta potential -29 mV.

From TEM images NPs are spherical in shape, as it can be seen in figure 3.7. Moreover the imaging technique confirms the monodispersity of the sample and

the average diameter obtained from the DLS measurements. NPs are stable for

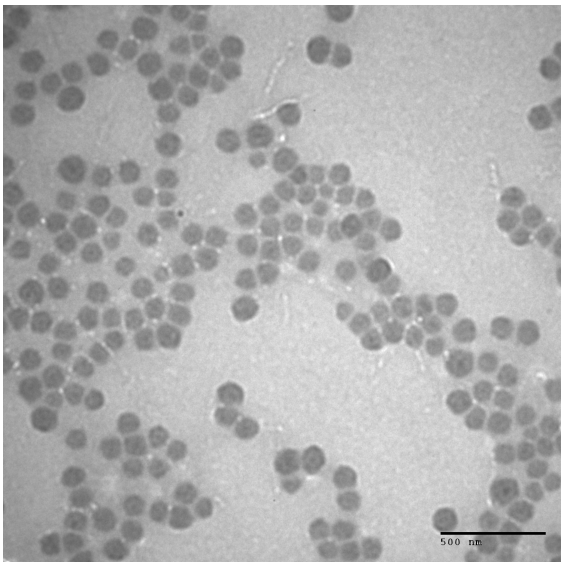

Figure 3.7: TEM image of the sample which DLS analysis is reported in figure 3.6; (scale bar = 500 nm).

months in water, with minimal precipitation.

Spectroscopic characterization

The fluorescence properties of NIR664 doped NPs are summarized in figure 3.8, which shows that the NIR664 dye has an excitation maximum at $\approx$ 670 nm and an emission maximum at $\approx$ 690 nm when embedded in the silica matrix.

To test the stability of dye entrapment inside the silica matrix, the samples were analyzed soon after the synthesis, and at various times after the synthesis. NPs are precipitated upon centrifugation at 10000 RPM for 15 minutes, and the collected supernatant is analyzed in the spectrofluorometer. No fluorescence signal was found in the supernatant, meaning that dye does not leach out from NPs. No dye leaching has been observed even after a few months.

To compare the fluorescence intensity of a single dye doped NP with the intensity of a single free dye molecule, measurement of the relative brightness has been carried out according to the following protocol: a known quantity of NIR664-

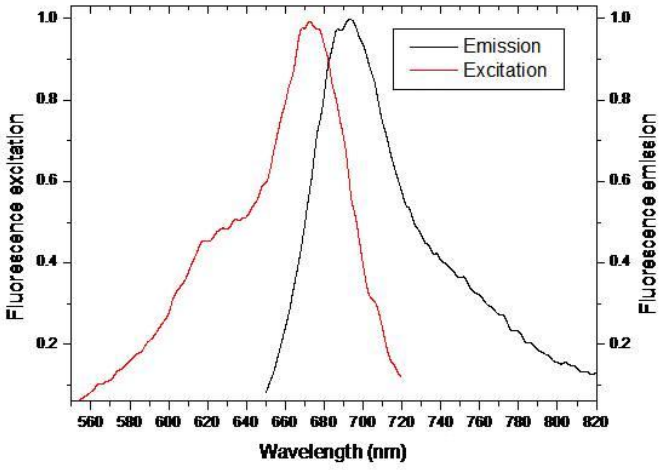

Figure 3.8: Normalized excitation and emission spectra of NIR664 NPs. Excitation spectrum: λ_{emiss}=740 nm; emission spectrum: λ_{exc}=640 nm.

iodoacetamide was dissolved in isopropanol and its absorbance was measured in a UV-VIS spectrophotometer in order to know its exact concentration from the Lambert-Beer law $A = \epsilon \cdot C \cdot l$. The sample was further diluted to give several samples.

NP samples were prepared in a similar way: from the absorbance spectrum of NPs dissolved in water is subtracted the scattering contribution of the NP. The absorbance value of the dye inside the NP at the peak is so recorded. This value is used to calculate the dilution ratio to obtain a sample of absorbance $\leq$0.05 and other samples with lower concentrations are prepared from it. The employed absorbance values ensure that the measurements of the fluorescence are in the linear range.

Synthesized NPs are freeze dried to determine the sample weight (see section 2.1.3 for further details on freeze drying process). The molarity of the sample is calculated using the mass per volume concentration, the density of silica, and the average diameter obtained by the DLS measurement.

The different dilutions of free dye and of NPs are put in multiple copies in a multi-well plate for integrated fluorescence measurement with a microarray scanner. In this configuration the values of the fluorescence from NPs and from free dyes are not comparable [55]. For the wells containing NPs, the illuminated volume has a different shape and dimension compared to the wells containing free dye

molecules. This is because the excitation light passing through the well is scattered by the large volumes of the NPs, hence enlarging the illuminated volume (see figure 3.9). To compensate for this error, when preparing the free dye samples, undoped silica NPs are added in solution together with the free dye molecules. These undoped NPs have to be of the same average size and polydispersity of the NPs under test. Undoped NPs are used just as scatterers to enlarge the illuminated volume in the free dye samples, thus ensuring that all the samples have equivalent scattering properties.

When the integrated fluorescence for all the samples (averaged over the multiple

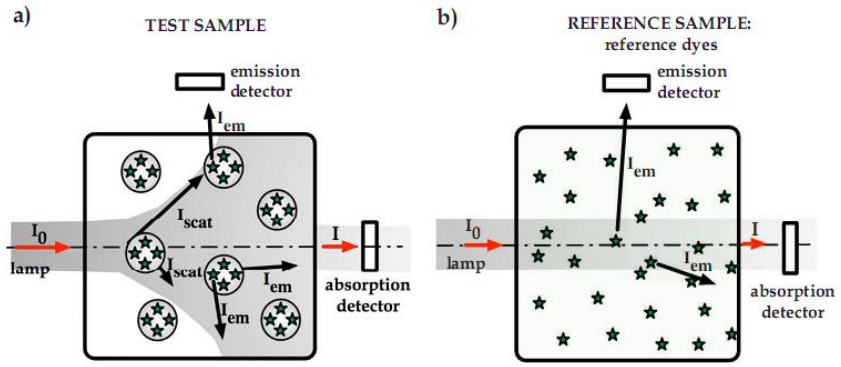

Figure 3.9: a) Solution of dye doped NPs and b) solution of free dye molecules, illuminated by a light beam. In the case of a test sample containing scattering objects (a), the zone illuminated by the incident beam (gray zone) is significantly enlarged compared to that of the reference solution (b). Ref: [55].

copies) is obtained, these data are plotted versus the concentration in moles per liter of free dye molecules or of NPs, as shown in figure 3.10.

Having used the same instrument and the same excitation/recording parameters, it is valid to assume the following:

$$\frac{F_{nps}}{F_{dye}} = \frac{\phi_{nps}}{\phi_{dye}} \cdot \frac{A_{nps}}{A_{dye}} \cdot \left(\frac{\eta_{dye}}{\eta_{nps}}\right)^2 \tag{3.1}$$

where F is the integrated fluorescence, ϕ the quantum yield, A the absorbance and η the refractive index of the medium in which the components are diluted. The extinction coefficient of the dye in solution can be assumed to be the same as that of the dye when embedded in the silica matrix. The optical path can also be considered the same for the samples containing NPs and the samples containing free

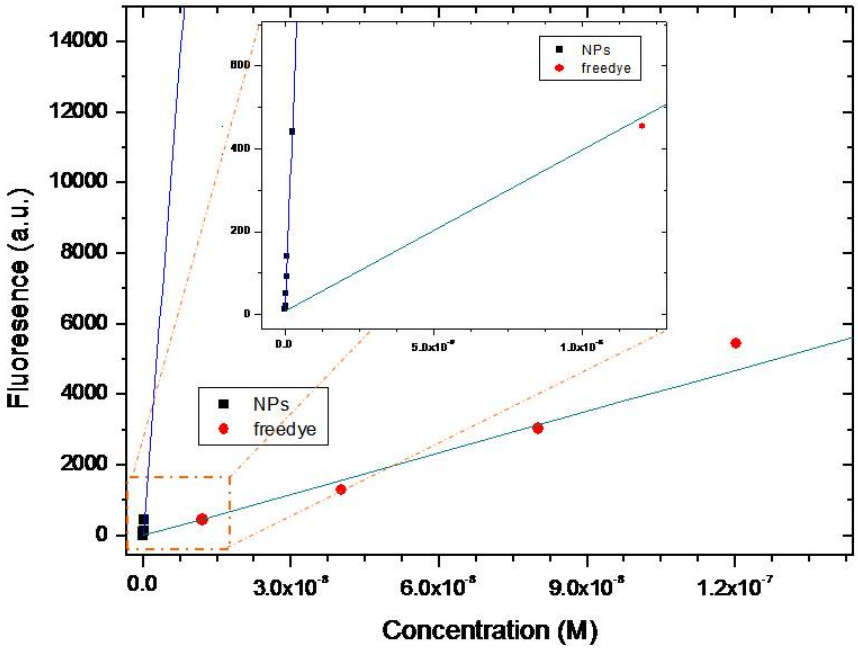

Figure 3.10: Integrated fluorescence for a sample of NIR664 doped NPs in water versus NP concentration, and for a sample of NIR664 free dye molecules in isopropanol versus dye molecule concentration including linear fit of the data.

dye molecules, since undoped NPs have been introduced to compensate scattering errors. Therefore equation 3.1 can be rewritten as

$$\frac{F_{nps}}{F_{dye}} \approx \frac{\phi_{nps}}{\phi_{dye}} \cdot \frac{C_{nps}}{C_{dye}} \cdot \left(\frac{\eta_{dye}}{\eta_{nps}}\right)^2 \tag{3.2}$$

Thus, calculating the slope obtained by the linear fit of the integrated fluorescence versus molar concentration, the equation become

$$\frac{Slope_{nps}}{Slope_{dye}} \approx \frac{\phi_{nps}}{\phi_{dye}} \cdot \left(\frac{\eta_{dye}}{\eta_{nps}}\right)^2 \tag{3.3}$$

From this it can be calculated the ratio ϕ_{nps}/ϕ_{dye} that is defined as *relative brightness*. Using this method it can be shown that the NPs are brighter than a single molecule dye. The dye doped NPs are brighter than one molecule of NIR664, as the slope of the linear fit is steeper than that of the free dye samples, as it can be seen in figure 3.10. From the calculations, the NPs are ≈ 60 times brighter than a single dye molecule.

3.2.4 Summary of results

In this section the optimum synthesis of silica NPs doped with a near infrared dye obtained after protocol optimization was presented. The initial syntheses (not described here) were focused on the understanding of the Stöber and microemulsion processes, by repeating some experiments taken from literature and by varying parameters. Optimization of the synthesis has been carried out in order to obtain NPs with the characteristics required for the project, like optimum size, monodispersity, and high brightness.

NPs obtained in this way remain suspended in solution due to their negative surface charge (which is measured by the zeta-potential), are stable in water for a long time, have a diameter variable between 80 nm and 100 nm suitable for the project and have a low polydispersity. The dye is successfully entrapped in the silica matrix without any leaching. This is an important point for the stability of NPs and for their toxicity when used on biological samples.

NP brightness is sufficient to start the experiments on interaction of NPs with platelets, but further optimization is desired. The aim is to obtain a super bright label for activated platelets. A super bright label entails a decrease in the limit of detection, which is a highly desired feature for a diagnostic assay.

3.3 Antibody conjugation to nanoparticles

For this project, NPs have to be modified with a platelet specific tag. Herein, we conjugate the NPs with an antibody towards specific surface platelet receptors. An antibody is a gamma globulin protein used by the immune system to identify and neutralize pathogens such as bacteria and viruses. Each antibody is specific for a target molecule (called antigen) with a highly specific interaction. A monoclonal antibody recognizes only one epitope on an antigen, while instead a polyclonal recognizes multiple epitopes on any one antigen. The basic structural unit of antibodies are similar, with two large heavy chains and two small light chains, as illustrated in figure 3.11. At the extremity of the protein there is a small variable region which is the antigen binding site. The unique part of the antigen recognized by an antibody is called the epitope. These epitopes bind to their antibody in a highly specific interaction that allows antibodies to identify and bind only their

unique antigen.

As discussed in 1.2.1, an activated platelet can be distinguished by looking at

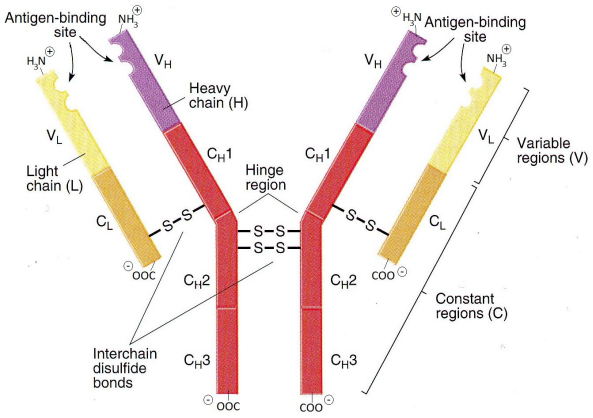

Figure 3.11: General structure of an antibody. Ref: adapted from http://apbrwww5.apsu.edu/thompsonj/Anatomy%20&%20Physiology/2020/2020%20Exam%20Reviews/Exam%202/CH21%20antibody_structure-giant-diagram.htm

the conformational state of its αIIbβ3 receptors. PAC-1 is an antibody, available on the market, that binds only to the activated form of the platelet glycoprotein IIb-IIIa complex (or αIIbβ3). It recognizes an epitope on the αIIbβ3 complex critical for fibrinogen binding. The integrin αIIbβ3 can also be targeted by the antibody anti-CD41, which binds to every state of the αIIbβ3 receptor.

For the initial development of the assay it was decided to use mouse anti-human CD41 monoclonal antibody, for the purpose of labelling both resting and activated human platelets.

3.3.1 Conjugation techniques

Two techniques of antibody conjugation are used. The first is the direct conjugation of antibodies to NPs and the second one involves the use of a crosslinker. In the direct conjugation, synthesized NPs are redispersed in phosphate buffered saline (PBS) at physiological condition (pH = 7.4), and antibody dissolved in PBS are added in a concentration which was 3 to 5 times higher than the NP concentration. The solution is then left under gentle stirring at 4°C over night. Conjugation

of antibodies to NPs can take place because of the reaction between carboxyl groups, -COOH, present on the antibody's constant region (see figure 3.11) and amine groups, NH_2 present on the NP surface, forming therefore an amide bond.

Using a crosslinker, the reaction between the amine and the carboxyl group is accelerated and the efficiency increased. 1-Ethyl-3-[3-dimethylaminopropyl]-carbodiimide hydrochloride (EDC) is a zero-length crosslinker which couples carboxyl groups to primary amines. The reaction between EDC and a carboxyl group

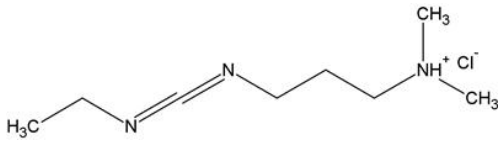

Figure 3.12: Chemical structure of 1-Ethyl-3-[3-dimethylaminopropyl]-carbodiimide hydrochloride (EDC).

creates an amine-reactive intermediate. If this intermediate encounters an amine a stable bond is formed, otherwise hydrolyzation of the intermediate and regeneration of the carboxyl group will take place.
Adding N-hydroxysulfosuccinimide (Sulfo-NHS), which acts as a catalyst, the in-

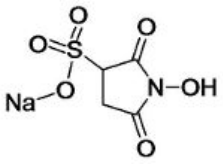

Figure 3.13: Chemical structure of N-hydroxysulfosuccinimide (Sulfo-NHS).

termediate is an amine-reactive Sulfo-NHS esters with a life-time longer than the life-time of the intermediate obtained using only EDC. Thus EDC-mediated coupling reactions have greater efficiency. The coupling reaction is represented in figure 3.14.

For NP conjugation, EDC and Sulfo-NHS are used to bind the carboxyl group of the antibody with the amine group of the NPs. EDC and Sulfo-NHS are dis-

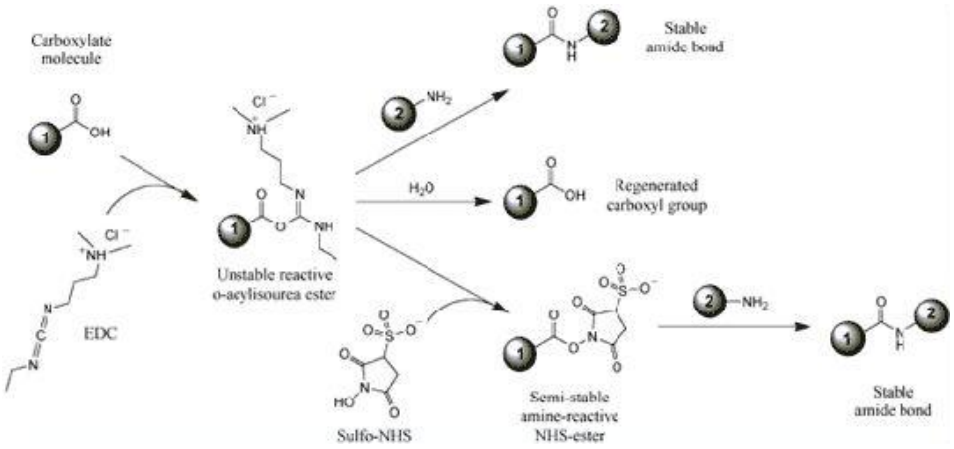

Figure 3.14: EDC reacts with a carboxyl group on molecule 1 and an amine-reactive intermediate is formed. A stable bond is created when the intermediate conjugates to an amine on molecule 2. The addition of Sulfo-NHS makes the life time of the amine-reactive intermediate longer. Ref: http://www.piercenet.com/media/

solved in MES buffer in a molar ratio of 1:1. This solution is then added to the antibody dissolved in PBS, in the same molar ratio. The vial is left for 15 minutes in incubation at room temperature without stirring. A longer incubation time is to avoid in order to inhibit further binding between the amine-reactive Sulfo-NHS esters antibodies and the antibodies themselves (since amino groups are present in the variable region, as shown in fig. 3.11). After incubation, NPs are added to the antibody solution, and gently stirred for about 30 minutes. After this time, the vials are centrifuged at 10000 RPM for 15 minutes to spin down the NPs, and the supernatant is discarded to remove any unreacted product as well as free antibodies. The antibody-treated NPs are then resuspended in PBS and stored in a fridge until usage.

3.3.2 Testing for the presence of antibodies

To determine the presence of the antibody on the NP surface and to quantify the amount of effectively loaded antibody, the bicinchoninic acid (BCA) protein assay was used. This is a colorimetric test, based on chemical reactions, able to determine the concentration of a protein present in a solvent. The test utilizes the reduction of Cu^{2+} to Cu^{1+} by protein when in an alkaline medium, followed by the

reaction of BCA with the reduced copper ions. The product of this reaction is a purple colored complex that can be measured by absorption. For a protein concentration not greater than 0.6 mg/ml the intensity of the BCA complex absorbance is linear with the concentration of the protein under investigation as described by the Lambert-Beer law.

To perform this test, undoped silica NPs are used in order to avoid any interference with the measurement of the absorbance from the BCA reaction. Undoped NPs were synthesized using a Stöber technique. The NPs synthesis protocol was adjusted to obtain NPs which are similar in size and with comparable zeta potential values to the dye doped NPs. In this case the Stöber technique is preferable over the microemulsion because a similar protocol without the dye cannot be obtained. We found in fact that in the developed microemulsion protocol the dye solution works as a catalyst in the synthesis. Thus a synthesis technique with a higher yield and less consumption of materials was chosen.

For the NP samples preparation, the NP solution was previously freeze dried in order to know the concentration of the solid mass per volume. Subsequently, a volume of solution containing 10 mg of solid mass is used to proceed either with the direct conjugation technique or with the EDC-mediated conjugation (both protocols are described in section 3.3.1). For this test we use bovine IgG as an antibody, which is a standard antibody easily available on the market and largely used in standard assays. IgG is used in a set of concentrations spanning from 30 μg/ml to 0.3 μg/ml. Bovine serum albumine (BSA) is used as a reference protein to build the calibration curve. BSA is diluted in concentrations spanning from 250 μg/ml to 0 μg/ml. The test is performed with a BCA assay kit, mixing the reagents with the standard protein samples and with the NPs samples and leaving the vials in incubation at 37 °C for about 1 hour. Afterwards all the samples are put in several replicates in a multi-well plate and their absorbance values is measured at $\lambda = 562$ nm with a microarray scanner. The absorbance of the wells containing BSA are firstly averaged between the replicates and then plotted versus theirs concentration. In this way is built a linear calibration curve which connects the measured absorbance with the associated protein concentrations. This trend is then used to estimate the quantity of antibody present on the NP surface.

The results obtained for the direct conjugation technique of IgG antibody on silica NPs show a huge variance of the values between the replicates, as illustrated

by the error bars in figure 3.15, meaning a not highly reproducible antibody loading efficiency. The amount of antibody effectively loaded for the higher concentration

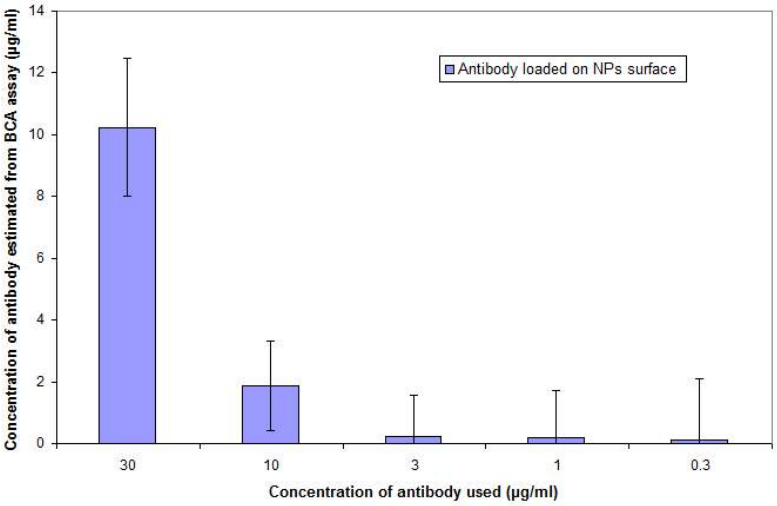

Figure 3.15: Concentration of IgG antibody conjugated to the NP surface through direct conjugation technique estimated with a BCA assay. Standard deviations from 4 replicates are depicted with error bars.

analyzed is around one third of the initial concentration. For IgG concentrations from 10 μg/ml to 0.3 μg/ml the results cannot be considered due to their large relative errors.

For NPs treated with ECD and Sulfo-NHS the variance is lower, as shown by the smaller error bars of figure 3.16. The amount of antibody loaded on the NP surface is about 40% for a concentration of 30 μg/ml and of 20% for a concentration of 10 μg/ml, but with a percentage error as high as 36% for the latter one. Again, the relative errors are too large for the samples with lower concentrations.

This test was repeated using different diluting solvents, like PBS, 1:10 PBS and water, and all lead to similar results, showing the actual presence of the antibody on the NPs when treated with either direct or crosslinker mediated techniques as well as the reproducibility of the results.

To investigate the behavior of the NPs when conjugated with an antibody, AFM imaging was performed. The samples examined were the NIR664 doped silica NPs synthesized according to the protocol described in section 3.2.2 and conjugated to

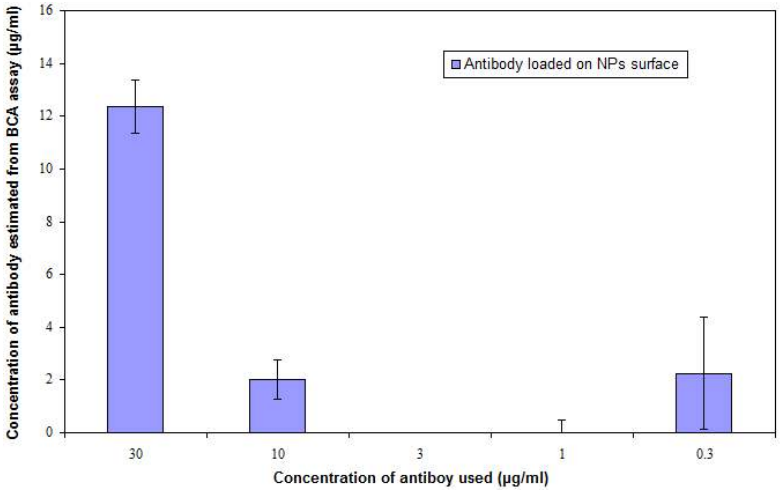

Figure 3.16: Concentration of IgG antibody conjugated to the NP surface through crosslinker-mediated conjugation technique estimated with a BCA assay. Standard deviations from 4 replicates are depicted with error bars.

the antibody anti-CD41 with the techniques described in section 3.3.1. NP samples were first diluted in water at a low concentration and then dried under nitrogen flux on glass slides. In figure 3.17 the AFM images of a sample of unconjugated NPs, and of antibody conjugates one, imaged in contact mode in air, are shown.

From AFM analysis it can be seen that dried NPs tend to aggregate when no antibody is present on the surface. When the antibody is conjugated to the NPs (figure 3.17B) there is a decrease in the degree of clustering. NPs conjugated to anti-CD41 through the crosslinker EDC show a behavior similar to NPs conjugated directly, resulting in less aggregated samples when deposited dried on a surface.

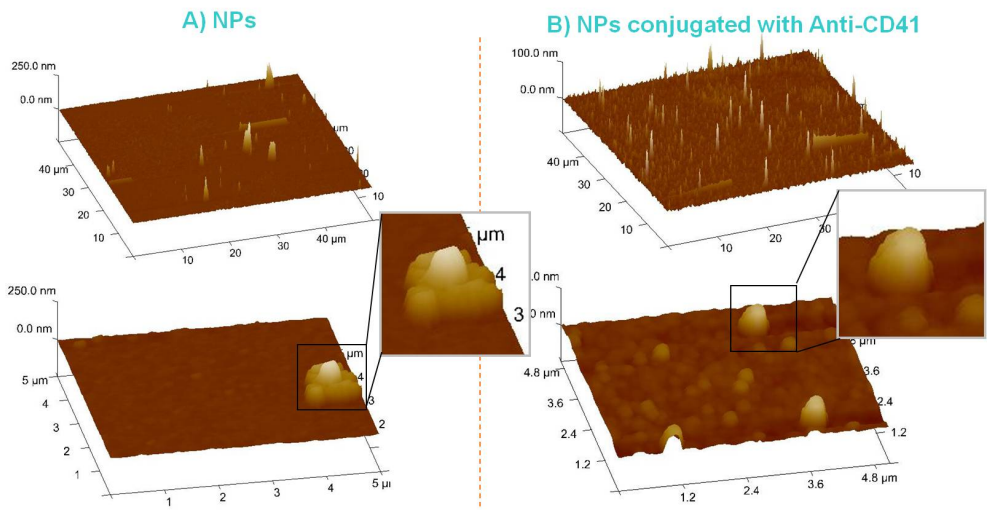

Figure 3.17: AFM image of NPs deposited on a glass surface. A) NIR664 doped NPs unconjugated, B) NIR664 doped NPs conjugated -directly- with antibody anti-CD41 as described in the text. There is less clustering when NPs are conjugated with antibody.

3.3.3 Summary of results

Antibody conjugation on the NP surface has been carried out with two different protocols. Antibody concentration determination by the BCA method shows the presence of the antibody on the NP surface. Tests with AFM show the decrease in NPs clustering behavior when the antibody is present.

In order to check if covalent conjugation has been achieved, experiments involving the antigen have to be done. In section 4.3.2 will be presented the fluorescence data obtained when targeting platelets with NPs.

Chapter 4

Development of a 2D platelet assay platform

4.1 Introduction

This chapter describes the experiments involving:

- platelets immobilization protocols
- nanoparticle compatibility with blood platelets
- nanoparticle labelling of human platelets.

4.2 Platelet immobilization protocols

To analyze single platelets with techniques like confocal microscopy or atomic force microscopy, platelets have to be immobilized on a surface. A key issue is to immobilize and fix the platelets without changing their original condition. This is indeed a major issue when the analysis is done for diagnostic purposes.
Two protocols have been investigated for platelet immobilization. The first one involves incubation of PRP on a glass slide; the second one uses whole blood on glass that has been printed with a fibrinogen pattern.

4.2.1 Immobilization on glass

The reason why a protocol to immobilize platelets on glass has been developed is to have a fast and easy technique to prepare the blood sample. The only instrument used is a centrifuge, which is an instrument easy to find in any laboratory. The immobilization of platelets on glass is based simply on the platelets affinity to a glass surface: if platelets are left on a glass surface for a time, they will start to spread and to attach to it.

Blood is obtained and processed as described in section 2.3. After PRP extraction, the platelets are concentrated in a smaller volume, in which platelets can cluster together. To avoid this happening, the plasma has to be diluted straight after the centrifugation process. The platelet concentration of a normal healthy donor gives a concentration of $\approx 150 \times 10^3$ platelets per mL. Diluting the plasma 1:3 in HEPES buffer gives a concentration of $\approx 50 \times 10^3$ platelets per mL, which is low enough to avoid clustering, as established by our partners in Royal College of Surgeons Ireland (RCSI). Diluted PRP is placed on a glass coverslip in incubation at room temperature and static conditions. From figure 4.1a and 4.1b it can be seen that an incubation time of 5 or 10 minutes is not enough to have a significant number of platelets on the glass. In figure 4.1c and 4.1d, representing incubation times of 40 and 60 minutes respectively, the platelets spread and attach on the surface; moreover the glass coverage is significantly higher than for shorter incubation times. With a 60 minute time, a high coverage of the surface is achieved and the platelets are all connected to each other and/or clustered together. For this reason an incubation time of ≈ 40 minutes was chosen as the optimal time to obtain good glass coverage and few clusters. After the incubation, the coverslip is washed three times with HEPES buffer and fixed with glutaraldheyde 1% in water or paraformaldheyde (PFA) 3.7% in buffer for 30 minutes, washed again three times with PBS and then mounted on a glass slide for microscopy analysis.

Variations between different experiments can be explained by the platelet count of a person being different on each day or by the variable amount of plasma versus other blood components. The diet of the donor prior to the blood drawing gives also a source of variability in the platelet properties. Some researchers in DCU experienced that a vegetarian diet enhances the autofluorescence signal (see section 5.2), due to the presence of more carotene. Moreover, samples from dif-

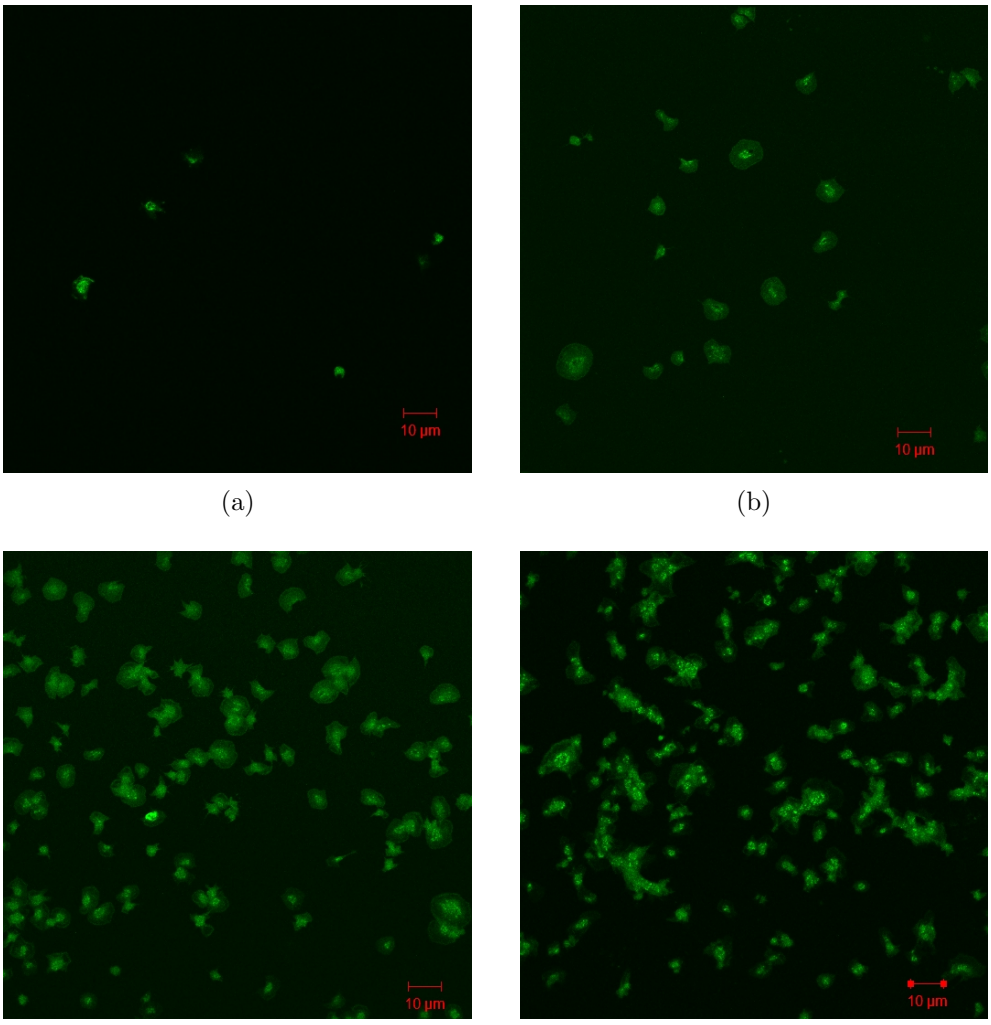

(a) (b)

(c) (d)

Figure 4.1: Platelets from PRP incubated on glass coverslips for a) 5 minutes, b) 10 minutes, c) 40 minutes, and) 60 minutes. The samples are fixed with glutaraldehyde for 30 minutes to enhance platelet autofluorescence and allow, therefore, confocal analysis without any further dye labelling.

ferent donors/ethnic groups/physical conditions can be largely different. Another parameter playing an essential role in the quality of the platelet immobilization is the way in which the blood is handled. Any shear stress to the platelets when pipetting or transferring from vial to vial should be avoided. It is also important the way in which the blood is drawn out from the vein. A larger needle is to be preferred for smaller shear stress, and the blood suction has to be carried out slowly and at constant speed. The use of vacuum vials is therefore to be preferred over manual syringe extraction. Particular care should also be taken in introducing as small an amount as possible of vein tissue in the blood stream: when platelets get in contact with exposed subendothelial components, like collagen, the avalanche activation process starts, as described in section 1.2.1.
In the recent experiments an improvement in the sample quality has been obtained by discarding the vial of blood that has first been drawn. In the vial that is extracted first are in fact present all the materials introduced by the needle puncture (like pieces of skin, molecules of dirt dragged from the skin layer, debris of the vein wall, and so on).

4.2.2 Fibrinogen printing for platelet immobilization

The second platelet immobilization technique is based on the printing of a platelet-specific protein on a glass coverslip. The main feature of this technique is that it allows separation of platelets from whole blood: when whole blood is left in incubation over the printed glass, platelets are specifically captured from the platelet-specific protein and adhesion of platelets only is achieved. Another feature is the possibility to control the confinement of platelets. By using different pattern sizes, single or multiple platelets can be confined per protein spot. Patterns can also be made of spots of different shapes, therefore allowing the analysis of how platelets spread in constrained conditions.

In the early stage of this work, protein patterned surfaces were supplied by our partners in RCSI. More recently we focused on reproducing these surfaces using the protocol described in Langmuir [56], and characterizing the printing quality using AFM, in order to improve and optimize the quality of the patterns.

The first step consists of the fabrication of the stamps. Stamps are made by pouring PDMS (polydimethylsiloxane) and a curing agent into a patterned

silicon master. PDMS is treated until complete curing occurs and solid stamps are extracted from the master. The stamps so obtained are elastic transparent cubes with less than 1 cm^3 of volume.

Before being used for fibrinogen printing, the PDMS cubes are oxidized by exposure to UV light for 15 minutes. In this way the stamp surface become hydrophilic, ensuring a homogeneous spreading of the protein. The platelet-specific protein used is fibrinogen diluted at 200 μg/mL in PBS and gently sonicated. Fibrinogen solution was freshly prepared on the day of printing. A drop of fibrinogen solution is then left incubating on the stamp for 15 minutes or more and, after that, stamps are gently rinsed with water and dried under nitrogen flux.

The stamp is placed upside down on a coverslip and left there for 10 minutes to print the fibrinogen on the glass. Also, the coverslip is previously activated under UV light for about 30 minutes.

The same stamp can be re-used to create successive prints, with a shorter time of fibrinogen incubation. To block the uncovered regions of the glass surface, the printed coverslips are left in a petri dish containing 10 mg/mL of albumin from bovine serum (BSA) solution until sample analysis.

When the pattern needs to be marked fluorescently, the printing solution is prepared by adding BSA fluorescein conjugated to the fibrinogen solution. The concentration of BSA used is 25 μg/mL. The printing process is then carried out minimizing the light exposure. The pattern is labelled in green using the fluorescent protein (see the spectra for fluorescein in figure 4.2) and can be visualized upon excitation with a 488 nm laser light beam.

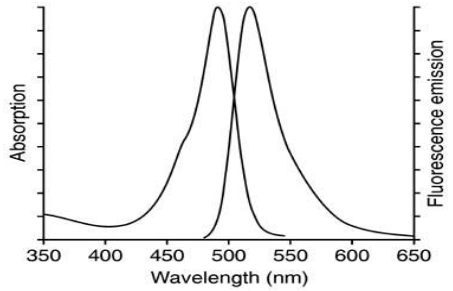

Figure 4.2: Normalized absorption and emission spectra for fhe BSA fluorescein conjugated dye.

Characterization of the fibrinogen pattern

The first attempts at protein printing had produced a patchy pattern or no pattern.
After several trails it was found that the main key for good printing is the way in which the stamp is handled. Great care has to be used when placing the stamp on the glass, moving it in the direction of the line normal to the glass surface and exerting a pressure just enough to make all the PDMS cube adhere to the glass. An extra pressure can push the pillars of the stamp in a way in which the fibrinogen contained in the inner-spaces of the pillars drop out. Extra care has also to be used when removing the stamp from the glass: the cube has to be gently peeled from the glass. A further improvement in the quality of the pattern was also achieved using fibrinogen solutions that had been slightly sonicated before deposition it on the PDMS stamp.

The printed pattern was not always produced successfully even when taking account of all these tips. Sometimes on the glass there could still be some areas with no pattern, with partial patterning, or with different fibrinogen concentrations. A good practice is, therefore, to always prepare multiple samples.

The printing quality was assessed with fluorescence microscopy and AFM. Fluorescence microscopy allowed to check the whole appearance of the pattern and AFM was used to investigate the height of the deposited fibrinogen layer and the uniformity of the protein within single spots.

For fluorescence imaging the pattern was composed of fibrinogen mixed with BSA conjugated to fluorescein (as described in the previous section). In figure 4.3 an example is shown of a typical printed surface, mostly homogeneous but with some small defects in some spots.

The most difficult shapes to reproduce were the 2 μm sized spots, which often were not present, partially or even totally. Nevertheless after a long practice it was possible to obtain good quality 2 μm sized patterns, like those shown in figure 4.4.

The fibrinogen could be printed in different shapes, circles, squares and teardrops. In figure 4.5 is shown the printing from a stamp containing all the three shapes in different dimensions.

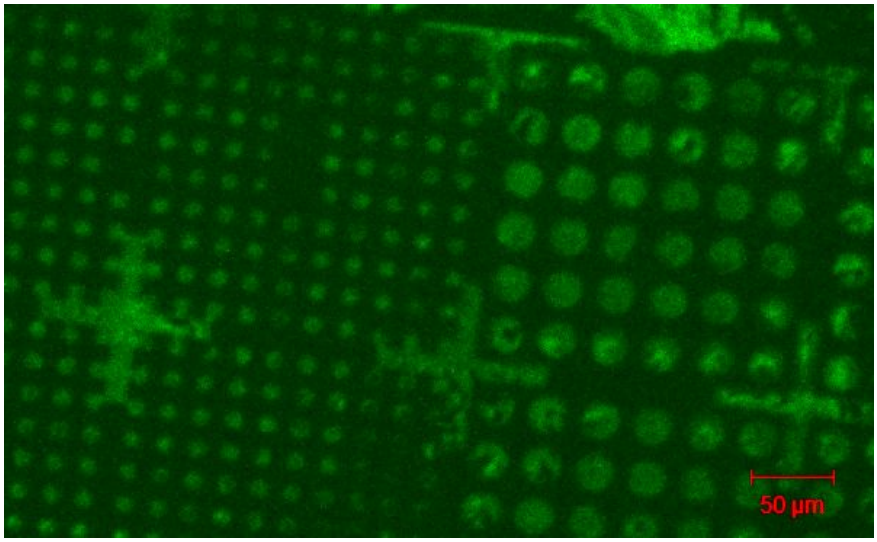

Figure 4.3: Fluorescence image of a printed pattern of fibrinogen. 6 μm and 12 μm circular spots are visible together with the crosses used for reference. The printing is homogeneous but with some defects. The image is obtained using a 10X object in air and completely opening the pinhole aperture of the confocal microscope.

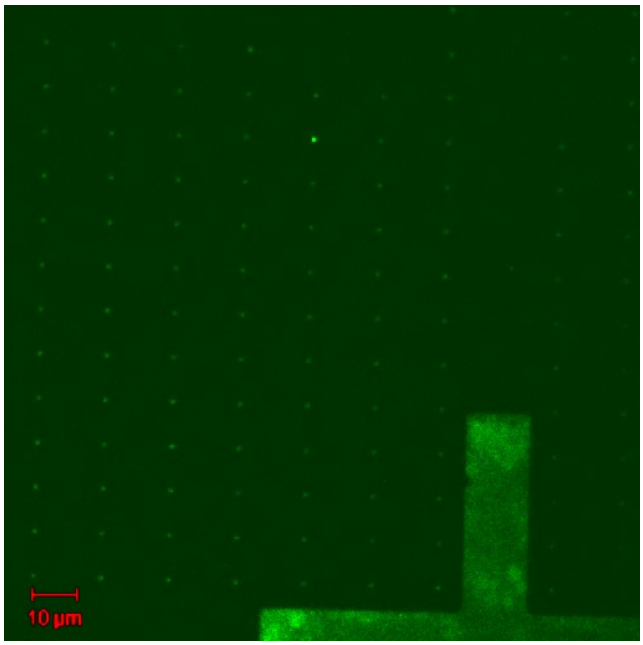

Figure 4.4: Confocal image of 2 μm fibrinogen spots. The image is obtained with a 60X oil immersion objective lens and pinhole aperture of 1 Airy unit.

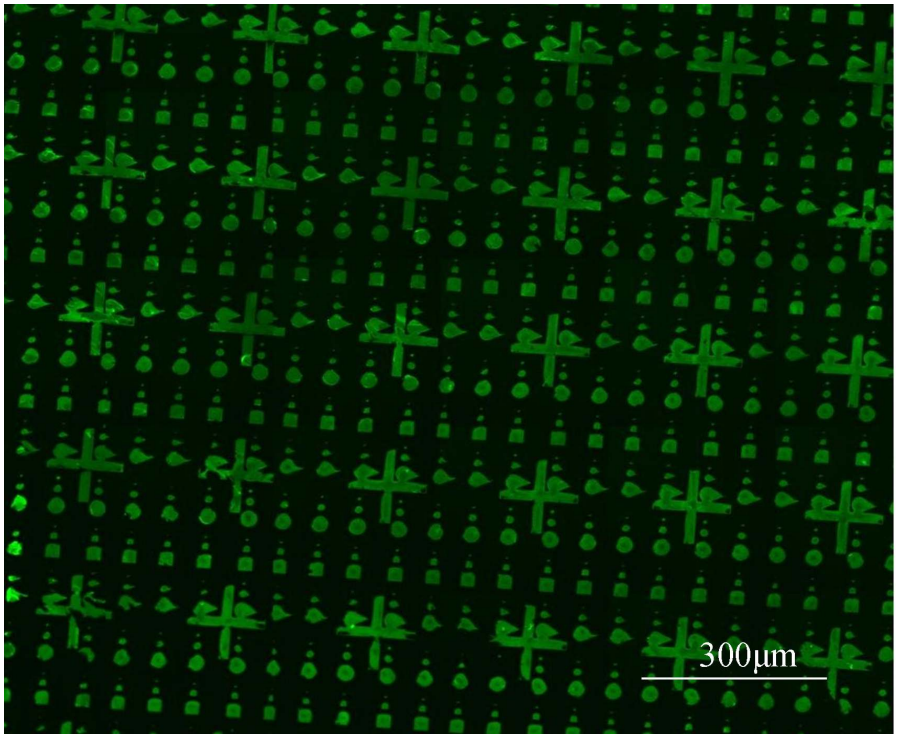

Figure 4.5: Confocal image of mixed shaped fibrinogen printed spots. The image is obtained with a 60X oil immersion objective lens and pinhole aperture of 1 Airy unit.

To investigate the nano-scale quality of the pattern, fibrinogen-printed coverslips are imaged with atomic force microscopy. AFM is a very powerful tool for high-resolution surface mapping. For our purposes it is a key component in the analysis of the homogeneity of the fibrinogen and the estimation of the number of layers deposited.

The imaging is carried out directly on the printed coverslip without any prior surface treatment and imaged in PBS to maintain the proteins in their natural state. The tip used is a silicon nitride probe specific for fluid tapping mode imaging, with resonance frequency of 65 kHz and force constant 0.35 N/m. The tip is never driven at a speed higher than 15 μm/s to achieve a high resolution and to preserve the integrity of the sample.

Figure 4.6 displays the 2-D and the three dimensional surface plots of a printed

pattern of nominal 6 μm circular spots. It can be seen that the printed areas are

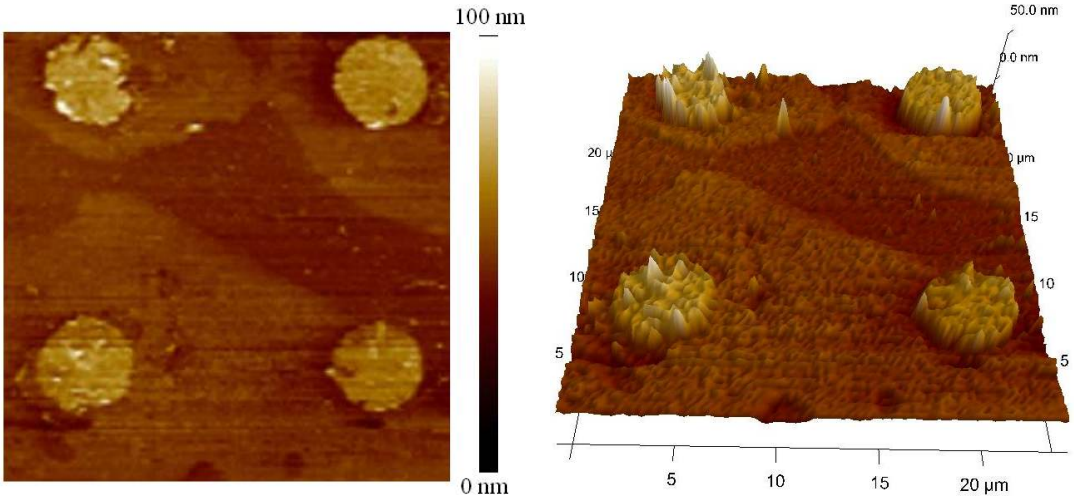

(a) (b)

Figure 4.6: a) AFM image of four 6 μm circular spots of fibrinogen and b) its 3D projection. The image was performed in tapping mode in liquid with tip speed of 10 μm/s.

actually circles regular in periodicity, with no fibrinogen printed outside of the pattern. A close up of a single spot performed at very low tip speed enables to view the profile of the deposited fibrinogen layer. The example in figure 4.7 shows a nominal 6 μm diameter spot. From the analysis of its height profile it can be seen that the actual diameter is around 5.5 μm, and the average height is around 2.5 μm. This corresponds to several layers of deposited fibrinogen, in fact the mean height of the fibrinogen molecules is 3.4 nm and the mean length is 65.8 nm [57].

The height of the fibrinogen layer deposited can vary according to the concentration of fibrinogen solution used for printing, the pressure exerted on the stamp and in general from the way in which the person performs the printing. The lowest height of deposited fibrinogen being imaged is 8 nm, which corresponds to a couple of layers of molecules.

The fibrinogen-printed surfaces so created are used for platelet immobilization. Whole blood is incubated on the coverslip for 30 minutes in rocking condition and then washed with HEPES.
A preliminary analysis of the capture efficiency can be performed using confocal

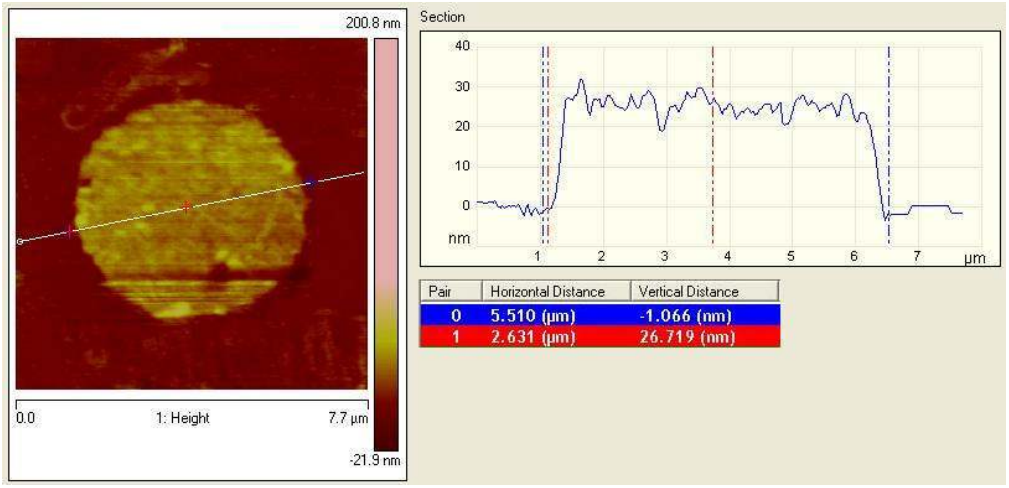

Figure 4.7: AFM image of a single 6 μm circular stamp and its height profile along a line. The image was performed in tapping mode in liquid with tip speed of 1.5 μm/s.

microscopy. The backscattered light signal enables imaging of the fibrinogen pattern. In figure 4.8 is shown a confocal image of a sample of platelets (fixed with a solution of 1% (w/v) glutaraldehyde in water) deposited on a fibrinogen printed glass slide with pattern of squares, circles and tear drops of different sizes. The printing is not neat, showing some protein deposited outside of the pattern. This was due to an excessive pressure exerted during the stamp printing. Platelet capture can be monitored by looking at the autofluorescence which was enhanced by the fixative.
Here it can be seen that platelets specifically bind to the fibrinogen pattern which provides the spatial control of cell deposition required for diagnostic purposes.

Other examples of platelets captured on fibrinogen patterns will be shown in section 5.4.

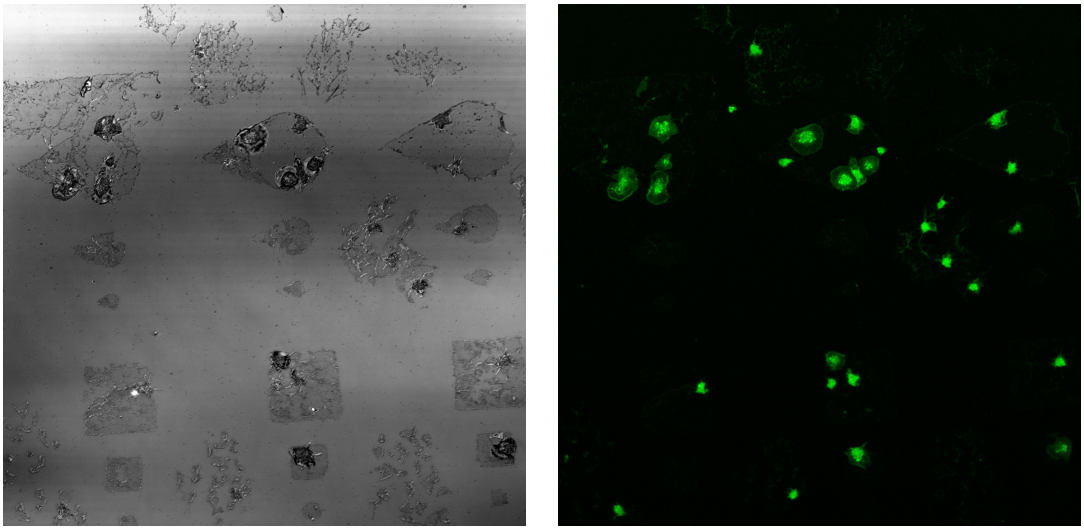

(a) (b)

Figure 4.8: WB incubated over a micro-patterned fibrinogen pattern, washed and then fixed with glutaraldehyde 1% (w/v). a) Backscattering image of the coverslip, clearly displaying in dark grey the fibrinogen pattern. b) Confocal fluorescence image showing the platelets autofluorescence enhanced by the fixation. Platelets are specifically captured by the fibrinogen and adhere to the pattern. Images obtained with a 488 nm argon laser line.

4.2.3 Summary of results

Two different protocols have been successfully optimized for platelet immobilization.
Immobilization on glass is preferred when a simple way of sample preparation is needed. Fibrinogen-patterned surfaces are chosen whenever it is required to immobilize platelets in a known shape and in a reproducible manner. AFM and confocal imaging of fluorescence or autofluorescence signals are efficient tools to characterize the surfaces.

4.3 Nanoparticles-platelet interaction

4.3.1 Compatibility of NPs with platelets

One fundamental point in developing an assay for diagnostic purposes is that the materials and methods employed do not interfere with the analyte to be measured, monitored or labelled.
In this project, NPs are to be used to quantify the number of activated platelets present in a sample of fresh blood. If the percentage is over a certain threshold, the patient is considered to be in risk for heart attack or stroke, as explained in section 1.2, and a specific medical treatment has to take place. To have a correct diagnosis it is therefore essential that NPs do not induce any aggregation or alter the functionality of the platelets.
Two tests have been performed to assure the NPs' biocompatibility with platelets: aggregometry test and flow cytometry analysis.

Platelet aggregometry test

An aggregometry test is performed in order to see if platelet aggregation kinetics are influenced by the presence of NPs. The instrument used was an aggregometer that measures the transmitted light of a platelet rich plasma (PRP) sample during platelet aggregation, as explained in section 2.1.4.

The experiment is performed as follows: whole blood, PRP, and platelet-poor-plasma (PPP) are obtained, as described in section 2.3. In aggregometry analysis the vials containing fresh blood must first stand for 30 minutes after collection. In this time the platelets regain their responsiveness. Blood samples must then be tested within 3 hours of collection to avoid deterioration of plasma and platelet procoagulants [48]. PPP is inserted in the aggregometer as a reference sample.

Before adding NPs to the PRP samples, a check is made to see how platelets aggregate and how much of the activator has to be used to obtain a standard aggregation profile. The activator used is adenosine diphosphate (ADP), which induced platelet aggregation (for further details see section 1.2.1).
From figure 4.9a it can be seen that when no agonist is added, the percentage of aggregation remains stable at 0%. A concentration of 6.5 μl = 5 μM of ADP gives

a normal aggregation curve. A concentration of 13 μl = 10 μM of ADP could result in clots, like in the curve recorded. Attention has to be paid to the agonist addition time: if the sample is left for too long in the measuring well, it can get damaged by the high speed of stirring. This can induce some shape change in the platelets that would alter the aggregometry test. Good practice is to add the agonist within the first 1-2 minutes after the measurement had been started.

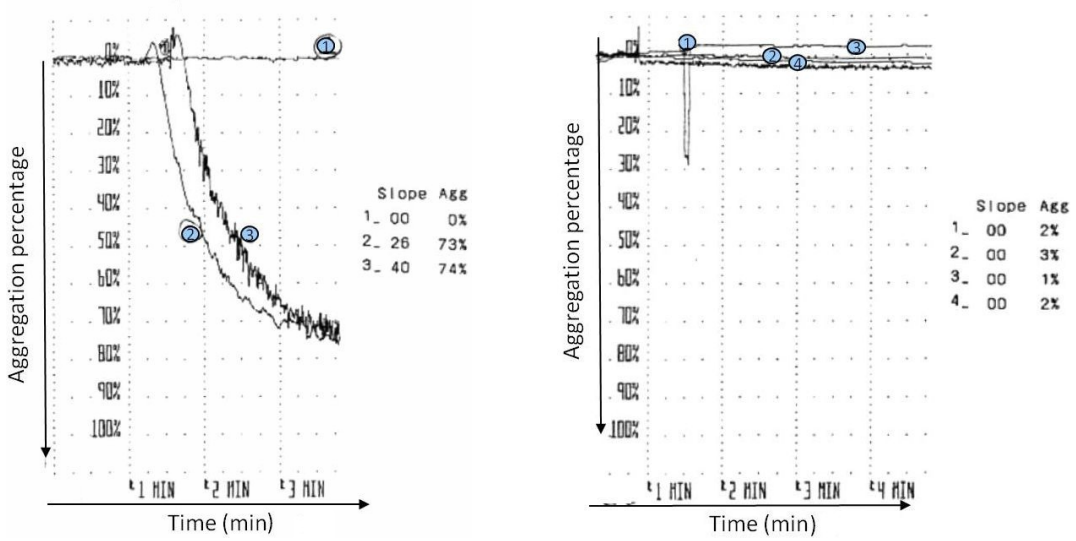

(a) (b)

Figure 4.9: a) Aggregometry profile of 250 μl of PRP with different amounts of agonist (ADP). Channel 1, no agonist added; channel 2, 5 μM; channel 3, 10 μM. b) Aggregometry profile of 250 μl of PRP with different samples added. Channel 1, 20 μl of ethanol; channel 2, 20 μl of NIR664 doped NPs in ethanol; channel 3, 20 μl of undoped NPs in ethanol synthesized in microemulsion; channel 4, 20 μl of undoped NPs in ethanol synthesized by the Stöber method. To each of the channels 5 μM of ADP is added following channel numerical order.

If the NPs are dispersed in ethanol, the aggregation of platelets cannot take place, as shown in figure 4.9b. The NPs have to be dissolved either in water, PBS, or HEPES buffer.

To see if NPs influence the platelet aggregation profile, four samples with different concentrations of NPs dissolved in water were prepared. From figure 4.10 it can be seen that the general aggregation trend is similar for all the samples inde-

pendent of NP concentration. Channel 2, with the lower amount of NPs, presents

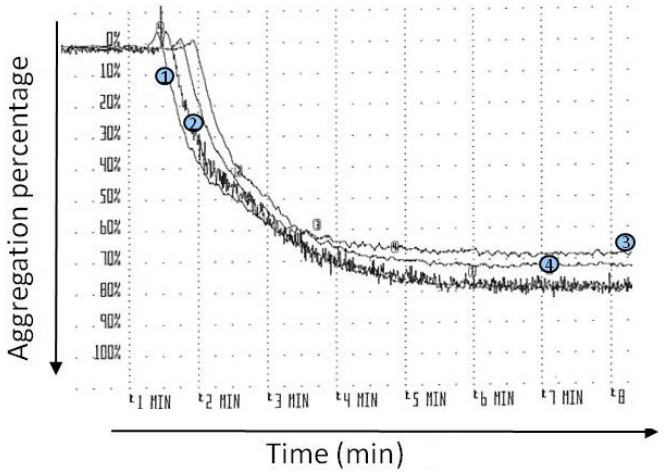

Figure 4.10: Aggregometry profile of 250 μl of PRP with added:(channel 1) 20 μl of PPP and 0 μl of NPs , (channel 2) 15 μl of PPP and 5 μl = 85 nM of NPs, (channel 3) 10 μl of PPP and 10 μl = 170 nM of NPs, (channel 4) 0 μl of PPP and 20 μl = 340 nM of NPs. After 1 minute to each of the channels, following the channel numerical order, it is added 6.5 μl = 5 μM of ADP.

a different behavior probably due to some damage induced by the stirring (since it had the same noisy profile even before the aggregation had started), but shows a similar aggregation trend as channel 1, where there are no NPs mixed with the PRP. Channel 3 and 4, with 170 nM and 340 nM respectively of NPs, have a final aggregation of 68% and of 72%, that differs from the aggregation reached by the reference sample (=79%). This variance is not significant, since a difference greater than $\approx$15% in the aggregation is considered to indicate an abnormal aggregation.

The data obtained from the aggregometry test shows the biocompatibilty of the silica NPs NIR664-doped with the platelets: the NPs do not alter the platelet aggregation properties.

Flow cytometry analysis

Flow cytometry, described in section 2.1.5, can be used to record the fluorescence arising from platelet activation products. With flow cytometry it can be shown whether or not the addition of NPs to platelet rich plasma (PRP), or to whole blood (WB), affects the activation of platelets.

In this flow cytometry experiment platelet activation status is monitored by looking at the conformational status of the platelet receptor αIIbβ3, and by detecting the presence of P-selectin expressed on the platelet surface. These two markers are a peculiarity of activated platelets only, as described in section 1.2.1. To target the open conformation of αIIbβ3, PAC-1 antibody, which binds to the fibrinogen binding site of the αIIbβ3 complex is used. To target the P-selectin exposed on the platelet surface an antibody towards P-selectin was used. When these two antibodies are conjugated with two different dyes they can be used to fluorescently label activated platelets. Choosing two dyes with overlapping excitation spectra but different emission regions allows the sample to be excited by a unique wavelength and permits the detection of the two different antibodies in two separate channels.

The dyes chosen for the experiment are fluorescein FITC and R-phycoerythrin (PE). The former has an absorption maximum at 495 nm, and the latter at 488 nm. Both dyes can be efficiently excited with an argon laser (excitation wavelength 488 nm). The emission of the two dyes can be easily separated using optical filters, since FITC has an emission maximum at 518 nm in the green region of the visible spectrum, and the PE emission is in the yellow/orange part, with emission peak at 578 nm.
PAC-1 antibody is conjugated with FITC, and anti-P-selectin is conjugated with PE.

The unique feature of flow cytometry is the ability of measuring the fluorescence per single cell (or particle). This contrasts with spectrophotometry in which the percent absorption and transmission of specific wavelengths of light is measured for the bulk volume of the sample.

The flow cytometry experiment of the data reported in table 4.1 was performed as follows: the whole blood (WB) and PRP obtained as detailed in section 2.3, are

divided into several vials, each of them of 250 μl to which a 20 μl volume of NPs is added. The samples are left in incubation for 30 minutes in different conditions: at room temperature in static conditions or on a rocking table, or at 37° C in static conditions. WB or PRP samples with no added NPs are prepared and incubated similarly, adding 20 μl of PBS to match the volumes. Meanwhile, the flow cytometry tubes are prepared with the antibodies towards platelet activation products, anti-P-selectin-PE and PAC-1-FITC, diluted in HEPES buffer. Some additional tubes are prepared as control samples with IgG, an antibody not conjugated to any dye.
When the NP incubation is finished, a volume is transferred from the incubation vials to the tubes containing the antibodies. The platelet activator TRAP (thrombin receptor-activated peptide) is then added at exact time intervals to the part of the samples where activation is induced. To the remaining tubes it is added HEPES buffer. After exactly 10 minutes the reaction of the activator is stopped by dilution with a large volume of HEPES buffer. The samples are then inserted in the flow cytometer one at a time, starting with the control sample.

The control samples, composed of WB or PRP with non-fluorescent IgG, are the negative control. These control samples are used to locate the platelet events in the histogram of Side Scatter (SS) intensity versus Forward Scatter (FS) intensity as depicted in figure 4.11. This can be done since the average size and granularity of the platelets are well known values.

The control sample is also used to set a threshold to cut out noise events. Since the negative sample has no fluorescence signal, all the collected fluorescence events are noise.
The fluorescence signals collected on each PMT are plotted in a one-parameter histogram. These histograms display the number of counts versus fluorescence intensity.
The samples are then processed and for each of the fluorescence channels it is recorded the percentage of platelet fluorescence events and the mean fluorescence intensity of these events. On the first fluorescence channel it is recorded the fluorescence from PAC-1-FITC, and on the second the fluorescence arising from anti-P-selectin-PE. The data are summarized in table 4.1.

			Flow cytometry values for distinctive activation products of platelets			
Incubation	**Activator**	**Sample**	**PAC-1 percentage of events**	**PAC-1 mean fluorescence of events**	**P-selectin percentage of events**	**P-selectin mean fluorescence of events**
Room temperature static conditions	none	PRP	0.30	1.06	3.01	1.00
		PRP + NPs	0.40	1.07	3.04	1.00
	TRAP	PRP	69.33	8.74	73.70	6.38
		PRP + NPs	69.27	8.58	72.46	6.10
37°C static	none	PRP	0.82	1.03	3.12	1.00
		PRP + NPs	0.59	1.02	3.33	1.00
	TRAP	PRP	69.81	5.19	72.19	4.55
		PRP + NPs	70.67	5.35	74.12	5.09
Room temperature static conditions	none	WB	0.42	1.13	1.63	1.00
		WB + NPs	0.87	1.15	2.29	1.00
	TRAP	WB	65.12	7.70	68.32	5.42
		WB + NPs	64.52	7.50	70.48	5.88
37°C static	none	WB	0.28	1.09	1.02	1.00
		WB + NPs	0.64	1.09	1.51	1.00
	TRAP	WB	31.41	3.25	49.84	2.49
		WB + NPs	32.67	3.28	50.28	2.55
Room temperature rocking table	none	WB	0.55	1.13	2.26	1.00
		WB + NPs	0.73	1.19	2.37	1.00
	TRAP	WB	29.87	3.40	54.60	3.72
		WB + NPs	49.98	5.88	70.26	7.10

Table 4.1: Table summarizing the flow cytometry data of distinctive activation products of platelets, obtained using PRP or WB with or without the presence of NIR664 doped NPs. The values obtained when NPs are present are close to the one obtained when NPs are absent for all the incubation conditions, meaning a insignificant influence of the NPs on the platelets. In the text the description of the experiment can be found.

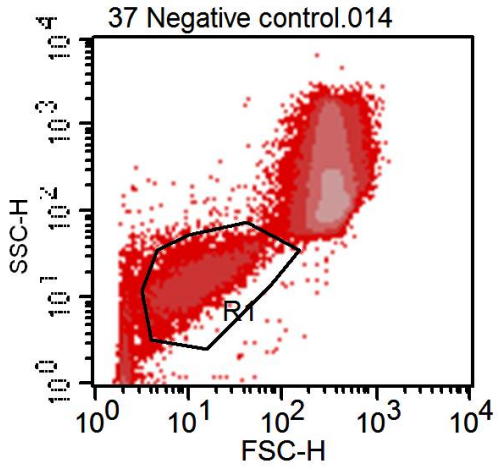

Figure 4.11: Histogram of SS versus FS for the control sample of WB incubated at 37°C in static conditions. The area outlined in R1 is where platelet events are located. The perimeter of R1 is a pre-known data which is reloaded for each of the flow cytometry experiments. It is drawn knowing the scattering properties of the platelets (size, granularity,..). No NPs are present in the control sample to not influence the settings for the experiment.

The percentage of fluorescence events originating from PAC-1 and anti-P-selectin is related to the degree of platelet activation of the sample.
From the results it can be seen that the percentages of PAC-1 and anti-P-selectin events are not significantly modified by the presence of NPs. In fact, the data obtained for samples of only PRP are similar to the data for PRP with added NPs. For incubation at room temperature in static conditions it can be seen that NP presence in PRP gives a percentage of PAC events of just 0.40% and 3% of P-selectin. These values are insignificant compared to the values obtained when activation is induced on PRP for the same incubation condition, which are 69% for PAC and 74% for P-selectin. Moreover, the values obtained for samples with NPs when the activator TRAP is present are close to those obtained in the absence of NPs and with TRAP. This is valid in all the investigated conditions. For whole blood samples the data do not suggest any change in platelet behaviour when NPs are present, except for the incubation on the rocking table, where the percentage of PAC and P-selectin events are significantly increased by the presence of NPs. This can perhaps be due to shear forces exerted by the NPs during the dynamic

incubation rather than from the NPs presence. In fact for incubation in static conditions this enhancement is not observed. From these data it can be deduced that NPs do not induce a change in platelet functionality.

4.3.2 Labelling of platelets by NPs

In this section the results obtained from labelling platelets using NIR664 doped silica NPs synthesized, as described in section 3.2 are shown.

The surface on which the platelets are immobilized consists of fibrinogen deposited on a glass slide in a micro-pattern. Platelets are captured on the micro-patterned fibrinogen, a platelet-specific protein, and, therefore, confined on specific areas. In the early stage of this work these surfaces have been provided by Royal College of Surgeons in Ireland from Miss Lopez-Alonso and Dr. Basabe-Desmonts, and later on prepared "in-house" according to the protocol developed by Basabe-Desmonts and others [56]. The fibrinogen printing technique and the characterization of the patterned surfaces is described in section 4.2.2.

The protocol for labelling platelets with NPs is divided in 4 steps. First, platelets are immobilized on the fibrinogen patterned glass. Second, platelets are incubated with NPs conjugated to anti-CD41 to test NP labelling efficiency. Third, as a reference platelets are incubated with an antibody towards the surface platelet receptor GPIX. Fourth, glass slides are examined under confocal microscopy to validate the labelling.
Anti-CD41 is an antibody specific for platelets that bind to all the conformational forms of the integrin αIIbβ3. NPs are conjugated to anti-CD41 as described in section 3.3. Anti-GPIX is used as a reference to fluorescently mark and locate the platelets. The GPIX antibody employed is conjugated with the fluorophore fluorescein (FITC).

The fibrinogen pattern is printed on a microscope coverslip, which is kept in a petri dish submersed in PBS until it is used. Fresh blood is obtained, as described in section 2.3. A volume of whole blood is added to the coverslip and the petri dish is placed on a rocking table. After 30 minutes of incubation, the coverslip is washed three times with HEPES, and then a solution of NIR664 doped NPs conjugated with anti-CD41 is added. NPs are left in incubation on the coverslip, on a rocking table, for 30-60 minutes, and then the glass is washed 3 times with HEPES buffer. A further 30 minutes incubation on a rocking table takes place for

a solution of anti-GPIX-FITC, followed by 3 washes with HEPES buffer. To fix the glass slide, a solution of paraformaldehyde 3.7% (w/v) in water is added to the sample for 15-60 minutes, and then washed away with PBS or HEPES buffer. The sample so obtained can be kept for few days in darkness in a petri dish immersed in PBS, or glued on a glass slide with a mounting medium, until confocal analysis takes place.

Samples prepared in this way are investigated through confocal microscopy (principles explained in 2.1.1), using a Zeiss LSM 510 Meta laser module confocal microscope with an excitation wavelength of 488 nm of an argon ion laser and of 633 nm of an helium-neon laser, and a 63X magnification oil objective (N.A.=1.4). The 488 nm laser light is used to excite the fluorophore FITC, which has an absorption maximum at 495 nm. Its fluorescence signal is collected through reflection from a dichroic beam splitter (545 nm) and the transmission of a band pass filter 505-575 nm. NIR664 NPs are excited with the 633 nm laser light, and the fluorescence separated through the transmission of a dichroic beam splitter (545 nm) followed by a low pass filter 650 nm placed in front of the second PMT. In this way it is possible to record the x-y fluorescence data obtained with two different excitation sources and relative to two different labels, the membrane label FITC conjugated anti-GPIX antibody in the green part of the spectrum and the NPs, in the near infra-red part of the spectrum.

In figure 4.12 confocal images from a sample labelled with anti-GPIX-FITC and with NIR664 NPs-anti-CD41 (direct conjugation method) are shown. The platelets are confined in fibrinogen patterned spots and are visible due to the FITC-antibodies which stain the membrane of platelets. From the fluorescence signal arising from NPs, it can be seen that NPs do not label the platelet membrane in the same way as anti-GPIX is doing. NPs are collecting into clusters located on platelet membranes. Unfortunately, it is impossible to quantify the number of NPs on the platelet surface, because the minimal resolution relates to the focal volume. For our system the lateral resolution is $\approx$ 300 nm. This means that a single "signal" pixel can contain more than one NP.
Control samples have been prepared following the same protocol but using NPs that are not conjugated with any antibody. In figure 4.13 the image obtained from fluorescence light between 505 and 545 nm, which corresponds to the signal from

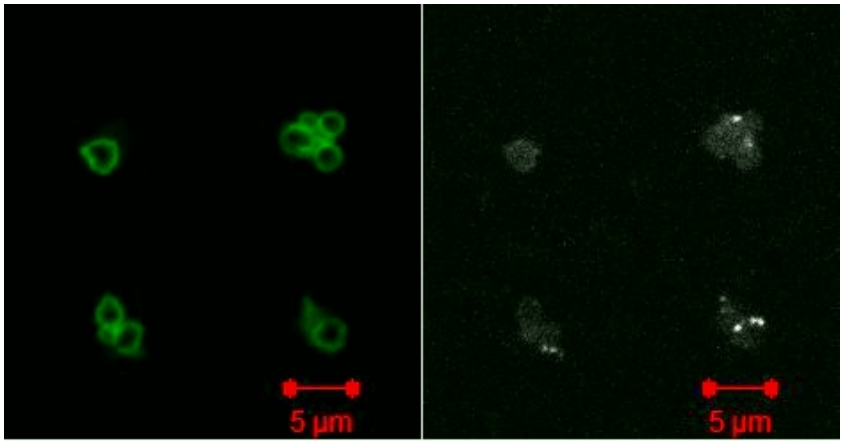

Figure 4.12: Confocal images of platelets from WB labelled with anti-GPIX-FITC (green emission) and with NPs (NIR emission) conjugated to anti-CD41 captured on a micro-printed fibrinogen pattern. The left panel shows the green fluorescence, the right one the NIR fluorescence. Average of 4 scans; λ_{exc} = 488 nm and 633 nm; pixel time 6.40 μs; pinhole diameter of 1 Airy unit.

anti-GPIX-FITC is shown, on the left and, on the right, the image obtained from the fluorescence collected in the near infra-red part of the spectrum is shown. Since in this case NPs are not supposed to attach to the platelet surface and should get removed during the washing, the collected signal of the near infrared light should be dominated by noise. This actually does not happen and the signal from the NPs is greater than the noise. Some clusters of NPs are still present even when NPs have no antibody on their surface. NPs clusters are located especially in the inner spaces between the platelets and in a few spots outside the platelets, showing some non-specific attachment. Comparing the control results with the NPs-anti-CD41 labelled samples it can be seen that the degree of NPs specificity to target human platelets is not enhanced by the direct conjugation of platelets specific antibody on the NPs. A visual comparison of the two cases is presented in figure 4.14.

The next experiments were done using NIR664 NPs conjugated to the antibody through the cross-linker EDC, as described in section 3.3. When NPs-anti-CD41 are incubated with the platelets (see figure 4.15), NPs still collect in clusters, as happened in the previous experiment. The percentage of clusters per platelet is slightly higher when using the crosslinker compared to when using the direct con-

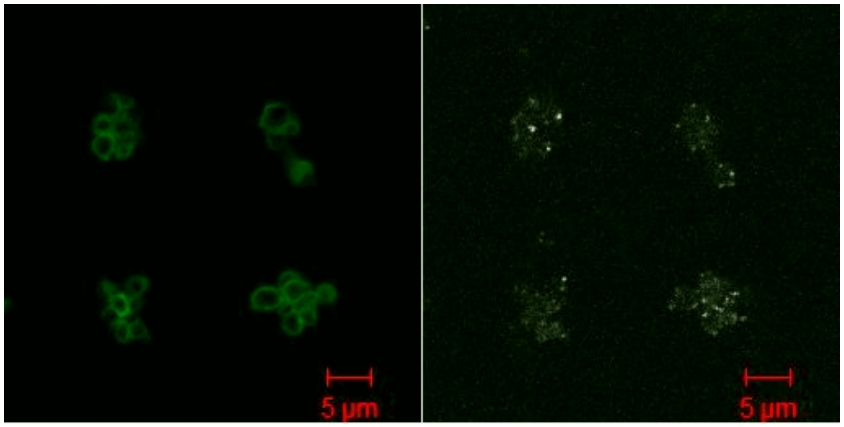

Figure 4.13: Control sample. Confocal images of platelets from WB labelled with anti-GPIX-FITC (green emission) and with NPs (NIR emission) not conjugated with any platelet-specific antibody captured on a micro-printed fibrinogen pattern. The left panel shows the green fluorescence, the right one the NIR fluorescence. Average of 4 scans; $\lambda_{exc} = 488$ nm and 633 nm; pixel time 6.40 μs; pinhole diameter of 1 Airy unit

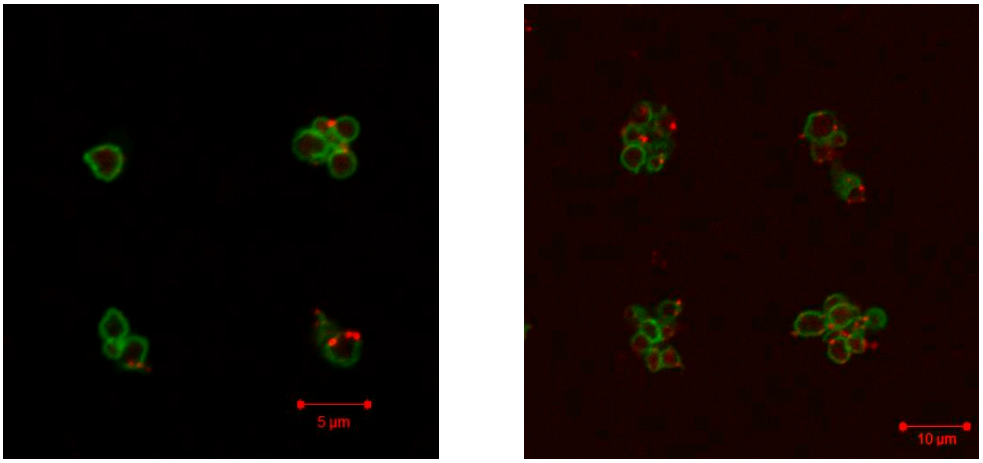

(a) (b)

Figure 4.14: RGB compositions of a) images displayed in figure 4.12 relative to the labelling from NPs-anti-CD41, and of b) images displayed in figure 4.13 relative to the control samples. No significant difference can be seen. Green channel: fluorescence from platelet membranes stained with FITC; red channel: fluorescence from NIR664 NPs.

jugation technique (≈ 3% more), but still not satisfactory enough for the aim of the project. The control sample, in which NPs do not have any antibody conju-

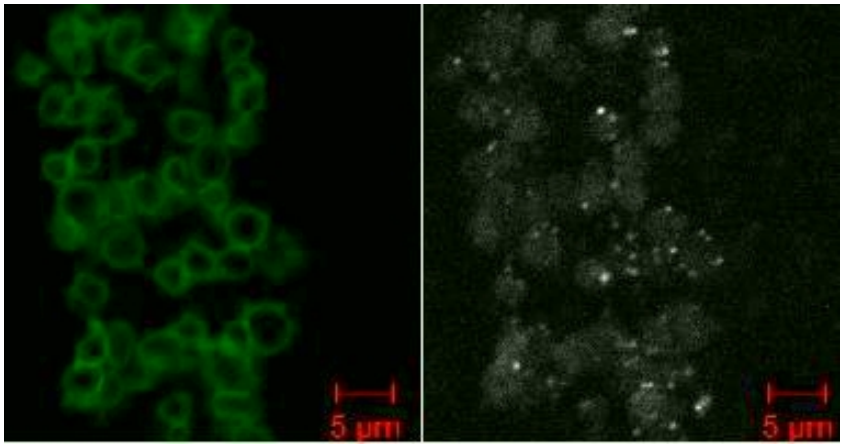

Figure 4.15: Confocal images of platelets from WB labelled with anti-GPIX-FITC (green emission) and with NPs (NIR emission) conjugated to anti-CD41 through the cross-linker EDC, captured on a micro-printed fibrinogen pattern. The left panel shows the green fluorescence, the right one the NIR fluorescence. Average of 4 scans; λ_{exc} = 488 nm and 633 nm; pixel time 6.40 μs; pinhole diameter of 1 Airy unit.

gated, is shown in figure 4.16. In both figures 4.15 and 4.16 the imaged area is a region of the coverslip where the fibrinogen is printed on a wide area. The area is shaped as a cross with arm dimensions of ≈ 40 μm X 15 μm. Since the platelet density is higher in the wider regions, possibility of having unremoved material in the inner spaces between the platelets is higher. The control and the samples can be visually compared in figure 4.17. The percentage of NP signals (coded in red) on the platelets surface is slightly higher for the NPs conjugated with anti-CD41 but still not satisfactory.

The results obtained are still far from the optimal, which is to obtain a uniform NP staining of the whole platelet membrane. The aim is to build up a platform that works as an effective tool to target platelets. No significant labelling of platelets by the antibody conjugated NPs was achieved. The antibody conjugated NPs have a very low specifity on the platelet membrane and they bind to the membranes in a degree similar to what unconjugated NPs do. More studies on the effective

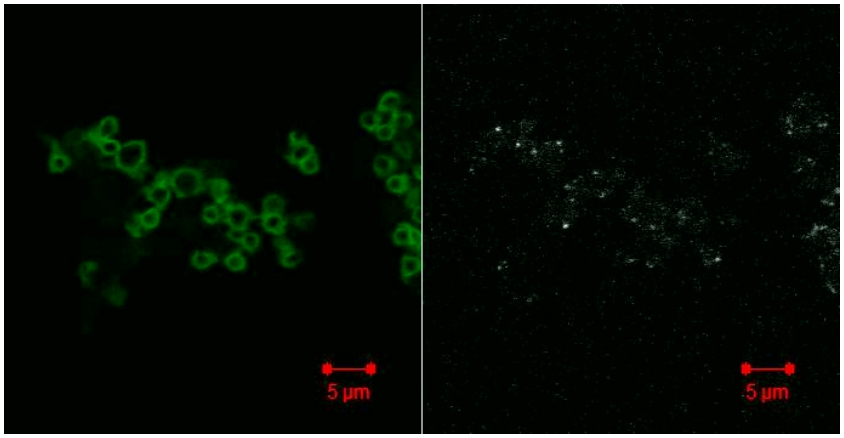

Figure 4.16: Control sample. Confocal images of platelets from WB labelled with anti-GPIX-FITC (green emission) and with NPs (NIR emission) not conjugated with any platelet-specific antibody captured on a micro-printed fibrinogen pattern. The left panel shows the green fluorescence, the right one the NIR fluorescence. Average of 4 scans; $\lambda_{exc} = 488$ nm and 633 nm; pixel time 6.40 μs; pinhole diameter of 1 Airy unit.

conjugation of antibody to NPs are required.
A further analysis of the cell signal also needs to be done. A contribution to the signal arising from the intracellular part of the platelets was found. This contribution is more visible for the images relating to the fluorescence collected through a low pass filter 650 nm (near infra-red channel), where the signal to noise ratio is lower compared to the images for the green wavelengths. Initially it was assumed that this signal could be associated with some degree of NP penetration through the platelets membrane. In later studies a similar background signal has been found also on samples prepared using whole blood or PRP without any addition of NPs. The intracellular signal seems therefore arise from platelets themselves. A deeper analysis of the fluorescence signal of unlabelled platelets will be shown in section 5.2.

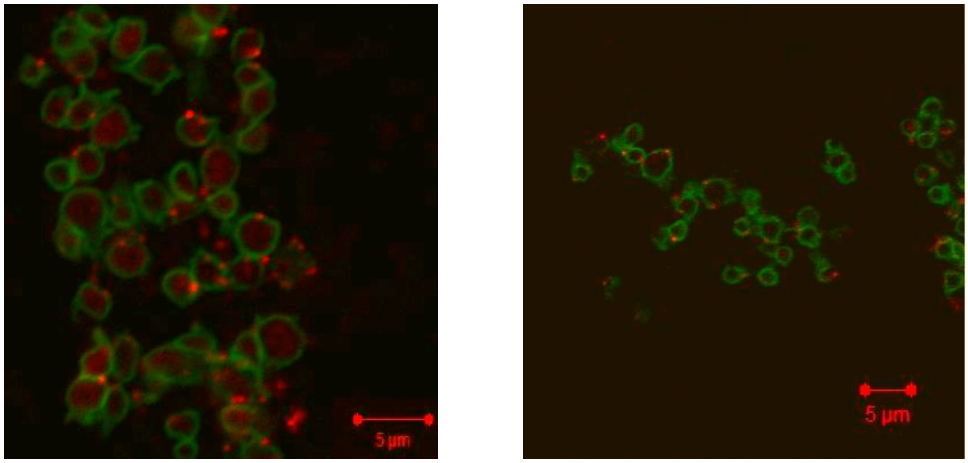

(a) (b)

Figure 4.17: RGB compositions of **a)** images displayed in figure 4.15 relative to the labelling from NPs-anti-CD41 (antibody conjugation through EDC), and of **b)** images displayed in figure 4.16 relative to the control samples. The percentage of NP signals on the platelet surface is slightly higher when NPs are conjugated to anti-CD41 through the crosslinker EDC. Green channel: fluorescence from platelet membranes stained with FITC; red channel: fluorescence from NIR664 NPs.

4.3.3 Specificity of antibody conjugated NPs

When using the NPs to label the platelets, a satisfactory uniform staining of the whole membrane could not be achieved. Moreover, data obtained using NPs conjugated with the antibody through the direct conjugation technique are not largely different from those obtained when using a cross-linker. The degree of labelling achieved suggests that covalent antibody conjugation has not been achieved or only partially achieved.

The BCA assay and the AFM test presented in section 3.3.2 show the presence of the antibody on the NP surface, but do not give any information about the nature of the bond. If the bonding with the antibody is electrostatic, the antibody is only adsorbed on the NP surface. For NPs with adsorbed antibodies the labelling of an external target is not efficient: this bond is not as strong as a covalent one and the NPs can be washed away during the washing steps.

For the two antibody conjugation techniques employed it cannot be excluded that the nature of the bond is electrostatic. The carboxyl groups (COOH) on the antibodies are negatively charged and the O^- is not a good leaving group. The creation of a covalent bond with an amine is very unlikely unless in the presence of a catalyst or of a heat source. In the direct conjugation technique no other chemical is used and no heat source can be employed so as not damage the antibody. In these conditions carboxylic acids can react with amines to form ammonium salts, creating therefore an electrostatic bond.

For the cross-linker conjugation technique an unsuccessful conjugation can occur if the amine-reactive antibodies react with amino groups of the other antibodies or of the NP surface.

AFM was used as a tool to investigate the actual specificity of the antibody conjugated NPs towards the antigen. If the specificity of the antibody conjugated NPs is comparable to the specificity of unconjugated NPs, the nature of the chemical bond achieved cannot be covalent.

In this experiment fibrinogen is used as an antigen and the NPs are conjugated to the antibody towards the fibrinogen. The system is kept simple, not involving any other elements than the antibody NPs and the antigens, therefore free of interaction with third materials. NPs are conjugated to anti-fibrinogen through the crosslinker EDC, as described in section 3.3. Fibrinogen is printed in a pattern on a glass cover slip following the protocol described in section 4.2.2. The fibrinogen

solution is prepared in a concentration of 100 μg/mL and mixed with 25 μg/mL of albumin from bovine serum (BSA) conjugated to the fluorophore fluorescein. By mixing the fibrinogen with a fluorescently labelled protein the pattern produced is fluorescently stained. The concentration of BSA used is low enough to not alter the fibrinogen printing quality, as already assessed by our partners in RCSI. The NPs are undoped to avoid any fluorescence interference with the imaging of the pattern.

Antibody-conjugated NPs are incubated on the fibrinogen surfaces for 30-45 minutes in static conditions and then washed out three times with HEPES buffer. The glass is then imaged using an AFM in a liquid environment, using a silicon nitride probe in tapping mode. An inverted microscope mounted on the AFM stage allows the acquisition of fluorescence images of the sample directly on the AFM platform. The fluorescence arising upon excitation of a mercury lamp with band pass filter of 460 - 495 nm is filtered through a band pass 510 - 550 nm filter and then recorded with a camera. In this way the protein printed pattern can be visualized in a fluorescence image, as shown in figure 4.18b. The AFM image of

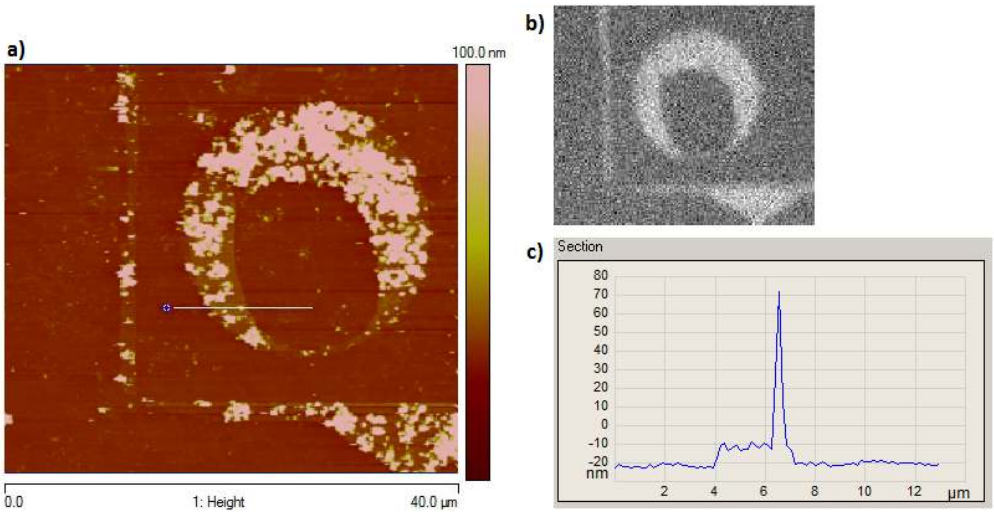

Figure 4.18: a) and b): undoped NPs conjugated to anti-fibrinogen and incubated over a fibrinogen pattern mixed with fluorescein conjugated BSA. a) AFM image, showing in white the NPs and in light brown the fibrinogen pattern; b) corresponding fluorescence image, showing in bright the printed pattern. c) Section of the AFM picture along the line of picture a), which intersects a 1.5 μm long and 10 nm thick fibrinogen layer with attached a single nanoparticle of 80 nm.

the same area is presented in figure 4.18a. The area coded in light brown is the fibrinogen pattern, as it perfectly matches the fluorescence data of figure 4.18b. The lighter spots are the antibody-NPs attached to the antigen surface. In figure 4.18c is shown a section of the AFM data taken along the line of figure 4.18a. As it can be seen, the fibrinogen has been deposited in an even layer with average thickness of 10 nm. The spike in the profile indicates a NP of size 80 nm.

From the comparison of the fluorescence channel, the AFM channel, and its profile it can be seen that antibody conjugated NPs bind to the fibrinogen pattern with a high specificity. Therefore the targeting of the antigen looks successful.

The control experiment employs undoped NPs not conjugated to any antibody and a fibrinogen printed surface prepared as previously described. The sample after the washing should consist only of the fibrinogen pattern with few or none NPs. The AFM image of the control sample is presented in figure 4.19. Once

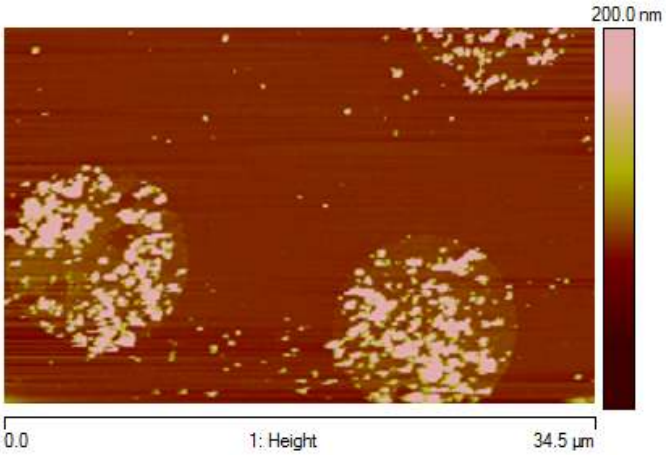

Figure 4.19: AFM image of undoped NPs (lighter spots) incubated on fibrinogen circular spots (light brown). NPs show a high specificity to the fibrinogen even if no antibody is present on the NPs surface.

again the fibrinogen pattern can easily be recognized in patterns (full circles in this case). Unsuccessfully, NPs do not get removed from the washing and they are still present over the pattern. NPs show a high specificity to the pattern even if no antibody is present on their surface.

These results clearly demonstrate that the antibody conjugation technique used

is not efficient enough to bind the antibody covalently to the silica surface, as similar results are obtained with or without antibody. Moreover, this experiment shows the necessity of an improved alternative surface chemistry of the NPs. In figure 4.19 infact can be seen that it is the plain silica surface itself which reacts and binds to the proteins. This feature can give rise to non-specific labelling when introducing antibodies on the NP surface.

4.3.4 Summary of results

Aggregometry and flow cytometry tests show the biocompatibilty of the dye doped silica NPs with the platelets. The presence of NPs does not alter platelet aggregation properties or induce change in platelet functionality.

Labelling experiments with antibody-conjugated NPs show an unsatisfactory labelling of the platelet membrane with a specificity comparable to the unconjugated NPs, as confirmed later on from NPs specificity tests. These results are fundamental in the project to understand that different alternative protocols of antibody conjugation have to be investigated. The experience obtained also suggests a deeper understanding of the nature of the antibody bond to the NP surface before proceeding with the platelet labelling. For more successful results, the work has to be integrated with a complete characterization of antibody conjugation, including immunoassays and binding tests where only the antigen is present.

The research is currently carried on with different antibody conjugation protocols from other researchers involved in the project. So far a higher and more specific degree of platelets labelling is obtained using dendrimers as linkers between the antibody and the NP surface.

Chapter 5

Characterisation of novel features of platelet physiology

5.1 Introduction

This chapter describes the experiments involving:

- platelets autofluorescence
- fluorescence assays on platelets in different activation conditions
- morphology of platelets in different activation conditions.

5.2 Platelet autofluorescence

5.2.1 Overview of biological autofluorescence

The enhanced brightness of NPs seeded with fluorescent molecules provides an attractive tool for the identification of both entire cells and sub-cellular features such as the location and concentration of specific membrane proteins. NPs containing surface-immobilized antibodies specific to the extracellular portions of transmembrane receptors would therefore act as a single step fluorescence membrane receptor reporter.

This section investigates the background to be expected when analyzing platelet samples using fluorescence-based techniques, like confocal microscopy. Understanding the endogenous fluorescence expected from untreated human platelets

provides information essential when engineering assays to report fluorescence signals significantly above the "contaminating" background. Fluorescence from a sample can be present when the sample has been labelled with an exogenous fluorophore. Often biological samples present a fluorescence signal even when not labelled. This fluorescence signal is called autofluorescence and comes from endogenous chromophores already present in the biological sample. In figure 5.1 the excitation and emission spectra of the most common endogenous fluorophores are shown. Some of the most common sources of autofluorescence are aromatic amino acid residues like tryptophan, tyrosine and phenylalanine. These are mostly concentrated in mitochondria and can also be present in cell cytoplasm which also contains NADH and NADPH, fluorescent molecules which are involved in the methabolism. Flavins are also autofluorescent; riboflavin FAD and FMN, which are mostly bound to enzymes, are concentrated in mithocondria, present in the cytoplasm as well as in the outer membrane. A prominent source of autofluorescence is the connective tissue, the presence of collagen and of elastin. Fluorescent products related to the aging of the cell are lipofuscins and porphyrins.

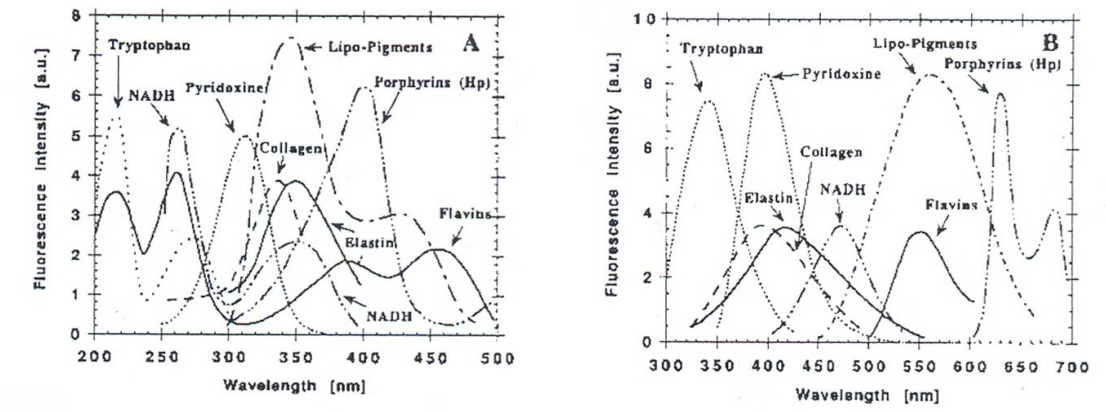

Figure 5.1: a) Excitation and b) emission spectra of some of the most common endogenous fluorophores.

5.2.2 Analysis of plasma autofluorescence

To investigate platelet autofluorescence, PRP and PPP was obtained from a freshly drawn sample of blood, as described in section 2.3. PRP and PPP are diluted in HEPES buffer according to the concentration required for the analysis.

Absorbance spectra of PPP and PRP in figure 5.2, collected using a UV-VIS spectrometer, show a non-zero absorbance of the plasma over all the visible region. In relation to the analysis shown in section 4.3.2, where the platelet samples la-

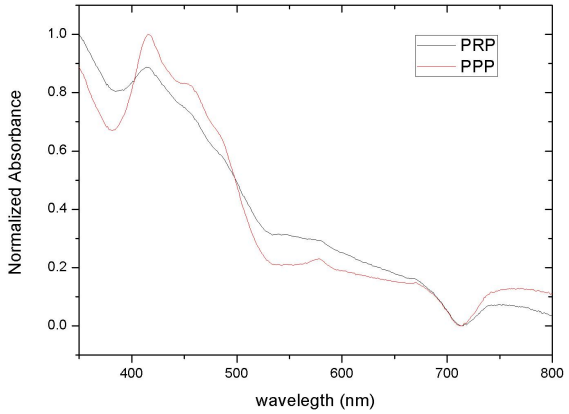

Figure 5.2: Normalized absorption spectra of platelet poor plasma (PPP) diluted 4 times in HEPES buffer, and of platelet rich plasma (PRP) diluted 8 times in HEPES buffer.

belled with anti-GPIX-FITC and with NIR664 NPs-anti-CD41 were excited with excitation wavelengths of 488 nm and of 633 nm, it can be seen that at those wavelengths the absorption of the plasma is significant, especially for excitation at 488 nm.

To measure the fluorescence of the plasma in solution, samples were monitored over time, to see if there is any relation between the aging of the sample and the magnitude of the fluorescence signal.
Fluorescence spectra were recorded for the PPP upon excitation at wavelengths 488 nm and 633 nm, as shown in figure 5.3. In general it can be seen that PPP has a peak in the fluorescence at 510 nm, and a smaller shoulder around 580 nm, when excited at 488 nm. Upon excitation at 633 nm, no clear fluorescence peaks are present. Interestingly there seems to be a recovery of the fluorescence 2 days after the sample was taken. Plotting the fluorescence intensity value of figure 5.3 (recorded at 580 nm for graph a) and at 680 nm for graph b)) versus the time in which the measurement took place after the blood drawing, it can be seen that the values remain almost constant on the day of the measurement, and increase after a few days. This is perhaps due to the production of same aging products (figure

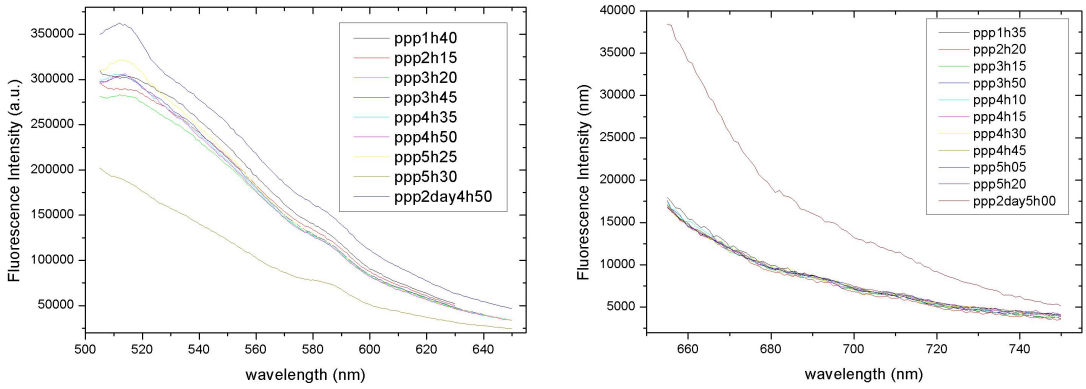

(a) (b)

Figure 5.3: Fluorescence emission spectra of PPP at different times after the blood has been extracted, upon excitation with a) a 488 nm light, b) a 633 nm light.

5.4). The same experiment repeated using PRP diluted 8 times in HEPES buffer

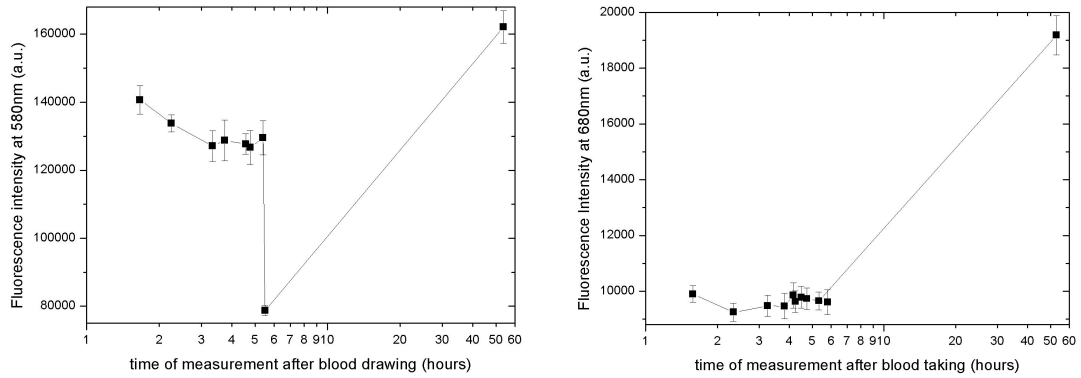

(a) (b)

Figure 5.4: Fluorescence intensity of PPP a) with 488 nm excitation, monitored at 580 nm; b) with 633 nm excitation, monitored at 680 nm.

produces the results shown in figure 5.5. The fluorescence spectra recorded after excitation at 488 nm and at 633 nm remain almost constant over time.
To see if there is any correlation between the aging time of the sample and the fluorescence intensity, the intensity value at 580 nm (for $\lambda_{exc} = 488$ nm) and at 680 nm (for $\lambda_{exc} = 633$ nm) are plotted against time (figure 5.6). From these plots, no clear behavior is observed and the fluorescence recovery found in the analysis of PPP is no longer present. Variation in the fluorescence intensity for long times

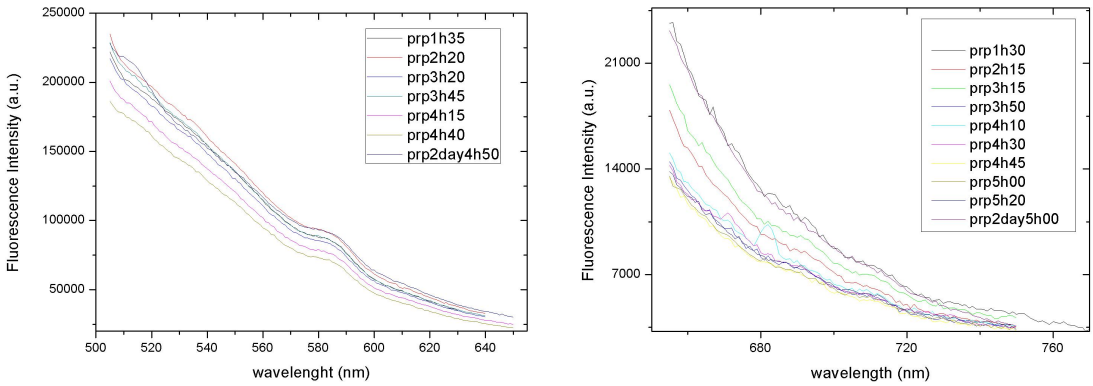

(a) (b)

Figure 5.5: Fluorescence emission spectra of PRP excited with a) a 488 nm light, b) a 633 nm light, at different times after the blood has been extracted.

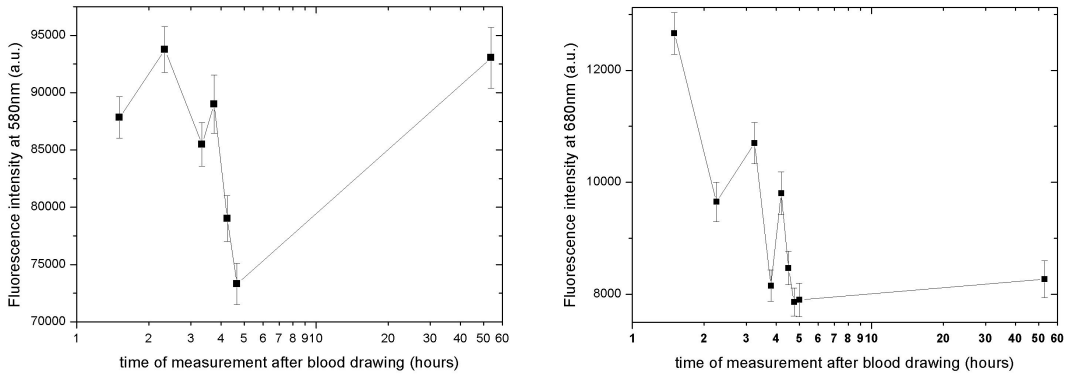

(a) (b)

Figure 5.6: Fluorescence intensity of PRP a) after 488 nm excitation, monitored at 580 nm; b) after 633 nm excitation, monitored at 680 nm.

could be due to contamination of the sample or to the presence of some molecules degrading over time. The fluorescence recovery for PPP can be due to some plasma protein and not to platelet themselves. In fact, the sample of PRP contains less plasma proteins than the PPP sample, since it is more diluted compared to PPP, in order to have an absorbance suitable for fluorescence analysis.

5.2.3 Analysis of single platelet autofluorescence

Fluorescence measurements with a spectrofluorometer are bulk measurements. It involves measuring the fluorescence of a cuvette of plasma which averages over all the platelets as well as over all the other plasma components. To analyze single platelets one at a time, samples are prepared as follow: PRP is obtained as described in section 2.3. The plasma is then diluted 1:3 in HEPES buffer and left for incubation on a glass slide for 45 minutes in static conditions. After the incubation time, the coverslip is washed 3 times with HEPES buffer and was fixed with glutaraldehyde for 30 minutes. Glutaraldedhyde is a fixative known to increase the autofluorescence [53] (for more details see section 2.2). After fixation, the sample is washed 3 times with PBS and the coverslip mounted on a microscopy glass slide. The protocol for immobilization of platelets on glass is illustrated in more detail in section 4.2.1.

Samples were then analyzed with confocal microscopy. An argon laser is used to excite the specimen at 488 nm and the various wavelength regions of the fluorescence signal are spectrally separated. A slit placed in front of the detector allows the collection of a fluorescence image for each of the wavelengths between 513 nm and 673 nm in steps of $\approx$ 10 nm. In figure 5.7 it is shown a composition of 16 fluorescence images color coded according to the emission wavelength intervals. All these images are then combined together in a single image. In this way it is possible to see which components of the specimen have a higher signal in a certain region of the spectrum compared to others. As it can be seen from figure 5.7, there are some components/granules inside the platelet that have a high fluorescence contribution in the green part of the spectrum. The outline of the platelet is manually drawn over the image and the average fluorescence of the pixels enclosed in this region of interest (ROI) is plotted versus emission wavelength. In this way it is possible to obtain a fluorescence spectrum of a single platelet. The spectrum obtained for figure 5.7 is shown in figure 5.8. This spectrum is significantly different from the one obtained using a spectrofluorometer for a bulk sample of plasma (figure 5.5). Here it can be seen that a platelet mainly fluoresces in the green region, with a peak around 555 nm and a shoulder at 540 nm and that there are also some less intense peaks around 610 and 645 nm (red region of the visible spectrum). The fluorescence peaks for this platelet is characteristic for all the platelets. Similar spectra are obtained from single platelets, clumps of platelets and from platelets with different morphologies. In figure 5.9 several autofluorescence spectra of dif-

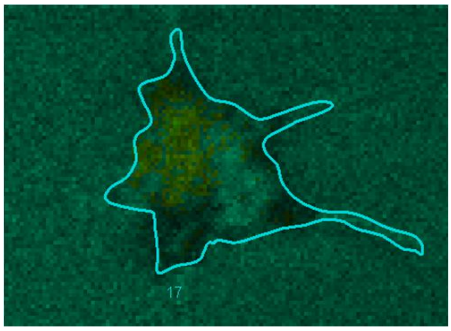

Figure 5.7: Composition of 16 images collected from 513 nm to 673 nm in steps of ≈ 10 nm for a platelet immobilized on a glass slide. Color coding is associated with the emission wavelengths.

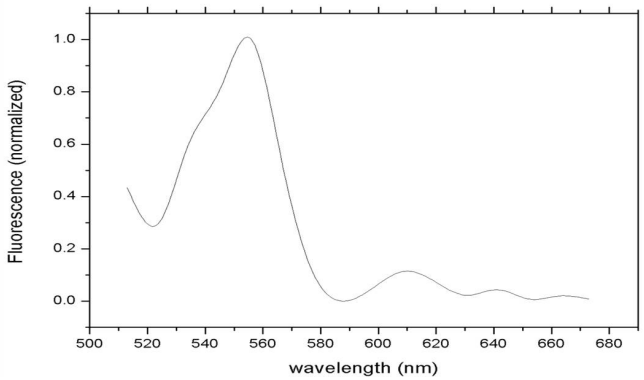

Figure 5.8: Average fluorescence of the ROI of figure 5.7 versus central wavelength at which the image is collected. The original data points are fitted with a polynomial (shown).

ferent platelets are plotted under the same conditions: same microscope settings (scan time, frame average, zoom, detector gain,...), same sample and same focal position on zeta axis. To standardize the analysis to screen platelets, the chosen ROIs are all circles of radius 5 pixels centered in the middle of the platelet. The peak magnitudes are actually not related to the visual appearance of the platelet, but to the intracellular contents. As can be seen in figure 5.7 there are some subcellular features that have a different fluorescence emission compared to the rest of the platelet.

Figure 5.10 compares the average fluorescence of small ROIs inside the same

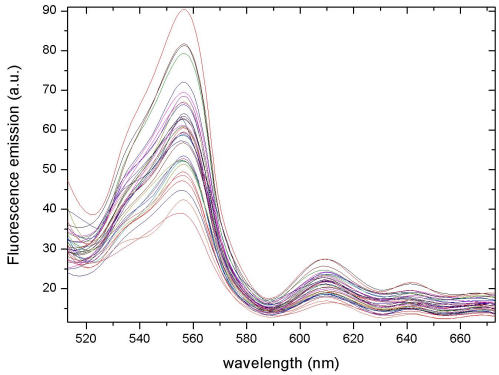

Figure 5.9: Fluorescence spectra for various platelets, collected and processed as described in the text.

platelet. The ROIs are circles of radius 2 pixels, and are distributed all along the y axis and numbered from 1 to 7 from upper to lower. In figure 5.10b is plotted the average fluorescence of a ROI relative to the emission around a certain wavelength versus the ROI number. It can be seen that different regions inside the platelet contribute more or less to specific emission wavelengths. ROI number 6, placed almost at the platelet membrane, has a higher contribution at 556 nm compared to the other ROIs, while having an integrated fluorescence lower or equal to the other ROIs for the other emission wavelengths. This behavior is not seen for the other peripheral ROIs of figure 5.10. ROI number 4, placed in the center of the platelet, has a lower fluorescence emission compared to the adjacent ROIs for all the wavelengths analyzed. All these data and observations are strictly related to the platelet content itself and cannot be predicted just by looking at the platelet shape or condition.

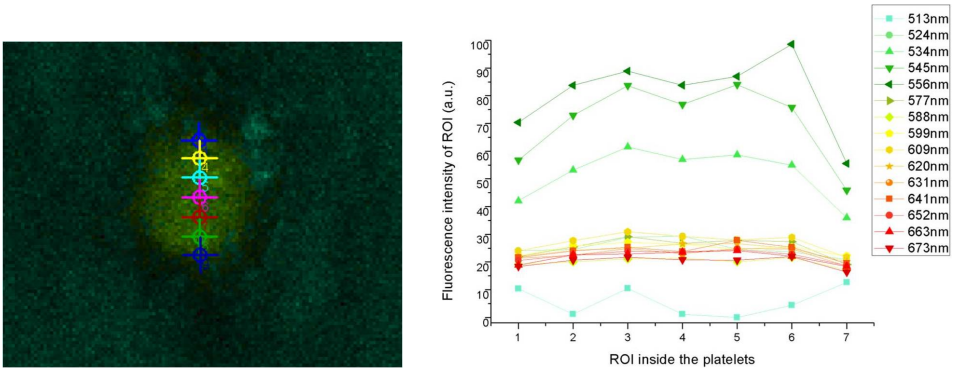

(a) (b)

Figure 5.10: a) Composition of 16 images collected from 513 nm to 673 nm in steps of ≈10 nm for a platelet immobilized on a glass slide. Color coding is associated with the emission wavelengths. b) Fluorescence emission of the ROI of figure a), versus ROI number, as explained in the text.

5.2.4 Summary of results

From the analysis in this section it is clear that platelet autofluorescence is a signal that cannot be neglected when developing a fluorescence assay for specific human platelet disease states. The limit of detection of an assay is strictly related to the background of the quantity measured. For a platelet assay, the autofluorescence is a non-removable background. Spectral analysis of bulk samples of plasma and of single platelets immobilized on glass did not show any correlation between the autofluorescence signal and characteristics like sample aging time, platelet shape and the platelet local environment. From the spectral analysis obtained using a confocal laser scanning microscope, it is clear that the autofluorescence signal is not uniform over the platelet and that different intra-cellular components have different fluorescence properties that cannot be predicted.

5.3 Fluorescence labelling of platelets

5.3.1 Antibody sandwich assays

Using the techniques of platelet immobilization on surfaces described in section 4.2, standard double antibody sandwich assays have been performed. The assays

have been performed to investigate if the immobilization protocols are suitable for targeting the platelet receptor αIIbβ3, which is the same receptor that needs to be targeted for the NP assay.

The primary antibody used is anti-CD41 mouse anti-human and the secondary is an IgG goat anti-mouse conjugated to the fluorophore Alexa488. The secondary antibody is added in a second step to bind to the primary antibody. When the sandwich assay is successful, the platelet membrane is fluorescently labelled with the Alexa488 fluorophore.

Samples are prepared as follow: platelets, immobilized either on glass either on fibrinogen printed pattern, are fixed with PFA 3.7 % (w/v) and subsequently incubated with a 200 μl solution of anti-CD41 in the ratio 1:1000 V:V in PBS for one hour on the coverslip at room temperature and in static conditions. The secondary antibody solution is diluted in PBS in a total volume ratio of 1:500 with the addition of 1.5 % (v/v) of goat serum. After the coverslip has been washed three times with PBS, a 200 μl drop of the secondary antibody solution is left on the glass in incubation for 30 minutes in static conditions and room temperature and then washed again three times with PBS. Afeterwards the coverslip can then be mounted on a glass slide for microscopy analysis.

The samples are imaged in confocal microscopy, using as excitation light a 488 nm argon laser line. The signal is collected on two separate channels, one recording the scattering information (using a band pass filter 465-510 nm) and the other recording the fluorescence (with a low pass filter 505 nm). The two signals are directed to the detectors using a dichroic glass 490 nm and the pin-hole aperture is set at 1 Airy unit for both of the channels for optimal optical sectioning. The scattering channel is used as a reference to identify the platelet position on the coverslip.

Platelets immobilized on glass

In figure 5.11 is shown the result of a double antibody sandwich assay of undiluted PRP immobilized on glass. The platelet membrane is homogeneously stained with the two antibodies, showing clearly the morphology of the platelets. When analyzing the samples in confocal microscopy the focus can be set to visualize the different areas of the membrane, like the bottom surface of the platelets

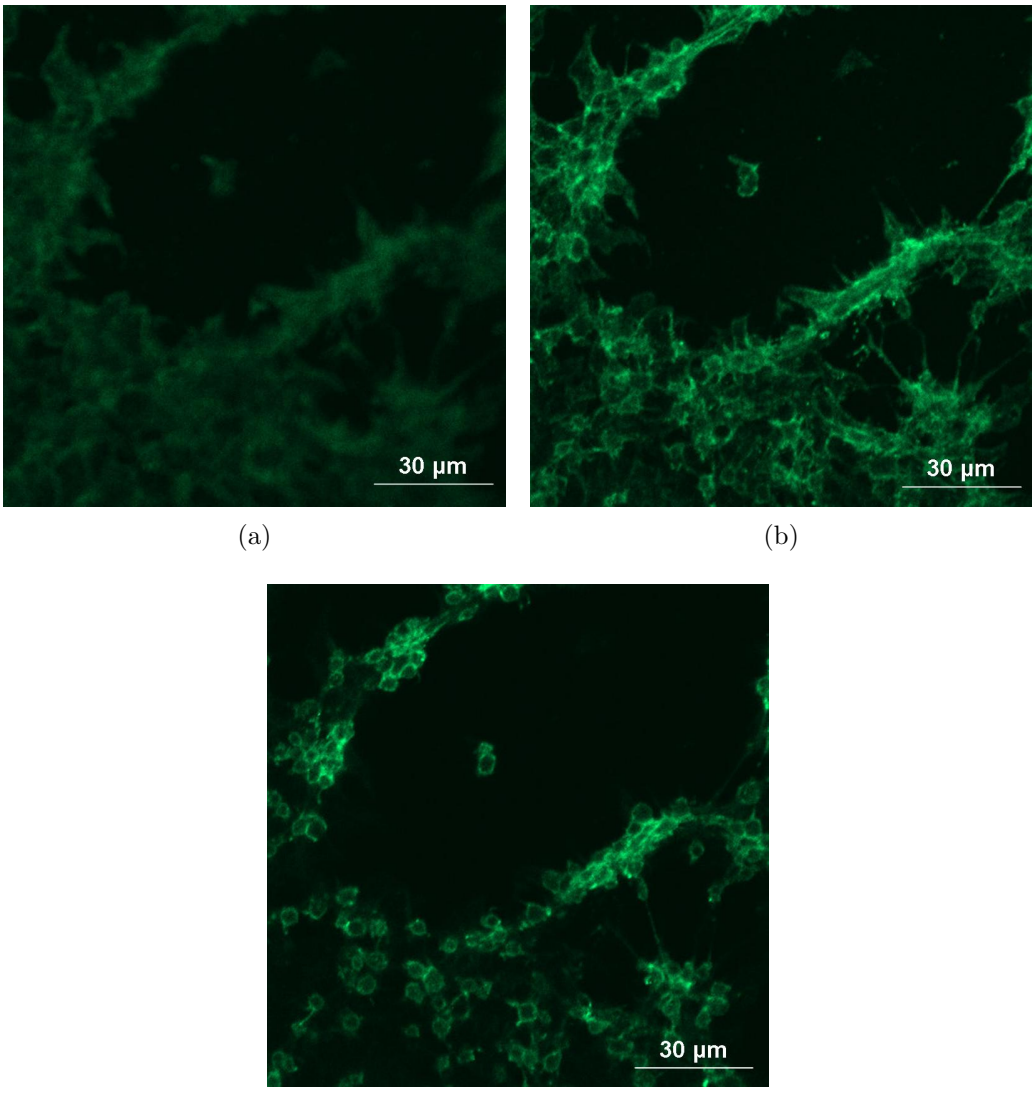

(a) (b)

(c)

Figure 5.11: Fluorescence image relative to the emission of Alexa488 for a double antibody sandwich assay using anti-CD41 as primary antibody. Platelets are immobilized on the glass slide after 30 minutes incubation and 30 minutes PFA fixation. In a) is shown an optical section along the z axis at the glass surface, in b) 1 μm above the glass surface and in c) 2 μm above the glass surface. The optical sections have a thickness of ≈ 0.8 μm.

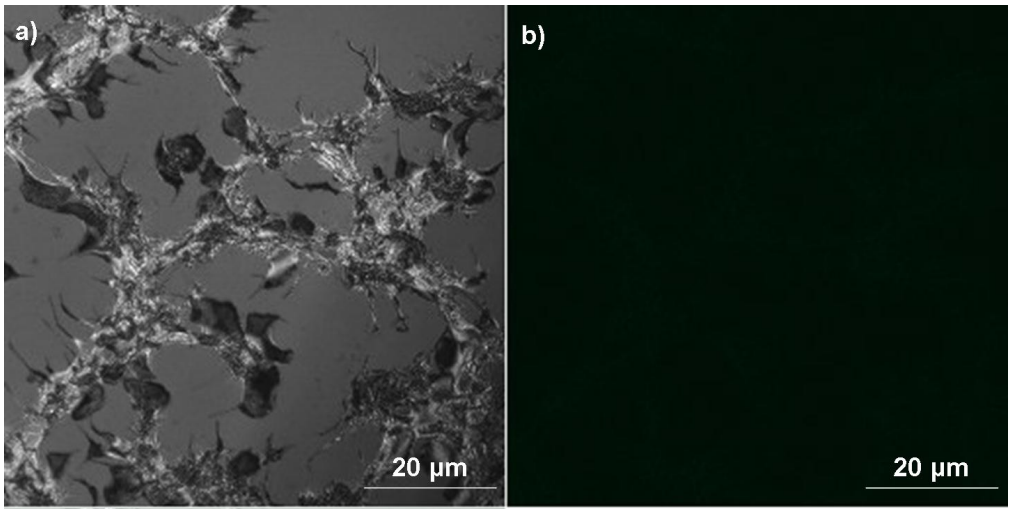

(a)

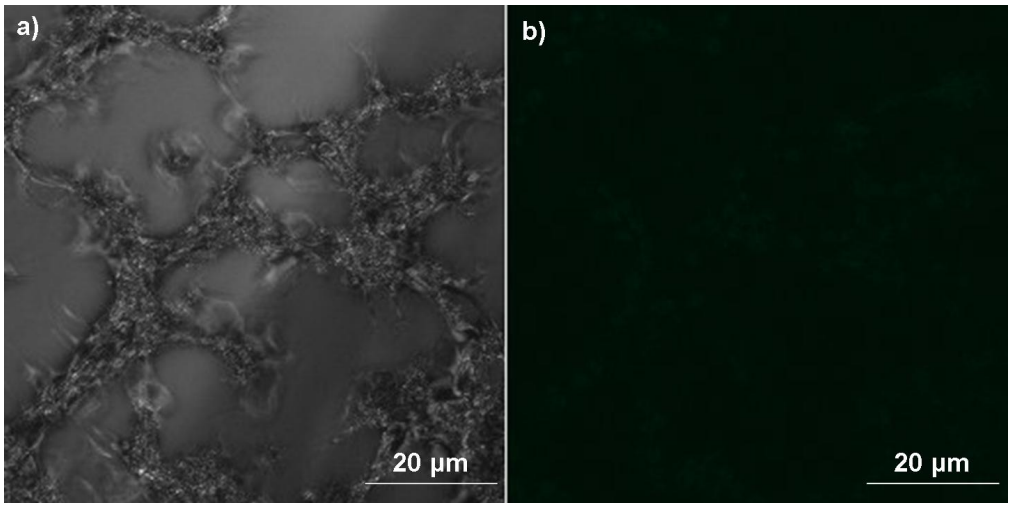

(b)

Figure 5.12: Control sample of the same assay described previously with using only the secondary (fluorescent) antibody. The platelets are visible in the scattering channel (left side) but not present any fluorescence (right side). No fluorescence is seen when moving the focus from the glass surface (top figures) to μm above the glass surface (bottom figures).

that is in contact with the glass (figure 5.11a), or the pseudopodia and filaments connecting platelets (figure 5.11b) or the upper section of the platelet membrane (figure 5.11c).

The control experiment in which only the secondary antibody is used presents no fluorescence signal, as it can be seen from figure 5.12.

This assay is used over the time of the research to investigate the functionality of the antibody after different storage times.

Platelets immobilized on fibrinogen patterns

In figure 5.13 is shown the result of a double antibody sandwich assay of platelets immobilized on a fibrinogen pattern using the technique described in section 4.2.

The results resemble what has been found for the sandwich assay of platelets immobilized on glass: a good staining of the platelet membrane and no signal from the control samples. The immobilization of platelets on fibrinogen micro-printed pattern is therefore suitable for targeting the platelet receptor αIIbβ3.

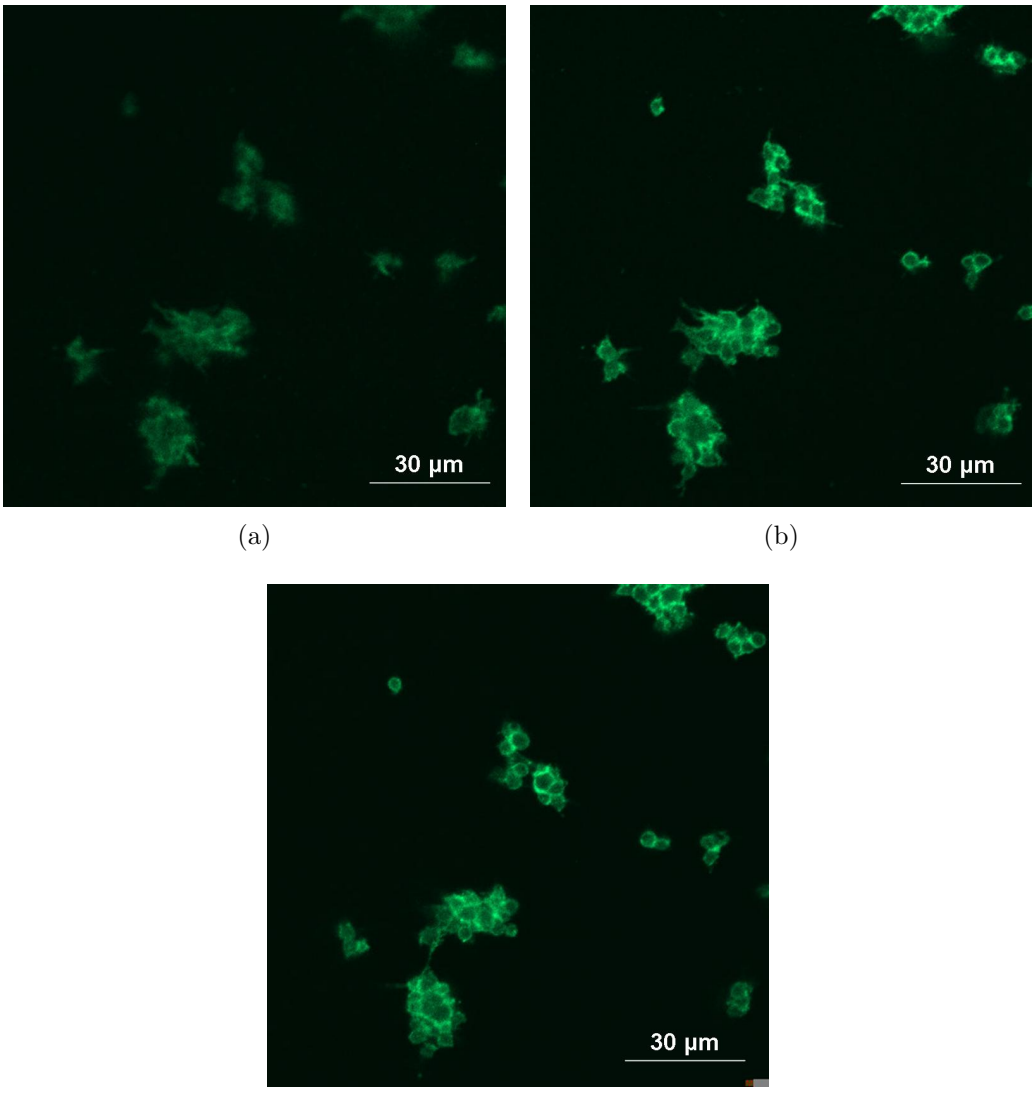

(a) (b)

(c)

Figure 5.13: Fluorescence image relative to the emission of Alexa488 for a double antibody sandwich assay using anti-CD41 as primary antibody. Platelets are immobilized on the fibrinogen printed glass slide after 30 minutes incubation and 30 minutes PFA fixation. In a) is shown an optical section along the z axis at the glass surface, in b) 1 μm above the glass surface and in c) 2 μm above the glass surface. The optical sections have a thickness of ≈ 0.8 μm.

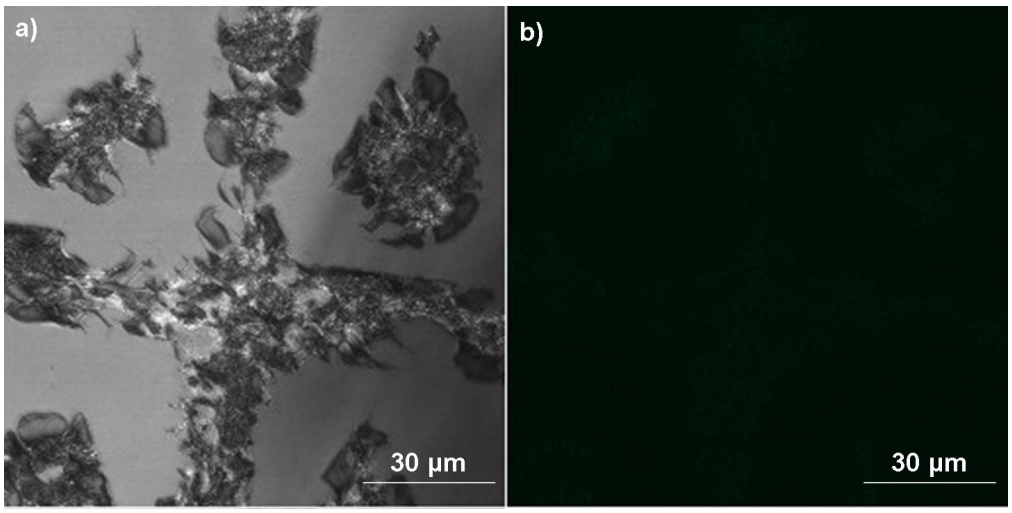

(a)

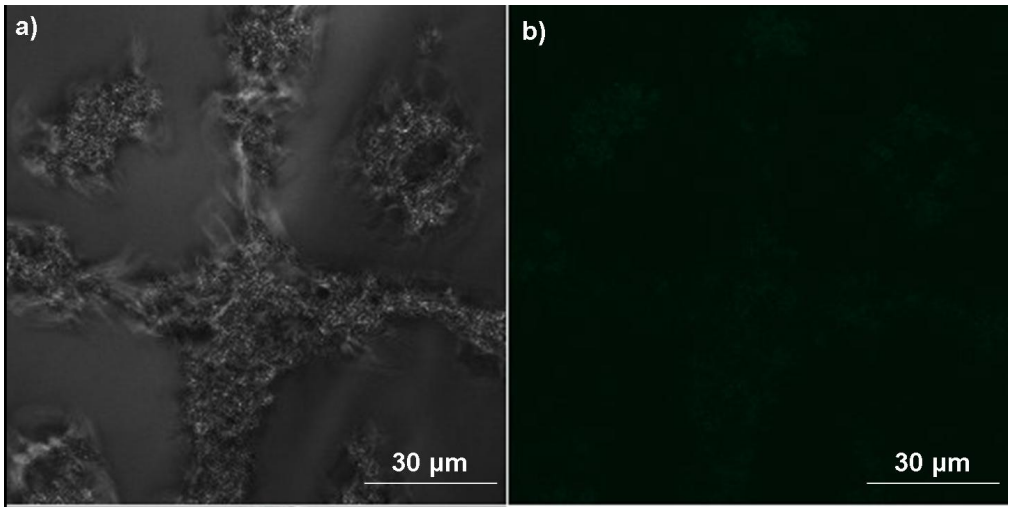

(b)

Figure 5.14: Control sample of the same assay described previously using only the secondary (fluorescent) antibody. The platelets over the cross and droplets-shaped pattern are well visible in the scattering channel (left side) but the fluorescence channel (right side) is black. No fluorescence is seen when moving the focus from the glass surface (top figures) to 1 μm above the glass surface (bottom figures).

5.3.2 Activation-specific antibodies

Activation-specific platelet antibodies are antibodies that bind to an element on the platelet that is characteristic of activated platelets only. In this experiment an antibody towards the molecule P-Selectin is used, which is stored in the granules of platelets and is rapidly transported to the plasma membrane upon activation (see also section 1.2.1). The aim of the experiment is to explore how the immobilization of platelets on micro-patterned proteins influence their activation and behavior.

Two different kinds of surfaces have been employed. The first one consists of fibrinogen printed in patterns of circles with diameter spanning from 2 μm to 24 μm, which is produced as described in section 4.2.2. The second type of surface has the same pattern but it is composed of anti-CD42b antibodies. These last plates are prepared by our partner in RCSI.

The reason why these surfaces are compared is because platelets are in two different states when immobilized on fibrinogen or on anti-CD42b [56]. Fibrinogen, binding to the αIIbβ3 platelet receptor, induces activation of the platelets, while anti-CD42b targets the GPIbα receptor which is not involved in platelet activation and therefore induces none or less activation of the platelets [56].

The analysis is targeted only to the platelets confined in the 6 μm spots in order to exploit best the potential of these micro-printed surfaces. Nowadays the majority of the studies focus on large groups of platelets. With the protein micro-pattering technology it is possible to explore what happens in constrained situations when platelets have just a small area to adhere to (as could happen in normal haemostasis, when just a small portion of endothelium is damaged). The current technology of surface patterning still does not permit the analysis of single platelets only. Single platelets are generally found on the 2 μm spots, but platelet adherence on these areas is too low to allow a statistically significant analysis.

The samples are prepared by adding the blood over the printed surfaces and leaving it in incubation for half an hour on a rocking table. The surfaces are then rinsed three times with HEPES buffer and fixed with PFA 3.7 % (w/v) . After fixation the coverslips are imaged with atomic force microscopy (AFM results will be shown in section 5.4). Subsequently the same slides are labelled with CD62P mouse anti-human conjugated to R-PE (R-Phycoerythrin) dye. This antibody

binds to P-selectin and it is fluorescently conjugated to a green emitting dye that can be excited with a argon 488 nm line (see its spectra in figure 5.15). As a reference a mouse anti-human CD41 antibody, which binds to the receptor αIIbβ3 presents on platelets surface is used. On top of the anti-CD41 is added a goat anti-mouse IgG antibody conjugated to Alexa Fluor 647. This fluorophore emits in the near infra-red region of the spectrum (see again figure 5.15) and can be excited with a helium-neon 633 nm laser line.

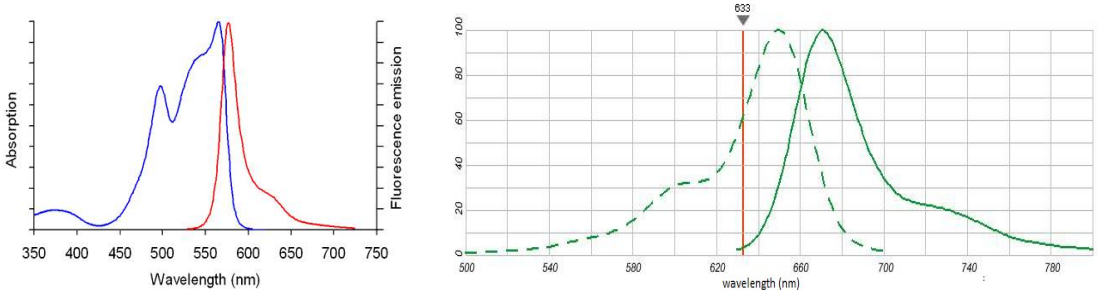

(a) (b)

Figure 5.15: Spectral characteristics of the two dyes used for platelet labelling. a) Normalized excitation (black curve) and emission (red curve) spectra for R-PE. b) Normalized excitation (dashed curve) and emission (solid curve) spectra for Alexa Fluor 647 conjugated to IgG, with overimposed the excitation line at 633 nm (red line).

For each of the samples, three signals have been detected and recorded through confocal microscopy. These signals are summarized in table 5.1 together with the setup details.

The fluorescence signal arising from labelled P-selectin is mainly found in the inner of the platelets, instead the signal from anti-CD41 is more intense from the outer membrane, as can be seen in figure 5.16. This can be better visualized in the RGB merging of channel 1 and 2, displayed in figure 5.17. Note also that for both of the pictures, the focus is placed at the bottom of the slide, as will be explained later. The two fluorescence signals are not colocalized, as shown by the colocalization scatterplots (figure 5.18). For platelets immobilized on fibrinogen there is a predominance of signal from regions with high contents of anti-P-selectin and low contents of anti-CD41.

	Signal	Source	λ_{exc}	Dichroic	Filter	Antibody	Relative to
Ch0	back scattering	reflected light	488	490	BP 465-510	/	**"objects"**
Ch1	green fluorescence	R-PE	488	490	LP 505	anti-CD62P	**P-selectin**
Ch2	NIR fluorescence	Alexa Fluor 647	633	545	LP 650	anti-CD41	**αIIbβ3**

Table 5.1: Recorded signals and specification of the microscope setup.

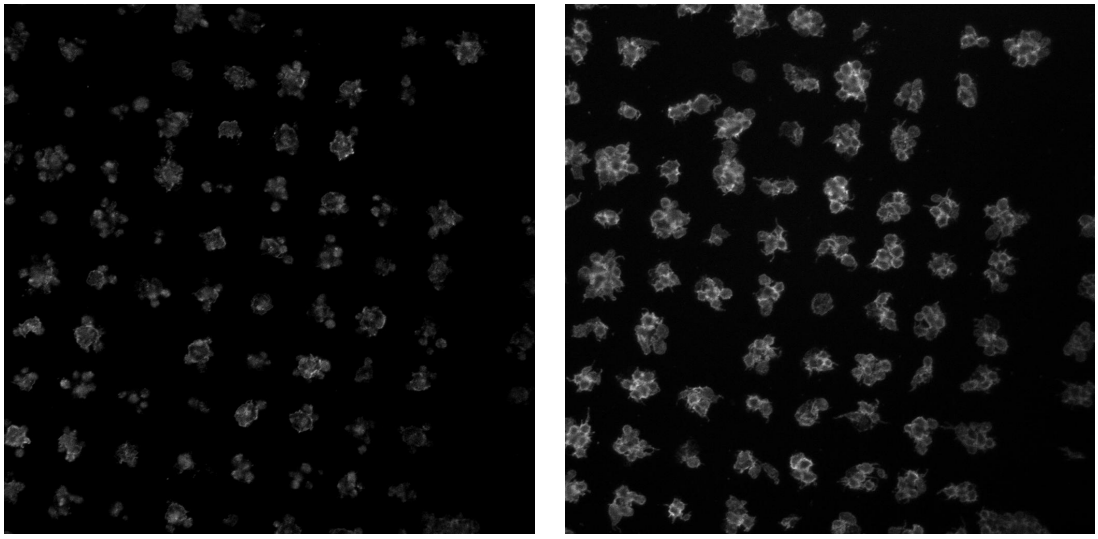

(a) Ch1 (b) Ch2

Figure 5.16: Fluorescence image of platelets from WB captured on fibrinogen 6 μm spots, a) from labelled P-selecting (green fluorescence) and b) from labelled αIIbβ3 (NIR fluorescence).

On anti-CD42b patterned surfaces the fluorescence information collected is significantly different, being the NIR fluorescence of labelled αIIbβ3 more dominant than the green signal of P-selectin events. In the colocalization scatterplots (figure 5.19) the main stripe is not anymore vertical but lays initially over the bisector and then binds horizontally.

A numerical analysis of the fluorescence intensity was also performed, as de-

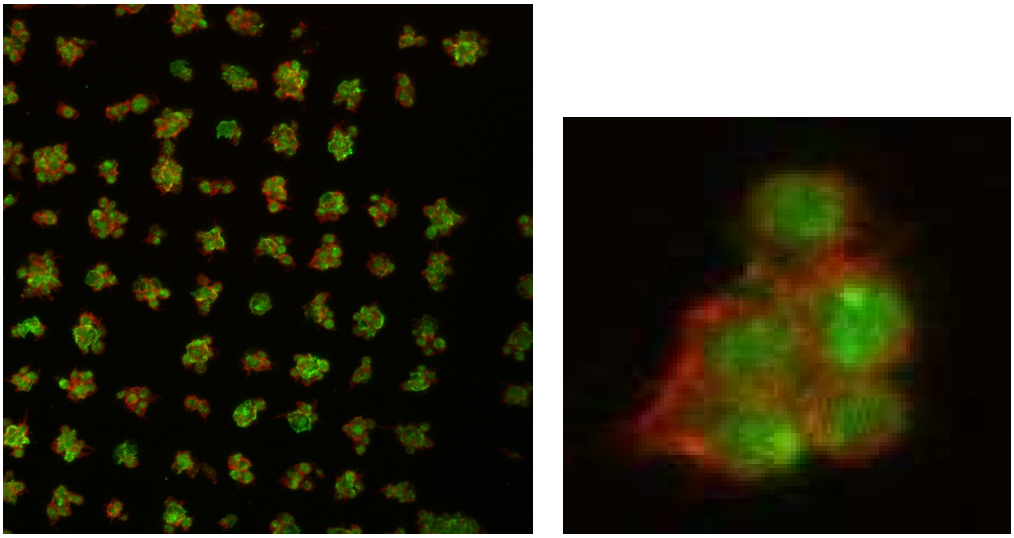

(a) (b)

Figure 5.17: a) RGB image composition of pictures in figure 5.16 and b) a zoom of a single 6 μm spot. Ch1 is coded in green and Ch2 in red.

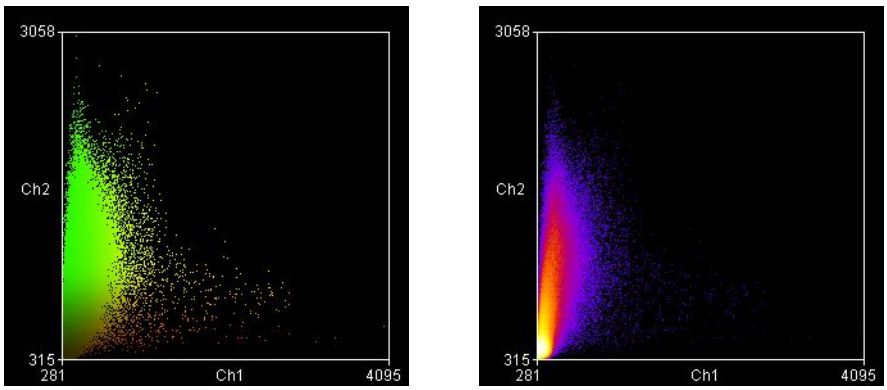

(a) (b)

Figure 5.18: Color (a) and density (b) colocalization scatterplots of the image in figure 5.16 of platelets on fibrinogen. Ch1 is relative to fluorescence of anti-P-selectin (labelled in green), Ch2 is from fluorescence of anti-CD41 (labelled in red).

scribed next.

Ch0, back scattered light, is used to identify the platelets and to create a mask to isolate the 6 μm circular spots. This channel is also used to set the focus for the im-

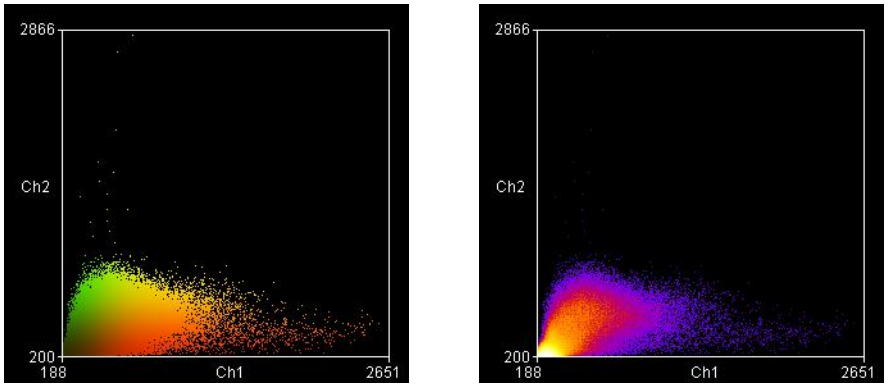

(a) (b)

Figure 5.19: Color (a) and density (b) colocalization scatterplots for platelets on anti-CD42b patterned 6 μm spots. Ch1 is relative to fluorescence of anti-P-selectin (labelled in green), Ch2 is from fluorescence of anti-CD41 (labelled in red).

ages collected in Ch1 and Ch2. In this way, between different slides, the z-position of the objective is relative and instead the focus is controllable and reproducible. The focus is always placed at the interface between the glass and the bottom of the platelets (see figure 5.20). The mask is created through an algorithm involving

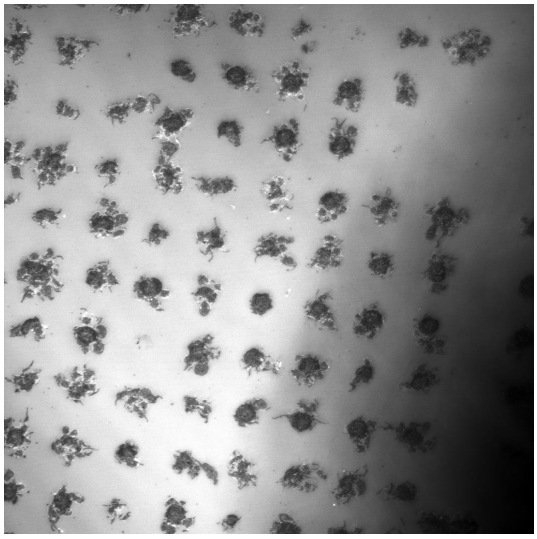

Figure 5.20: Back scatter image (Ch0) of platelets from WB captured on fibrinogen 6 μm circular spots. Platelets can easily be seen in backscattered light and so the image can be used to create a mask to locate the platelets.

the enhancement of contrast, the homogenization of the signal of local areas, the suppression of the background and the setting of a signal threshold (neglecting small sized areas). The mask so created identifies most of the platelet 6 μm spots, losing the ones located at the right-bottom border of the image, where the signal is hugely compromised by the tilting of the glass. This mask can be applied to any of the channels, as shown in figure 5.21. The mask was superimposed on a

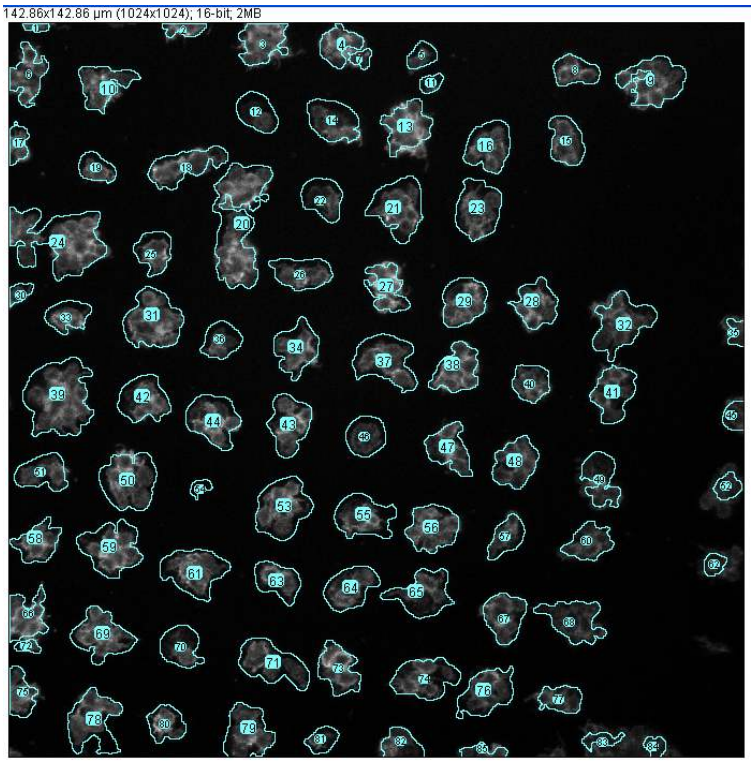

Figure 5.21: Ch1 green fluorescence channel with superimposed the mask which was created from the Ch0 back scattering (see also figure 5.20). Deleted ROIs are ROIs over unoccupied spots (like 54), ROIs overlapping platelets outside from the pattern (like 11), ROIs overlapping more than 1 spot (like 20), and ROI not completely overlapping a spot (like 52).

channel to manually remove the errors in the mask: the ROIs not overlapping to a platelet filled 6 μm spot are deleted. These errors arise from the recognition of the mask of the scattering of fibrinogen of unoccupied spots or from non-specific attachment of platelets outside the pattern.

For each of the ROIs is calculated the fluorescence intensity averaged over

the spot area, obtaining the "pixel fluorescence density" (ρ_{fluo}) of a single 6 μm spot. Table 5.2 summarize the results obtained when averaging ρ_{fluo} over more than 800 ROIs and the standard deviations (σ). The values obtained confirm a

	FIBRINOGEN SURFACE		ANTI-CD42b SURFACE	
	ρ_{fluo} $[au/pixel]$	σ $[au/pixel]$	ρ_{fluo} $[au/pixel]$	σ $[au/pixel]$
P-selectin events	783	170	443	45
αIIbβ3 events	529	194	519	89

Table 5.2: Pixel fluorescence density for platelets immobilized on 6 μm spots of two different surfaces. The displayed values are an average of over 800 spots.

larger presence of the activator product P-selectin for platelets immobilized on fibrinogen, as expected. Fibrinogen is in fact a molecule involved in the activation process of platelets. For platelets immobilized on 6 μm fibrinogen spots the ratio of ρ_{fluo} from P-selectin events and from αIIbβ3 events is 1.48. For platelets immobilized on 6 μm anti-CD42b spots the ratio is 0.85, below one. It can therefore be assumed that anti-CD42b micro-printed surfaces activate the platelets less than fibrinogen surfaces do. Nonetheless, assumptions regarding the degree of activation of platelets cannot be made. A percentage of the fluorescence from P-selectin could have been relative to some degree of penetration of the antibody within the platelet. The permeability of the membrane could in fact be increased by the usage of the fixative PFA which is needed for the slide preparation for AFM analysis.

Other experiments are performed introducing an activator at the time of platelet incubation. The glass slides were prepared, as previously described, printing fibrinogen in circular patterns on a glass and blocking the rest of the surface with BSA. Straight after putting the whole blood on the surface, adenosine diphosphate (ADP) is added as activator for a final concentration of 1 μM. The glass slide is then left in incubation for half-an-hour, washed and then stained with antibodies towards αIIbβ3 and P-Selectin, as previously described.

The slides so obtained present less adhesion compared to slides prepared without the activator. From the scattering channel Ch0 (figure 5.22) can be seen the unoccupied spots, since the fibrinogen circles are visible (lighter gray periodical spots). From the analysis of the fluorescence of platelets confined in the 6 μm

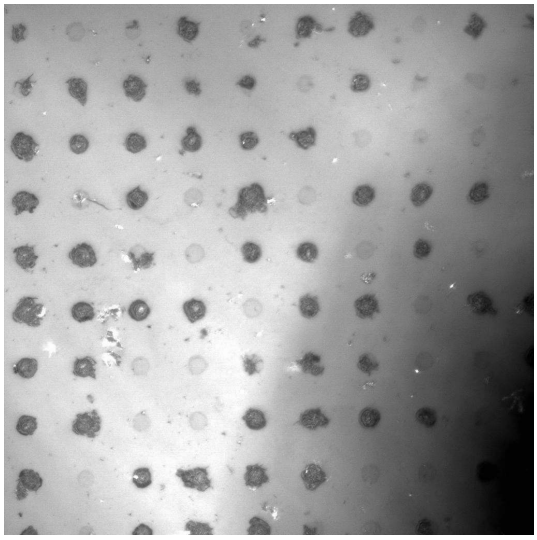

Figure 5.22: Scattering channel of platelets from WB treated with 1 μM ADP captured on fibrinogen patterned 6 μm spots. 35% of the fibrinogen spots are unoccupied.

spots it transpires that the value found for the pixel fluorescence density from P-selectin labelled antibody is still higher than the one from αIIbβ3 (see table 5.3), with ratio of the two 1.48.

The colocalization analysis of these samples is interesting. An example is shown in picture 5.23. The signal is still mainly distributed on the left side of the scatterplot, showing a predominance of signal from regions with high contents of anti-CD62P and low contents of anti-CD41, as seen before for the fibrinogen surfaces with untreated platelets, but also with a small contribution from regions with low anti-CD62P and high anti-CD41.

The introduction of an activator to the blood has minor influences on the results obtained, which in fact resemble the one obtained when no activator is used. The main difference is the level of adhesion that is diminished to around 50% in some plates.

After an exchange of opinion with our partner in RCSI we suggest that this

	FIBRINOGEN SURFACE with added ADP	
	ρ_{fluo} $[au/pixel]$	σ $[au/pixel]$
P-selectin events	480	107
αIIbβ3 events	325	99

Table 5.3: Pixel fluorescence density for platelets immobilized on 6 μm fibrinogen spots. ADP was added at the time of blood incubation. The displayed values are an average of over 600 spots.

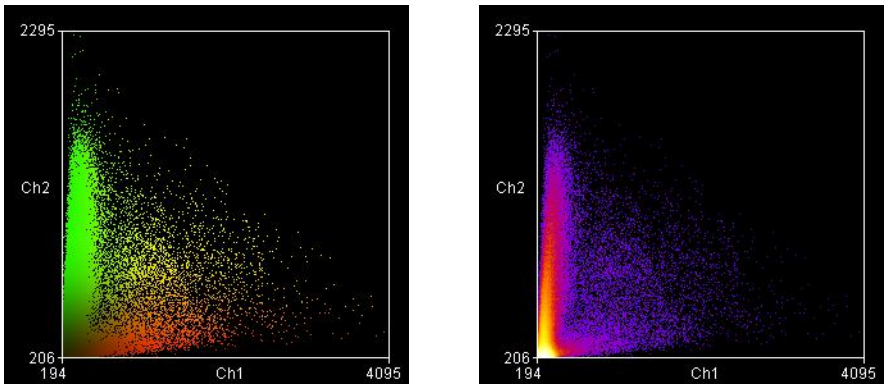

(a) (b)

Figure 5.23: Color (a) and density (b) colocalization scatterplots for platelets treated with ADP on fibrinogen. Ch1 is relative to fluorescence of anti-P-selectin (labelled in green), Ch2 is from fluorescence of anti-CD41 (labelled in red). Notice the bottom stripe of low intensity P-selectin events.

way of sample preparation can perhaps select a subpopulation of platelets. The scenario could be that platelets reacting to the activator upon its introduction become activated and recruit other platelets to which they bind, creating a cluster in the blood and not being able to adhere anymore to the 6 μm spots and maybe preferring bigger surface areas or no surfaces at all. The presence of a dim low stripe on the colocalization scatterplots could be related to this subpopulation

selection. Of course the situation can be more complex, involving factors like the age of the platelets, their responsiveness and many others.

This is indeed a new interesting topic encountered in this study, and it would be fascinating to study it to see if it could be used as a tool to discriminate some platelets from others. Additional experiments with others activators, as TRAP, should also be performed in both WB and PRP to ensure consistency of the results obtained. ADP in fact causes only minimal activation to the platelets when inserted to WB samples, since red blood cells contain a very active uptake system to remove plasma ADP (to prevent unwanted platelet activation in intact blood vessels).

5.3.3 Summary of results

Platelets immobilized on glass or protein patterns can be efficiently labelled with fluorescent antibodies. The use of activation specific antibodies allows to monitor the state of the platelets and reveal the effects that different kind of surfaces have on platelets.

5.4 High resolution morphological studies

5.4.1 Introduction

In this chapter was presented a series of experiments and analysis on platelets having as a main common topic the use of fluorescence as a signal. It was shown how to make platelets adhere to different kinds of surfaces, the platelet fluorescence properties were described , staining of platelets with antibodies was described and the information provided by staining platelets with activation-specific antibodies was discussed. From all these topics a particular interest emerged in knowing more about their morphology and topology.

As already discussed in section 5.3.2 most of recent studies are about large groups of platelets, either in bulk conditions when analyzing samples of plasma in a cuvette (like in aggregometry measurements), or depositing a layer of platelets on a large surface area. A typical scenario is like the one shown in figure 5.24, where a group of platelets are deposited on a large area of fibrinogen.

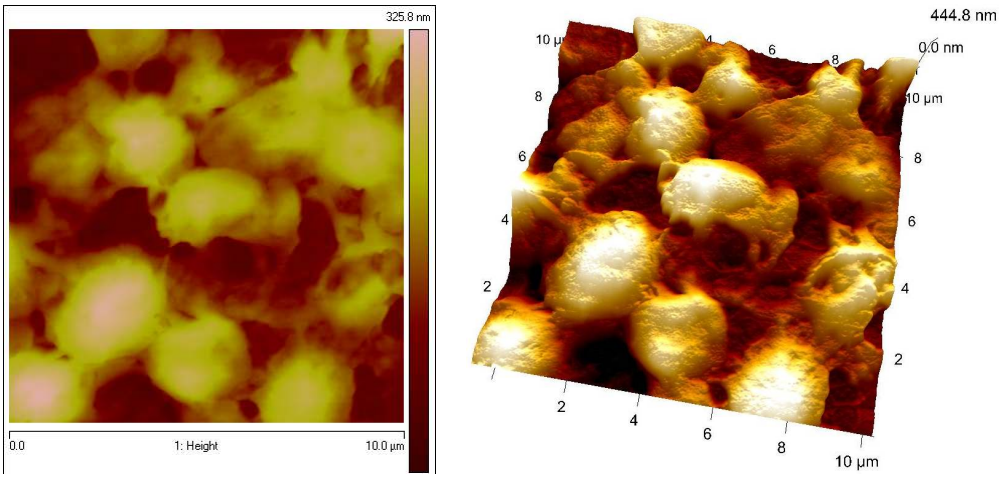

(a) (b)

Figure 5.24: AFM image of platelets immobilized on a wide fibrinogen area. a) height channel, b) 3D projection. Imaged in contact mode in air on dried platelets.

Thanks to the technology of protein printing in micro-patterns described earlier, a powerful tool for the analysis of small groups of platelets in constrained conditions is now available.

The data presented in this section are all obtained with AFM. AFM analysis requires much longer measurement times compared to fluorescence analysis, but it can image the nanometer-scale features of surfaces. This cannot be obtained with light based microscopies which are limited by the light diffraction constraints (see section 2.1.6 for further details about AFM).

The slides employed for the morphological study are the same as have been presented in section 5.3.2, where the samples are labelled with activation-specific antibodies and imaged in confocal microscopy. It is important to underline that the AFM measurements take place before the slides are stained with antibodies, in order to avoid any interaction between the probe and the antibodies. Samples are prepared leaving the blood in incubation for half an hour over a protein printed surface on a rocking table, washing it three times with HEPES buffer and fixing it with PFA 3.7 % (w/v). Samples are stored in a petri dish containing PBS until the time of AFM measurement.

At the time of the analysis the coverslip is washed with DI water and dried under nitrogen. The AFM is then operated in contact mode on dried platelets, using as a tip a silicon nitride probe with resonance frequency of 65 KHz and force constant 0.35 N/m.

The morphology data of platelets immobilized on micro-printed protein patterns are compared for two kind of proteins: fibrinogen and anti-CD42b. As already discussed in section 5.3.2, platelets behave differently when immobilized on fibrinogen or on anti-CD42b since the former induces activation on the platelets [56].

5.4.2 Platelets on fibrinogen printed pattern

In this section are presented some of the data collected for platelets immobilized on fibrinogen circular patterns of different sizes.

In figure 5.25 are shown platelets adhering on 12 μm spots. The platelet adherence on the fibrinogen spots is different. In some spots platelets spread all over the fibrinogen area (figure 5.25a) and in some others the fibrinogen coverage is just partial. In each of the cases can be seen a tendency of attaching to the fibrinogen in a "fried-egg style", with the membrane spread in a flat layer of about 30 nm height and with the rest of the cell organelles collected in a taller point. The example

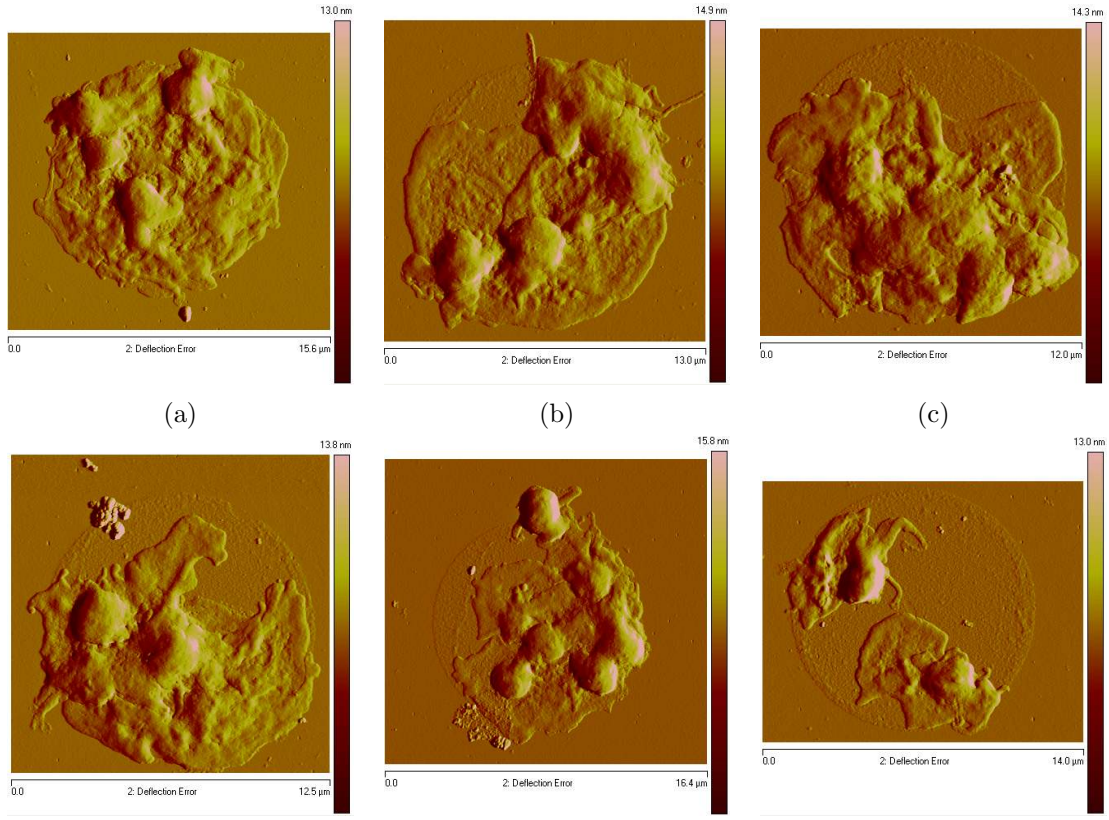

(a) (b) (c)

(d) (e) (f)

Figure 5.25: AFM deflection error images of platelets from WB captured on 12 μm fibrinogen spots. The adherence level is different between the spots. Imaged in contact mode in air on dried platelets with tip speed 12 μm/s.

of figure 5.25f, in which just two platelets are on the spot and with most of the fibrinogen unoccupied, was found quite rarely. The most frequent behavior that is observed is of platelets spreading almost completely on the spot, like in figure 5.26.

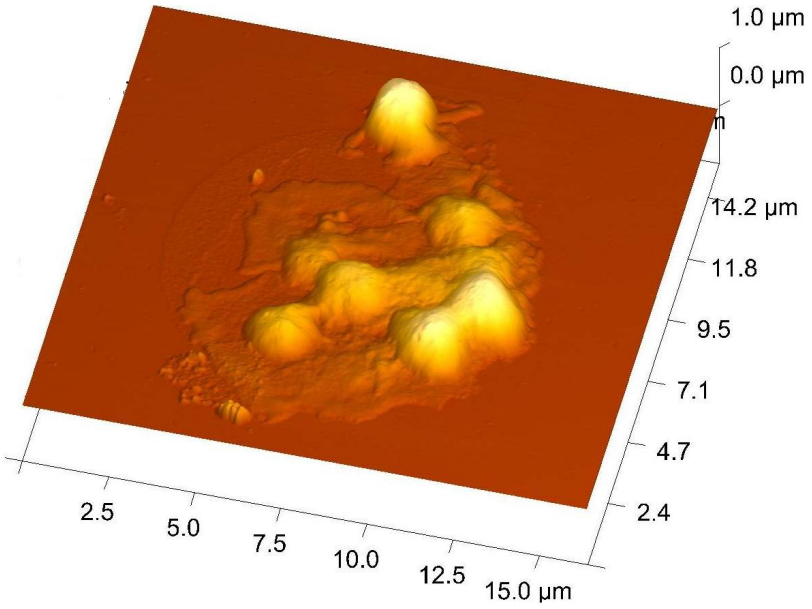

Figure 5.26: AFM 3D surface plot for the spot in figure 5.25e.

On the 2 μm spots the occupancy is very low as already seen in the session about the fluorescence analysis. Figure 5.27 shows a typical overview of a 2 μm patterned area, where almost no platelets are found, "preferring" instead the larger spots. Some non-specific attachment outside from the pattern is also present. Figure 5.28 depicts a high-resolution image of the platelet deposited on the spot of figure 5.27 taken with high line sampling and low tip-speed (12 μm/s).

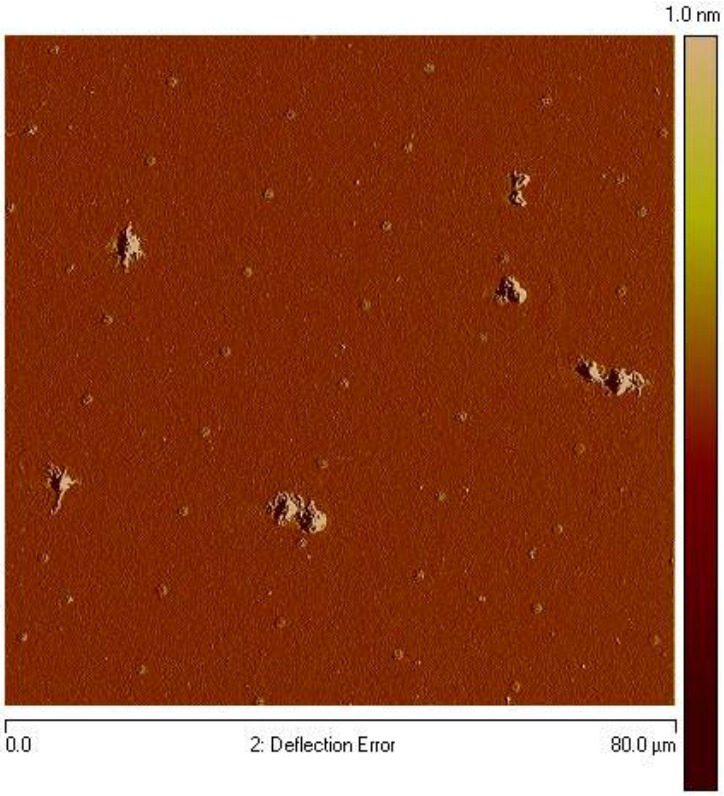

Figure 5.27: AFM deflection error image for platelets from WB captured on 2 μm fibrinogen spots. Platelet adhesion is almost null and too low for any statistically significant analysis.Imaged in contact mode in air on dried platelets.

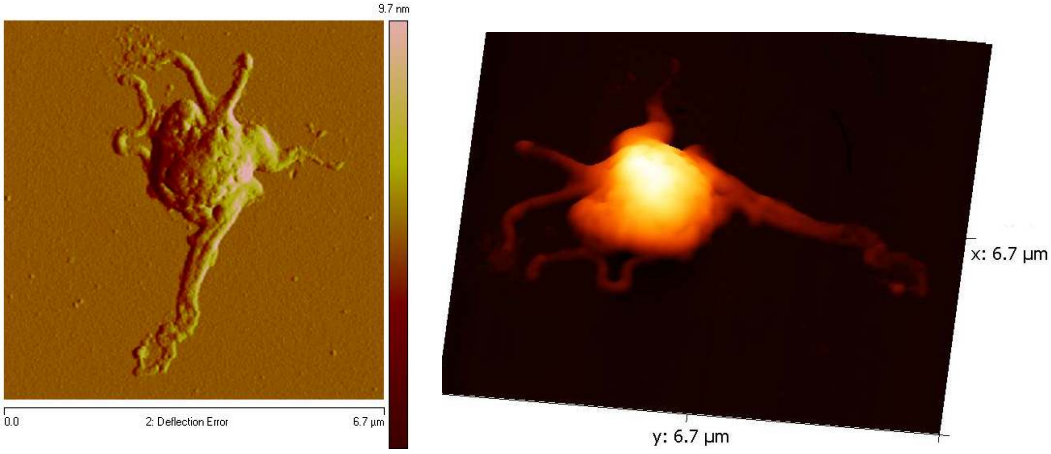

(a) (b)

Figure 5.28: AFM deflection error (a) and 3D surface plot (b) of a platelet on a 2 μm fibrinogen spot (high-resolution zoom of picture 5.27). Imaged in contact mode in air on dried platelets.

The morphology analysis was mostly focused on the platelets confined in the 6 μm spots. On these larger spots the occupancy is almost 100 %, as can be seen in figure 5.29 and in 5.32.

On the spots, platelets deposit in groups of more than one, like in 5.31f where 4 or 5 platelets are present, or, more likely, in groups of 2-3 platelets. In figure 5.30d two platelets are adhering on the same spot in a different way, one being completely flat and spread over the protein, and the second one globular-shaped on the top of the first one. Spots with only one platelet are also recognizable, like in figure 5.30a.

The average spot height is around 300 nm, and the minimum is about 150 nm. These spots are characterized by platelets flattening their membrane over the fibrinogen area, as in the examples shown. At times on the 6 μm spots there are found aggregates of platelets taller than 480 nm and presenting a globular shape, like the one of figure 5.33. The height of this agglomerate is 780 nm. The different degree of spreading and also the large presence of pseudopodia is to be noticed. The 6 μm circles are also generally fully occupied by the platelets with very few examples of platelets not spreading completely over the fibrinogen spot like the ones of figures 5.34b e 5.34d.

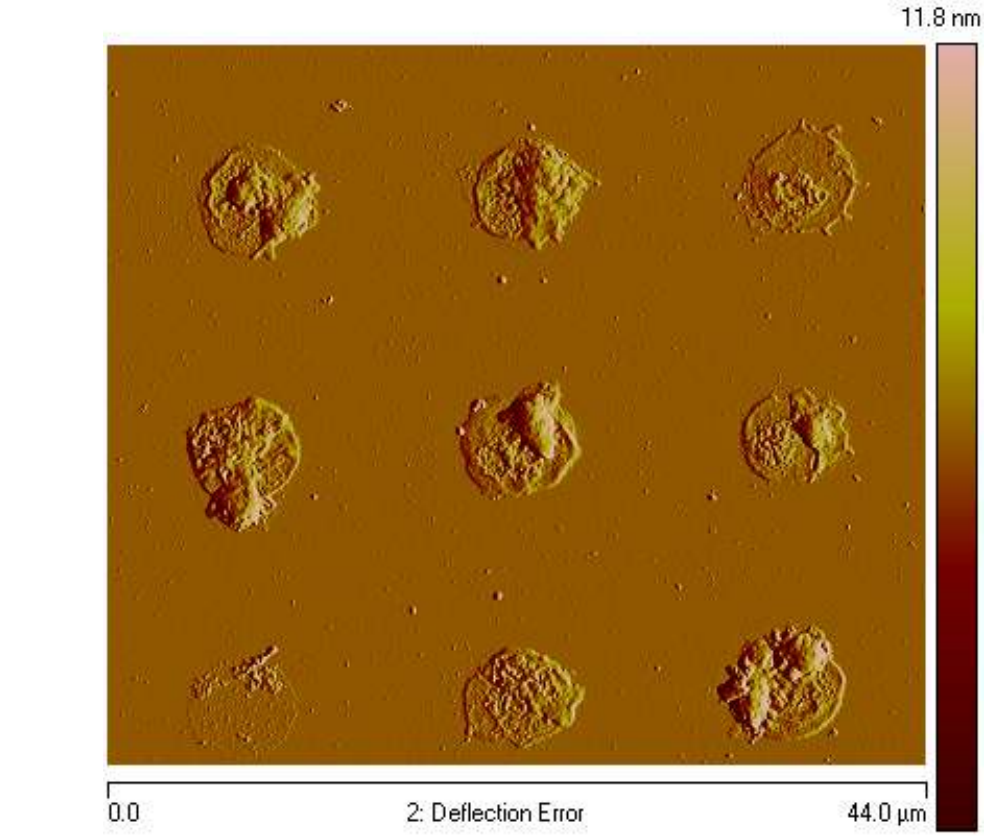

(a)

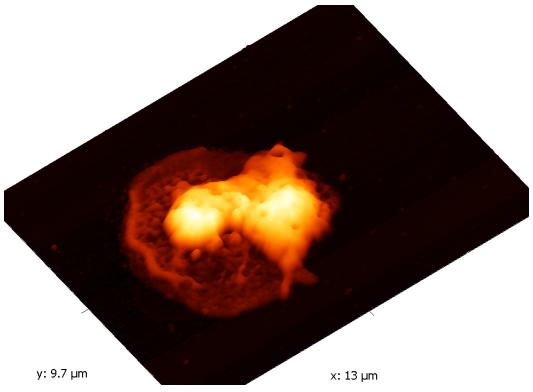

(b)

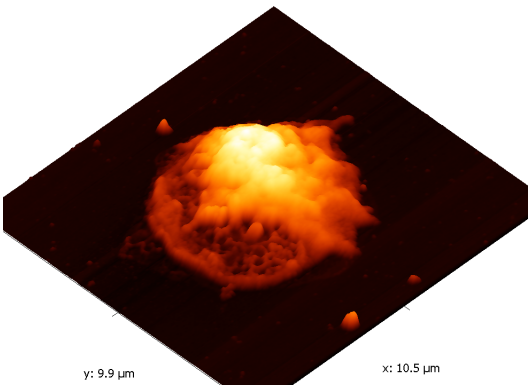

(c)

Figure 5.29: a) AFM deflection error of platelets from WB captured on 6 μm fibrinogen spots. b) and c) are the 3D surface plots of the top two spots. Imaged in contact mode in air on dried platelets with tip speed 12 μm/s.

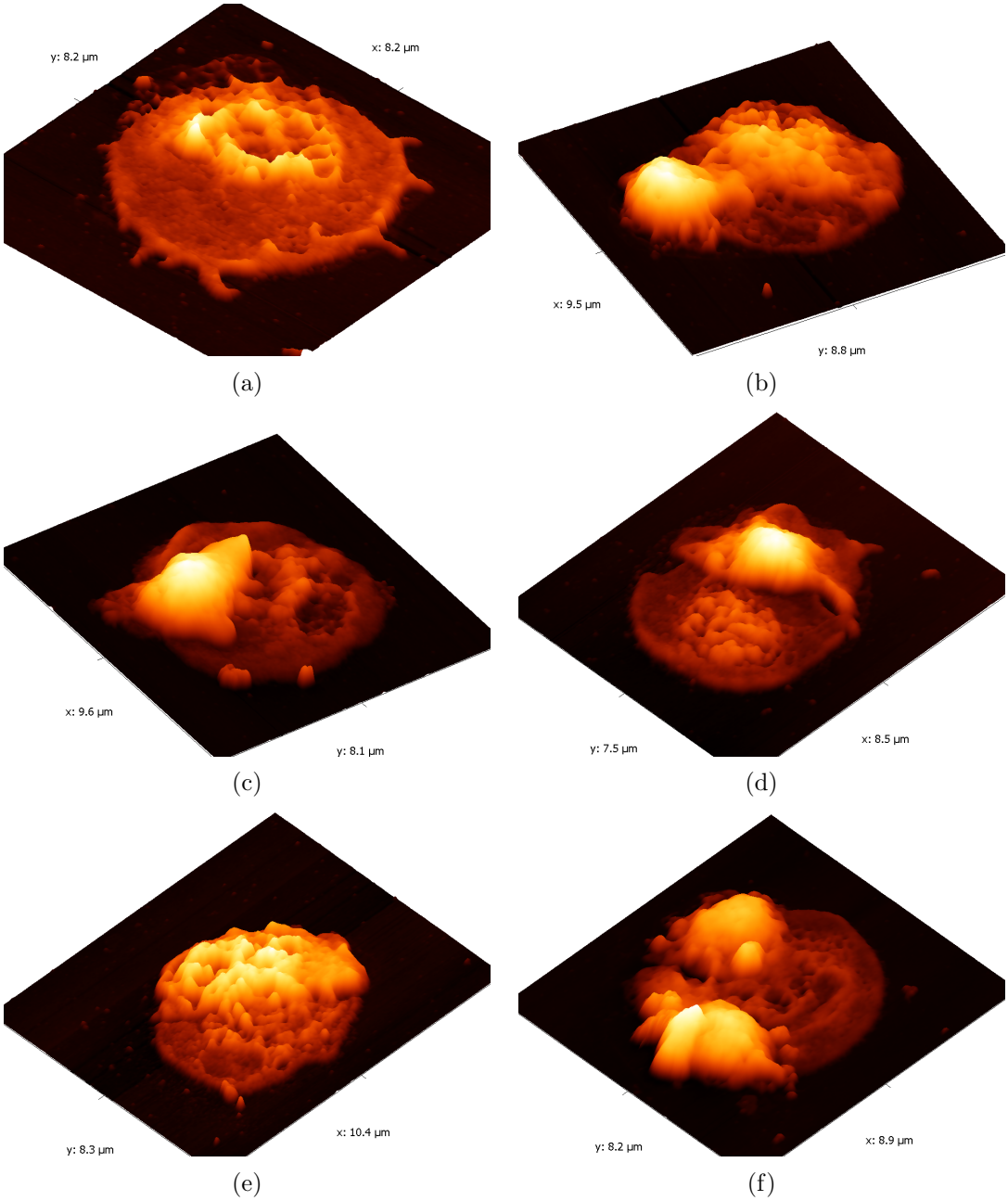

Figure 5.30: AFM 3D surface plots of the platelets in figure 5.29 (from the right top one to the last one).

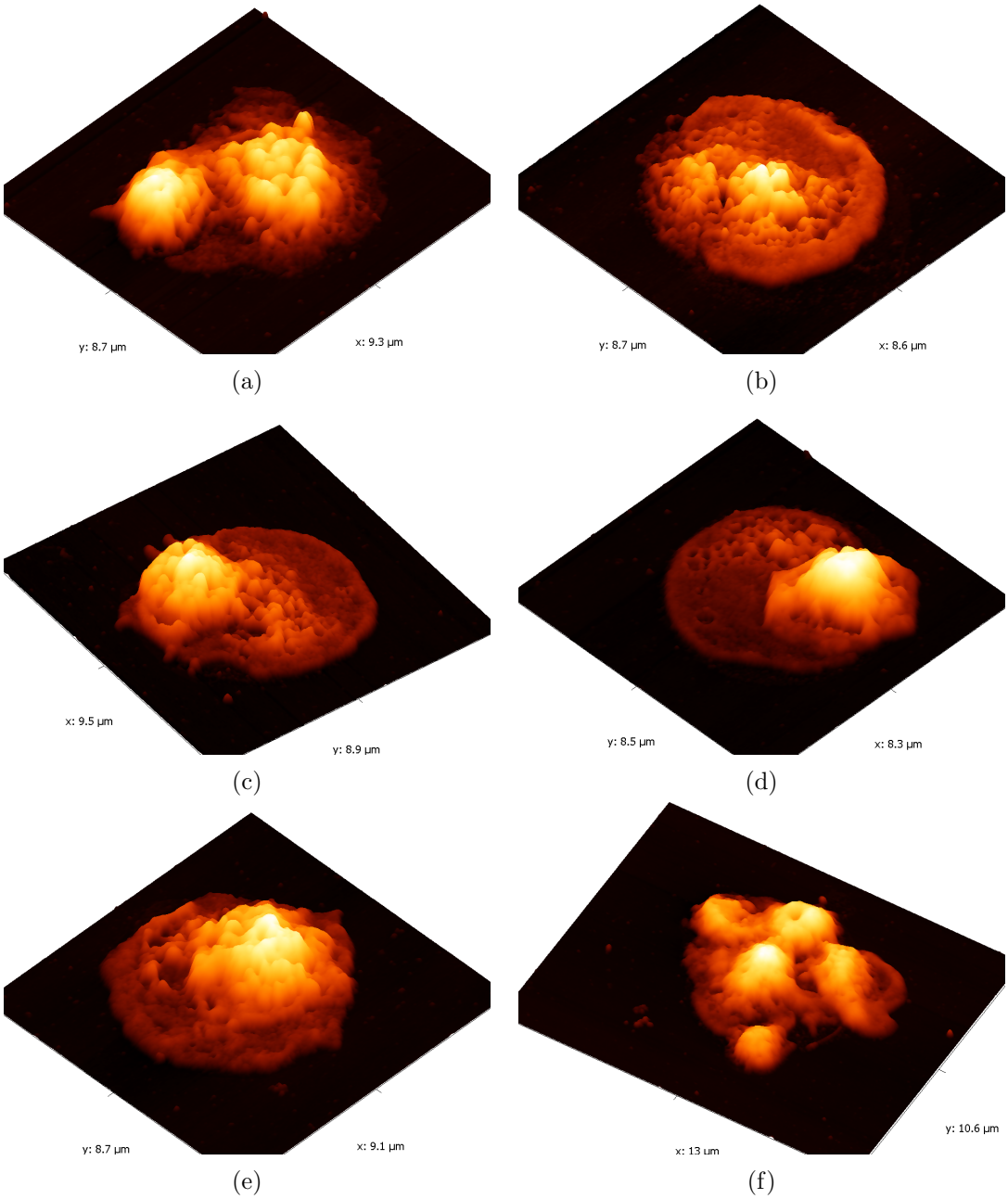

Figure 5.31: AFM 3D surface plots of the platelets in figure 5.32.

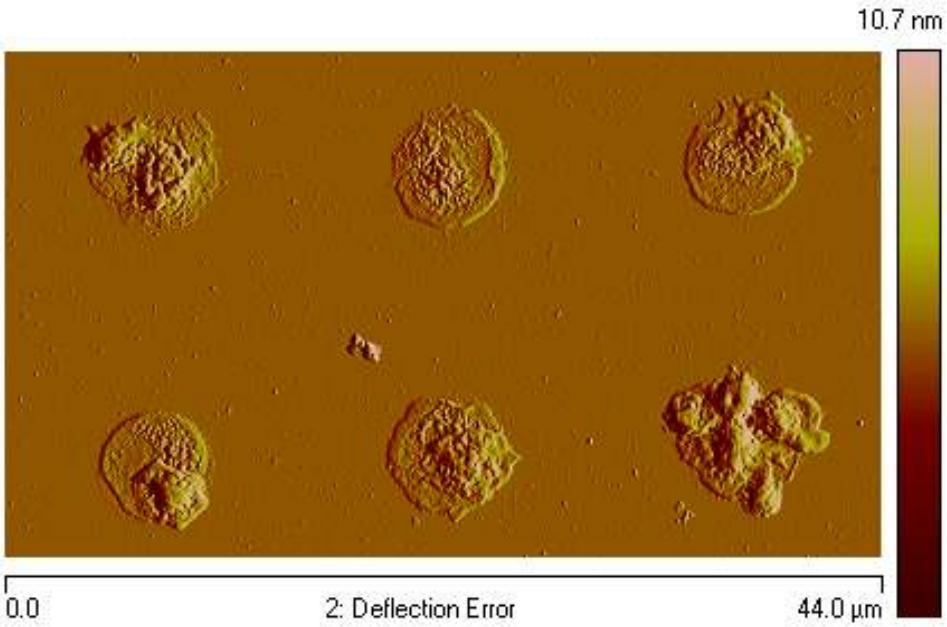

Figure 5.32: AFM deflection error of platelets from WB captured on 6 μm fibrinogen spots. Imaged in contact mode in air on dried platelets with tip speed 12 μm/s.

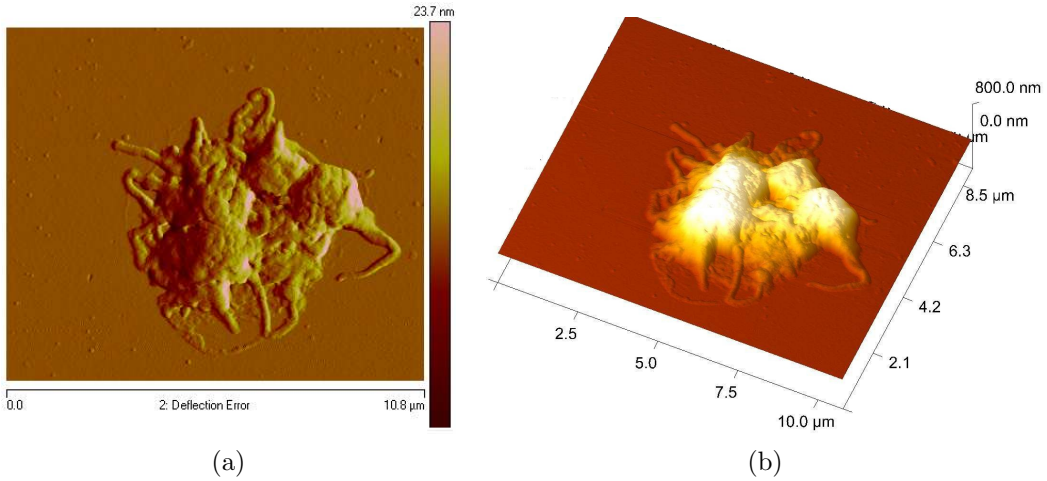

(a) (b)

Figure 5.33: AFM deflection error and 3D surface plots of a 780 nm tall aggregate of platelets from WB captured on a 6 μm fibrinogen spot.

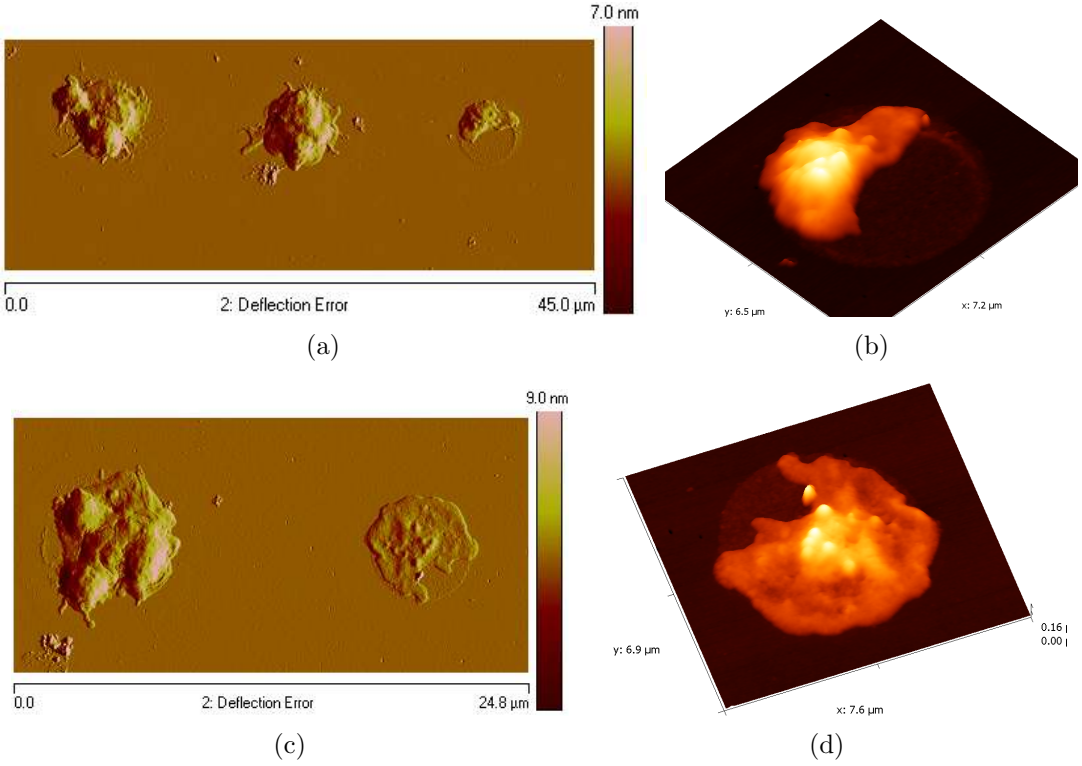

(a) (b)

(c) (d)

Figure 5.34: AFM deflection error and 3D surface plots of platelets from WB captured on 6 μm fibrinogen spots and not spreading completely over the fibrinogen area. Imaged in contact mode in air on dried platelets with tip speed 12 μm/s.

With the addition of an activator

As already seen in the fluorescence analysis with activation-specific antibodies (section 5.3.2) a further investigation was performed for samples in which the blood was pre-activated by adenosine diphosphate (ADP). 1 μM of ADP was added soon after putting the blood in incubation on the fibrinogen surface.

These slides present a lower platelet occupancy compared to the samples in which no pre-activation is induced (see figure 5.35).

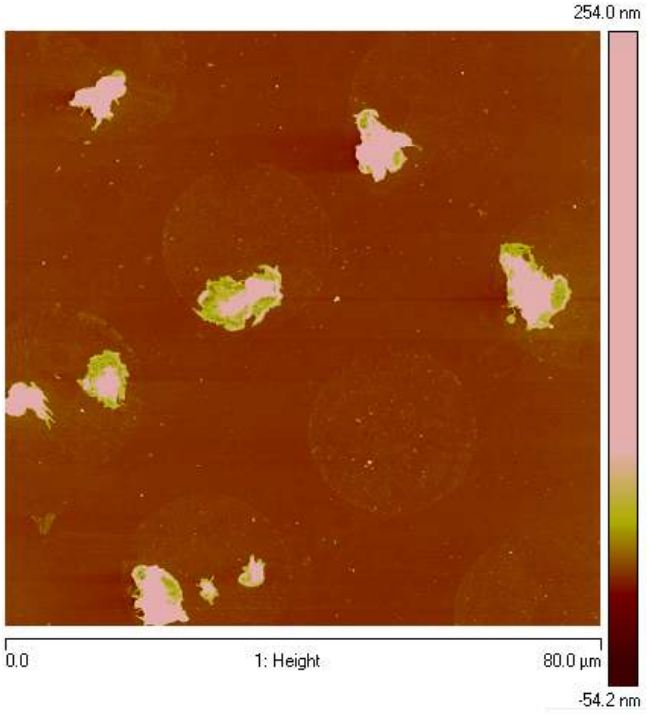

Figure 5.35: AFM height image of platelets pre-activated with ADP in WB and captured on 24 μm fibrinogen spots. Occupancy level is low. Imaged in contact mode in air on dried platelets with tip speed 12 μm/s.

An interesting behaviour was observed for some platelets adhering to the 12 μm spots, as reported in figure 5.36. Platelets connect to each other through their pseudopia in a chain maintaining their globular shape. The 12 μm spot of figure 5.36a shows a group of 3-4 platelets whose membranes spread flat over the fibrinogen area (as seen previously for platelets not pre-activated) and with a connected chain of globular platelets outside from the fibrinogen pattern. Also in figure 5.36c

platelets adhering to the fibrinogen are connected to a platelet outside the spot.

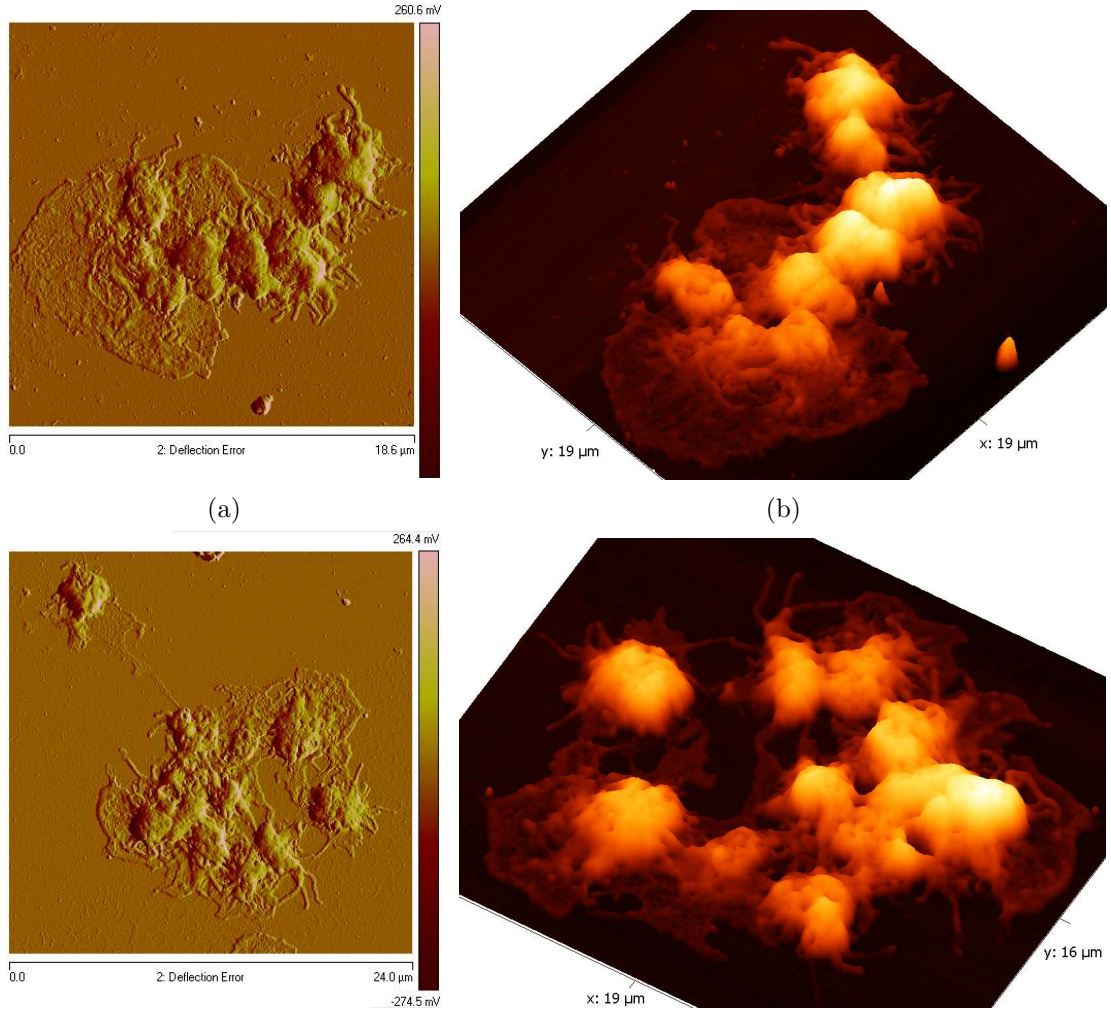

Figure 5.36: AFM deflection error and 3D surface plots of platelets pre-activated with ADP in WB and captured on 12 μm spots. Platelets connected to each other in a chain. Imaged in contact mode in air on dried platelets with tip speed 12 μm/s.

On 6 μm fibrinogen spots the occupancy level is around 60 %, as already shown in figure 5.22 of the confocal analysis. The morphology of the platelets confined in these areas does not present significant difference compared to when no activator is introduced. In figure 5.38 is shown a couple of platelets adhering to the 6 μm

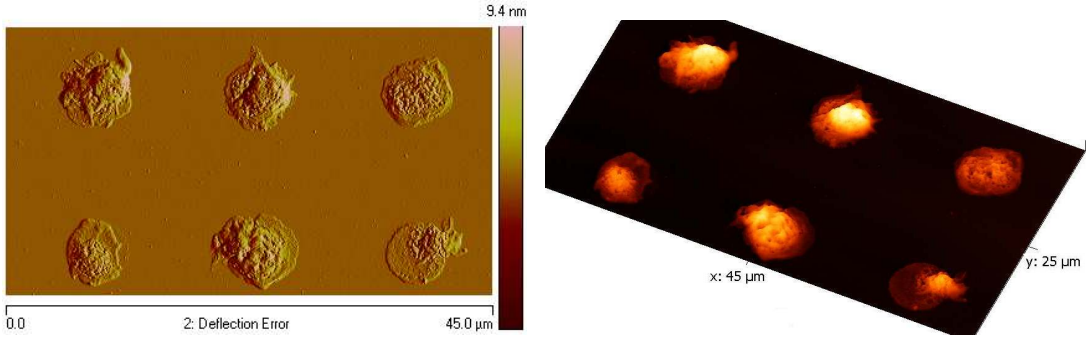

(a) (b)

Figure 5.37: AFM deflection error and 3D surface plots of platelets pre-activated with ADP in WB and captured on 6 μm fibrinogen spots. Imaged in contact mode in air on dried platelets with tip speed 12 μm/s.

spot in a way similar to what we saw in figure 5.30d of non-pre-activated platelets.

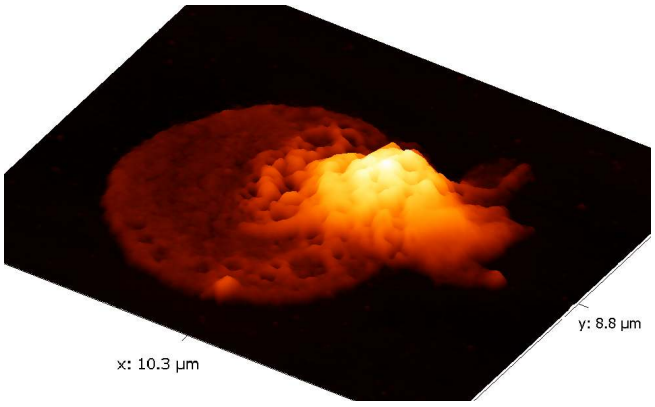

Figure 5.38: AFM height image of pre-activated platelets on a 6 μm fibrinogen spot. (Detail of picture 5.37b).

Other examples of the morphology of pre-activated platelets on 6 μm spots include groups of more platelets (figure 5.39), groups of one-two platelets spreading all over the protein (figure 5.40) and groups of platelets not totally covering the fibrinogen area (figure 5.41).

The results obtained for pre-activated platelets have minor differences to the

results acquired for platelets without the addition of an activator. Nevertheless they present few peculiarities which would be interesting to investigate in a specially designed study (see also the discussion for these surfaces reported at the end of section 5.3.2).

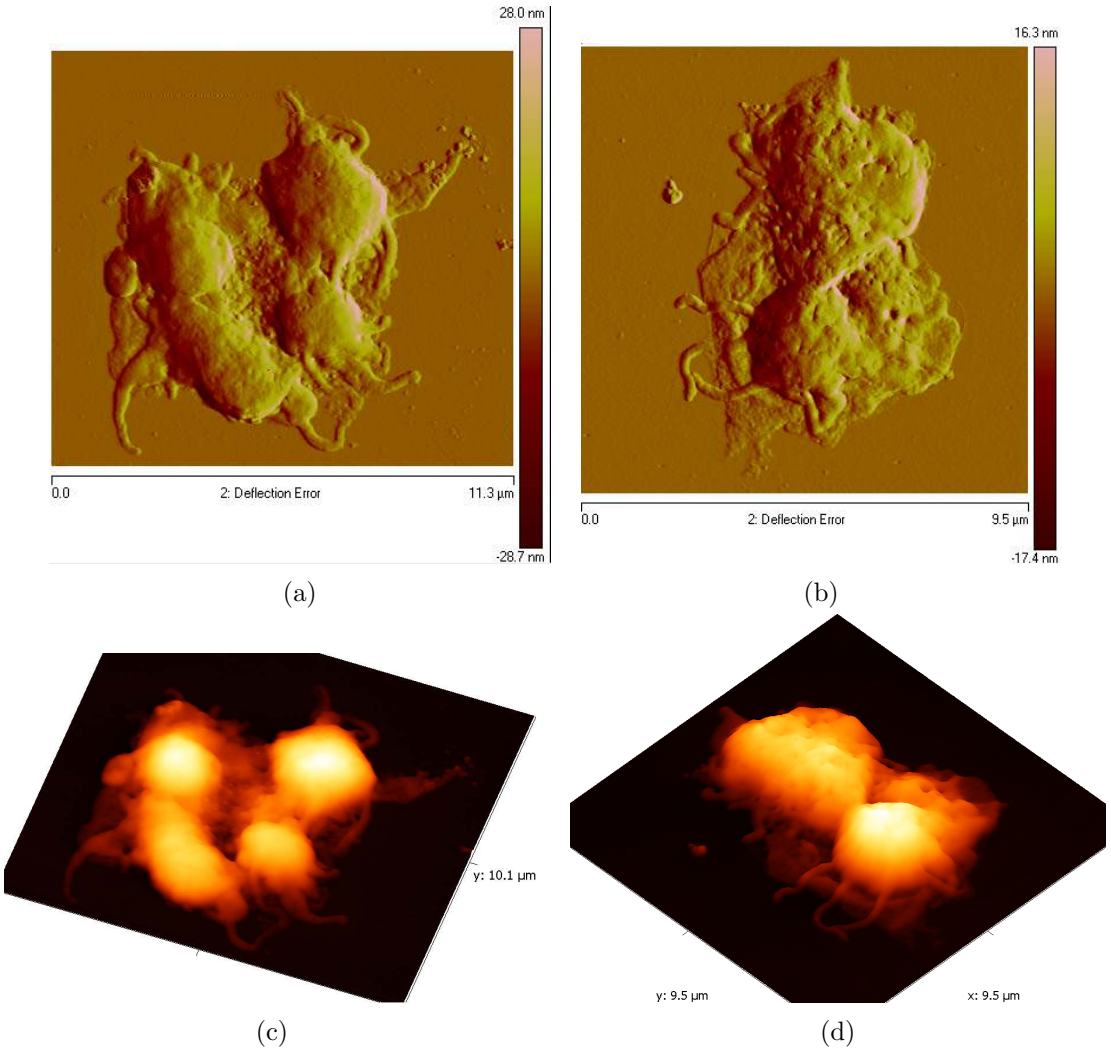

(a) (b)

(c) (d)

Figure 5.39: Examples of platelets pre-activated with ADP in WB and captured on 6 μm fibrinogen spots. Platelets adhere on groups of 3-4 platelets. a) and b) are the AFM deflection error images, and b) and c) their relative 3D surface plots. Imaged in contact mode in air on dried platelets with tip speed 12 μm/s.

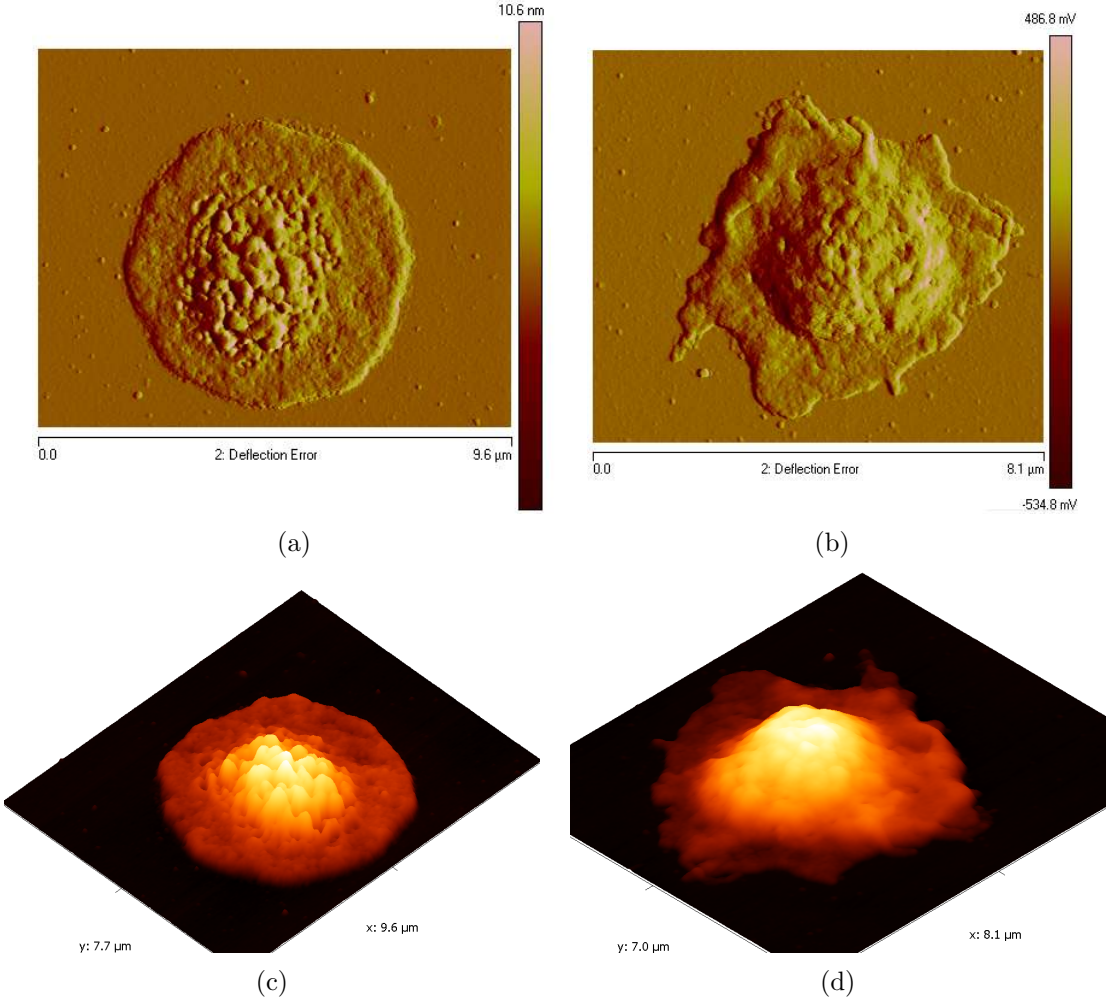

Figure 5.40: Examples of platelets pre-activated with ADP in WB and captured on 6 μm fibrinogen spots. Single platelets adhere on the spots spreading their membrane. a) and b) are the AFM deflection error images, and b) and c) their relative 3D surface plots. Imaged in contact mode in air on dried platelets with tip speed 12 μm/s.

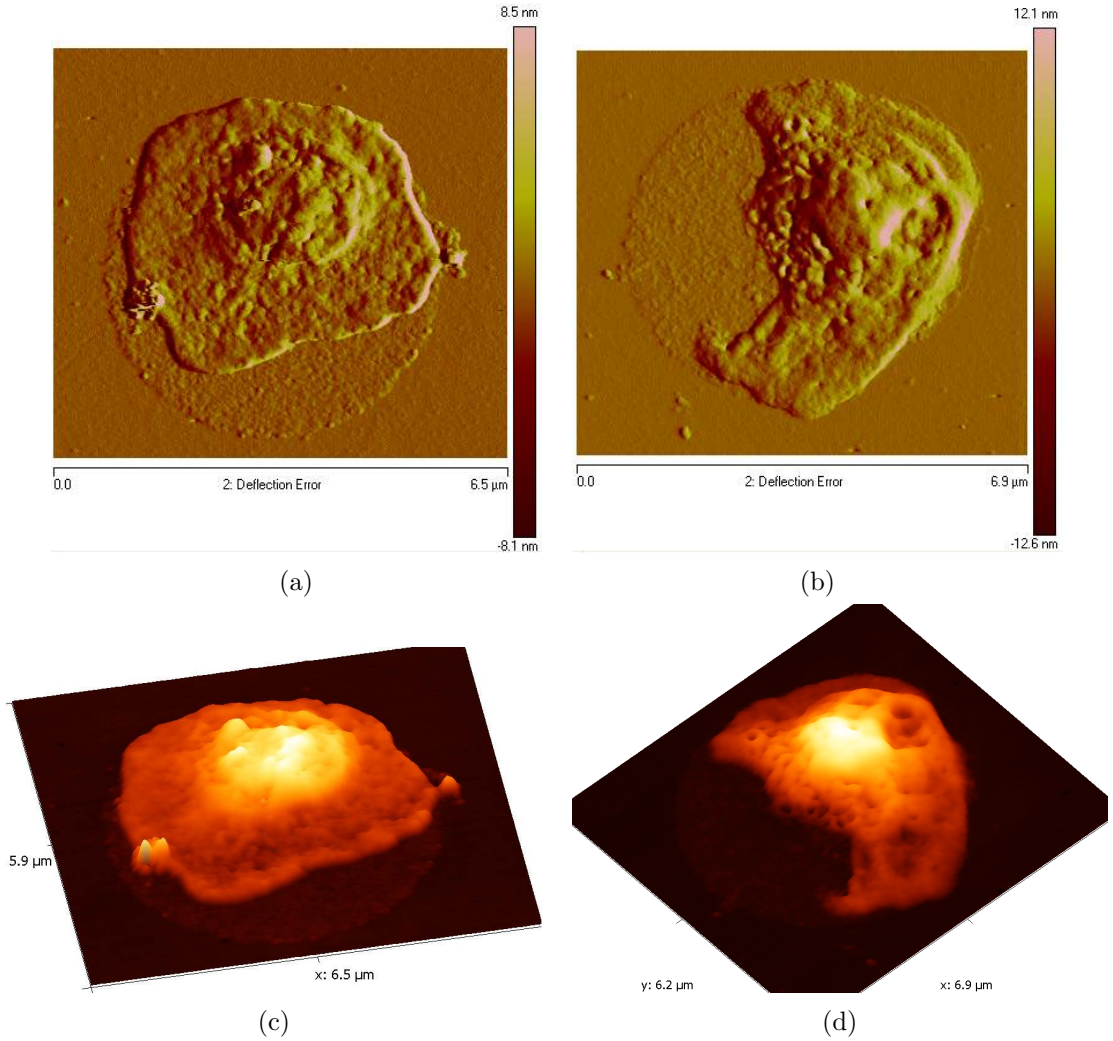

(a) (b)

(c) (d)

Figure 5.41: Examples of platelets pre-activated with ADP in WB and captured on 6 μm fibrinogen spots. Single platelets adhere on the spots partially covering the fibrinogen area. a) and b) are the AFM deflection error images, and b) and c) their relative 3D surface plots. Imaged in contact mode in air on dried platelets with tip speed 12 μm/s.

5.4.3 Platelets on anti-CD42b printed pattern

The second type of surface investigated was composed of anti-CD42b antibodies printed in the same circular micro-patterns of the previously presented samples. These surfaces were prepared by our partner in RCSI.

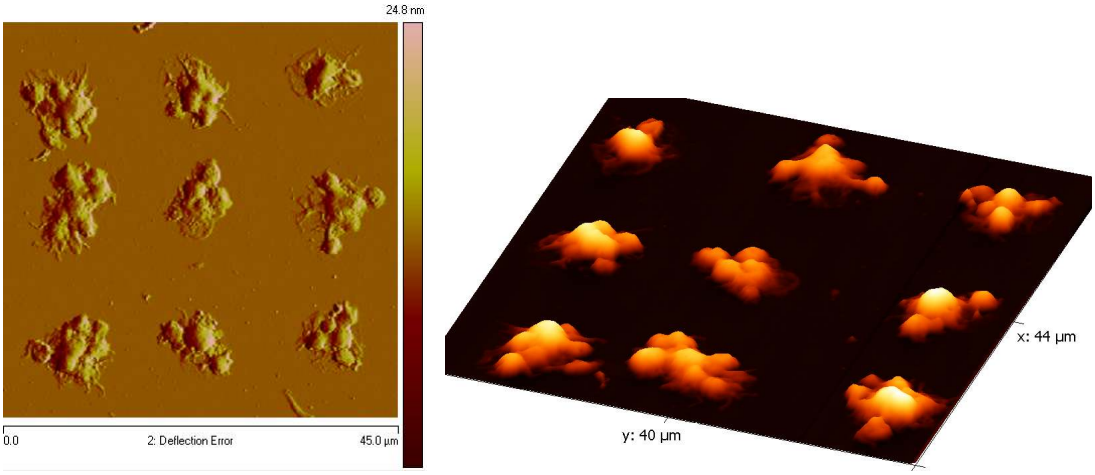

(a) (b)

Figure 5.42: Low resolution overview image of platelets from WB captured on 6 μm anti-CD42b spots. Each of the spot has a group of more than 3 globular-shaped platelets. a)AFM deflection error and b)3D surface plot. Imaged in contact mode in air on dried platelets, tip speed = 20 μm/s, samples/line =256 and lines = 256.

Platelets adhere on micro-patterned anti-CD42 spots in a way substantially different from what is seen on fibrinogen patterns. On 6 μm anti-CD42b spots platelets do not spread their membrane flat over the patterned area, but instead retain their globular shape. Moreover the number of platelets per spot is generally higher, with spots presenting 7 or more platelets.

The average maximum height is 780 nm, significantly greater than the height of platelets over fibrinogen patterned areas. On anti-CD42b platelets spread less and have a higher tendency to pile up one over the other.
Rarely is found a spot with the morphology characteristics observed for platelets on fibrinogen. One of the few example is shown in figure 5.44b where one platelet spreads its membrane in a thin layer over the spot and a second platelet adheres

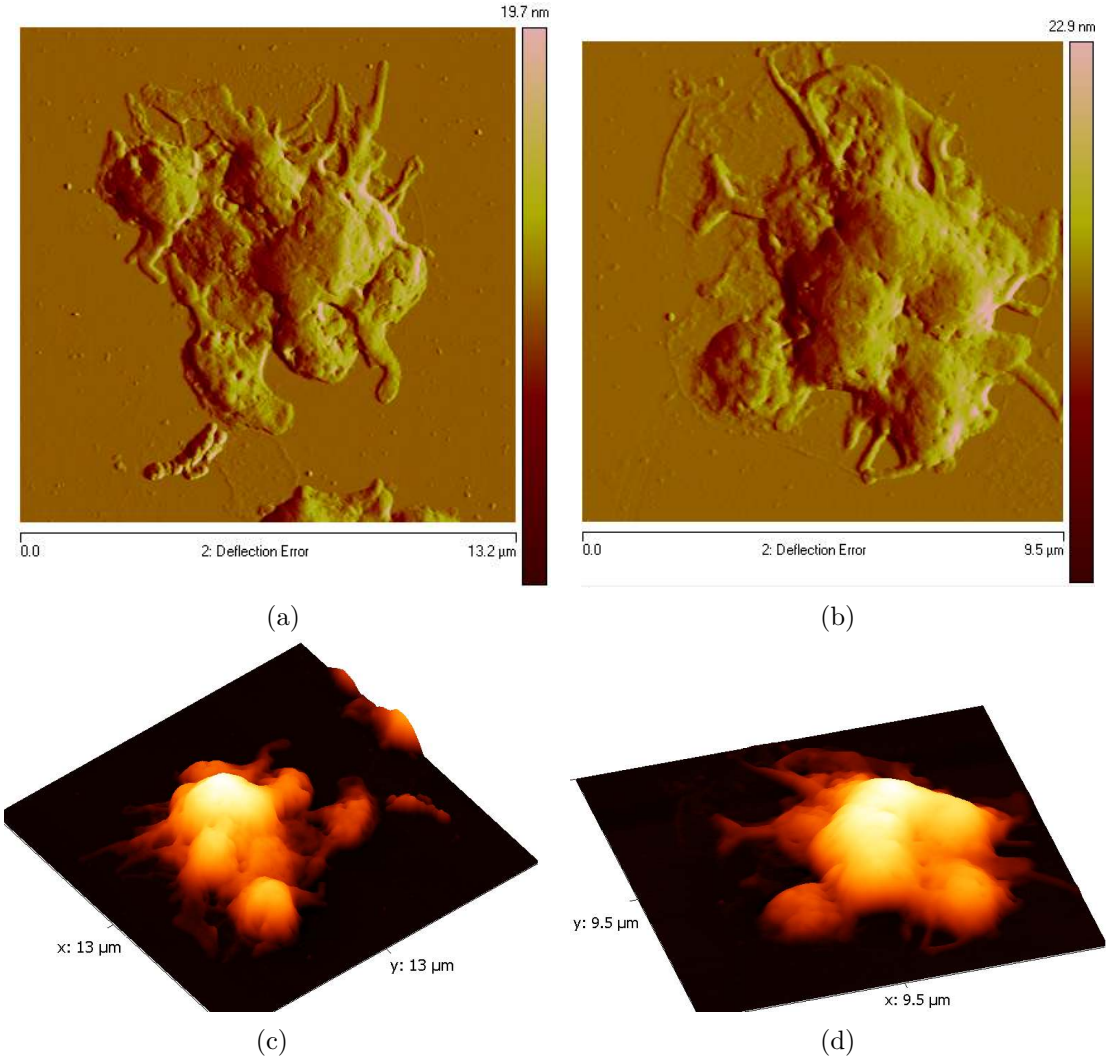

(a) (b)

(c) (d)

Figure 5.43: Examples of platelets from WB captured on 6 μm anti-CD42b spots. Big groups of platelets are adhering on the spots. The spreading of platelet membranes is low. a) and b) are the AFM deflection error images, and b) and c) their relative 3D surface plots. Imaged in contact mode in air on dried platelets with tip speed 12 μm/s.

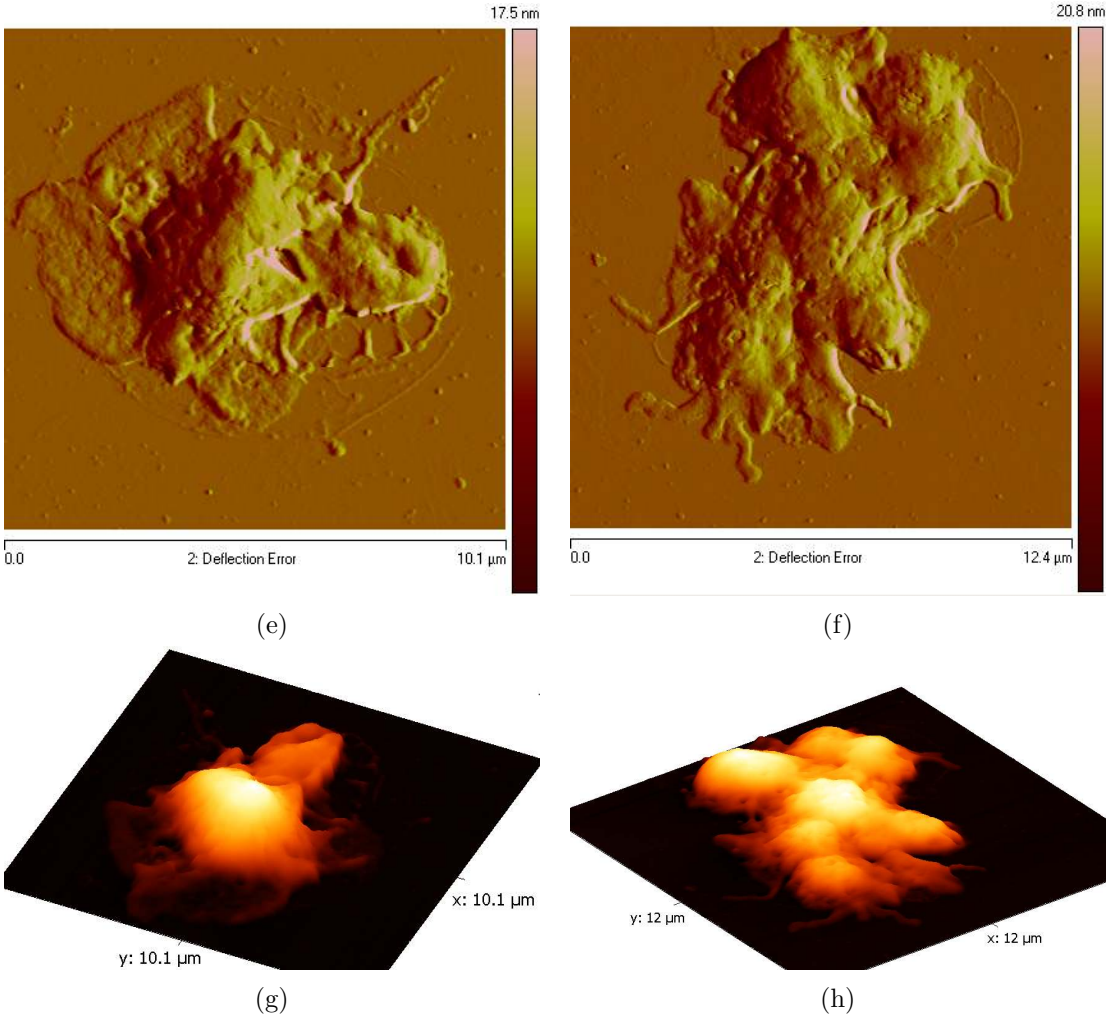

(e) (f)

(g) (h)

Figure 5.43: Examples of platelets from WB captured on 6 μm anti-CD42b spots. Big groups of platelets are adhering on the spots. The spreading of platelet membranes is low. e) and f) are the AFM deflection error images, and g) and h) their relative 3D surface plots. Imaged in contact mode in air on dried platelets with tip speed 12 μm/s.

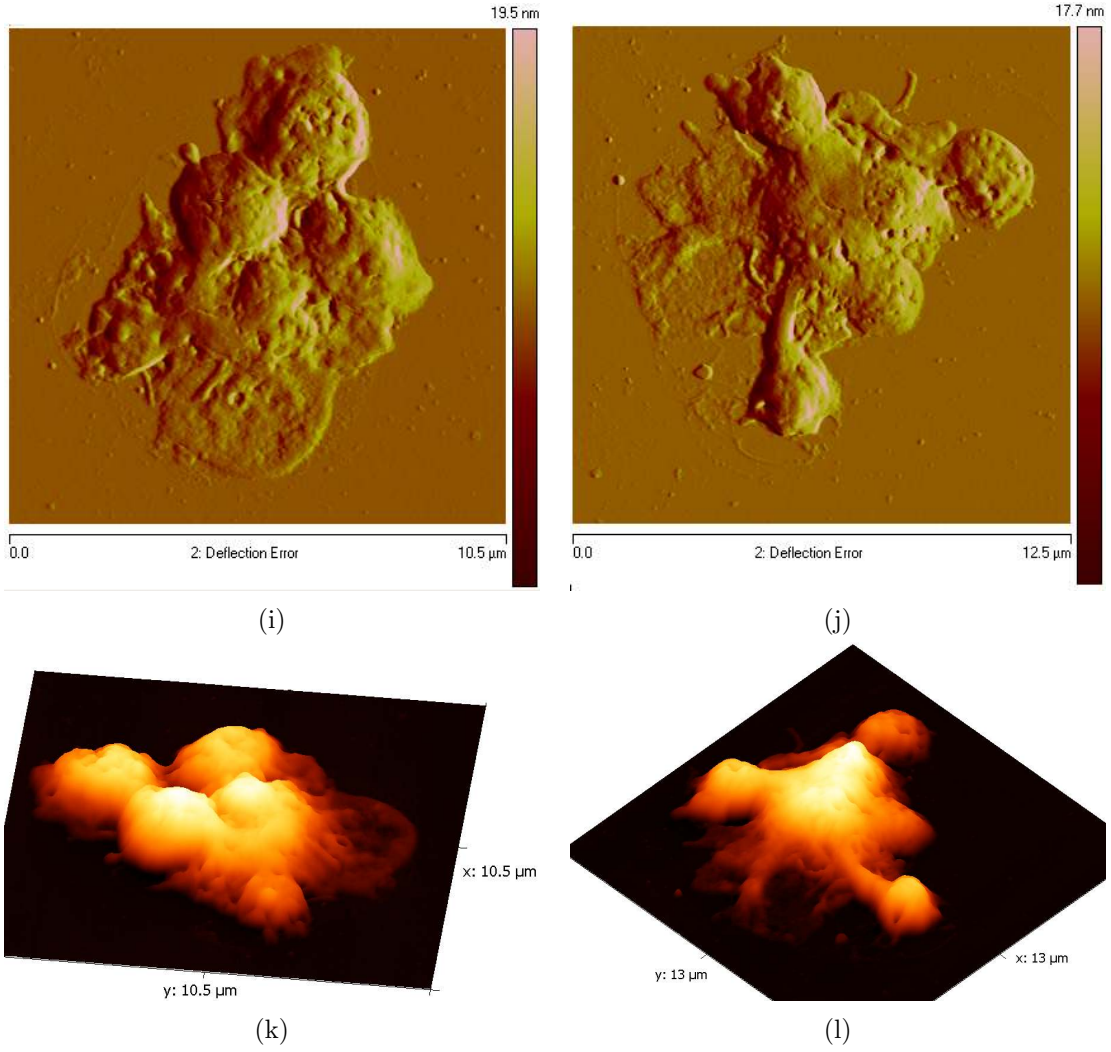

(i) (j)

(k) (l)

Figure 5.43: Examples of platelets from WB captured on 6 μm anti-CD42b spots. Big groups of platelets are adhering on the spots. The spreading of platelet membranes is low. i) and j) are the AFM deflection error images, and k) and l) their relative 3D surface plots. Imaged in contact mode in air on dried platelets with tip speed 12 μm/s.

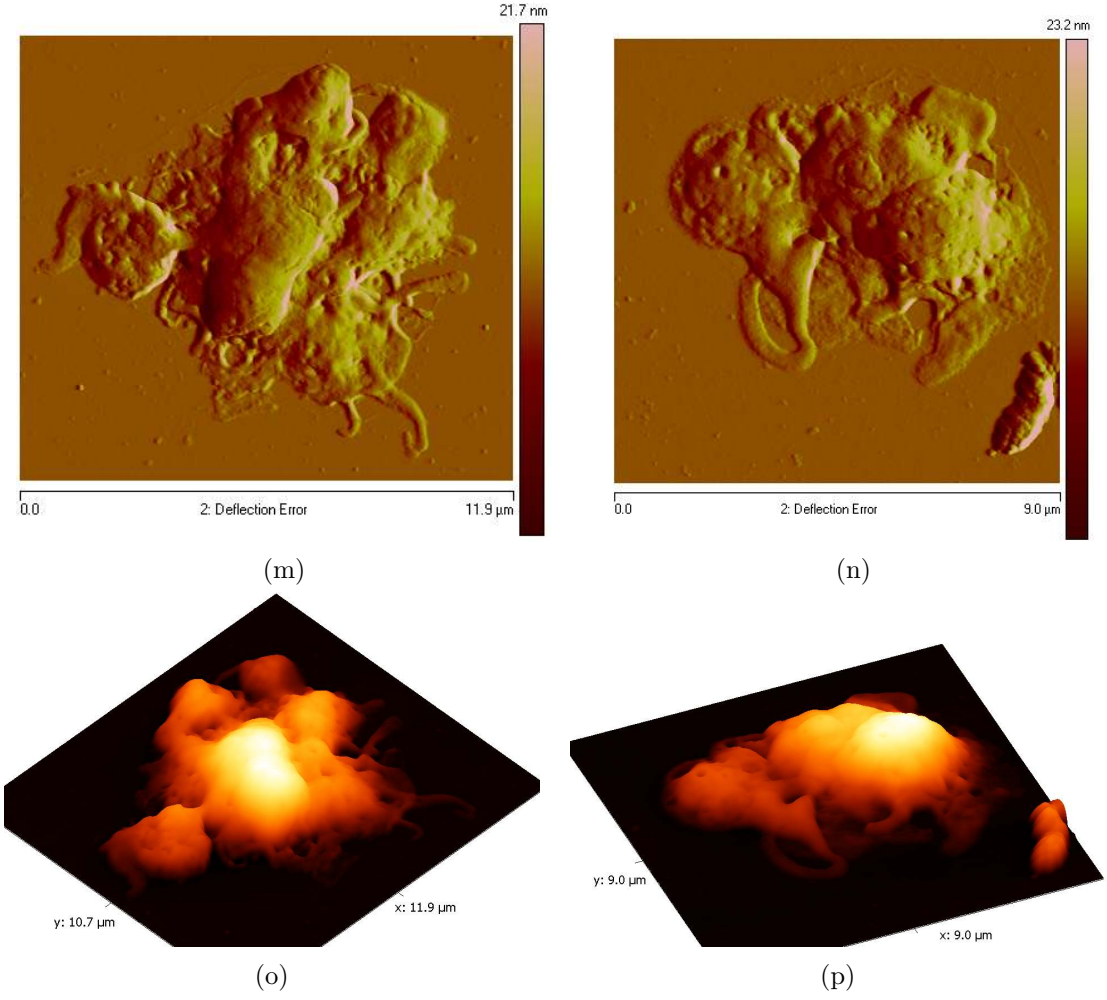

(m) (n)

(o) (p)

Figure 5.43: Examples of platelets from WB captured on 6 μm anti-CD42b spots. Big groups of platelets are adhering on the spots. The spreading of platelet membranes is low. m) and n) are the AFM deflection error images, and o) and p) their relative 3D surface plots. Imaged in contact mode in air on dried platelets with tip speed 12 μm/s.

on the top of the first one.

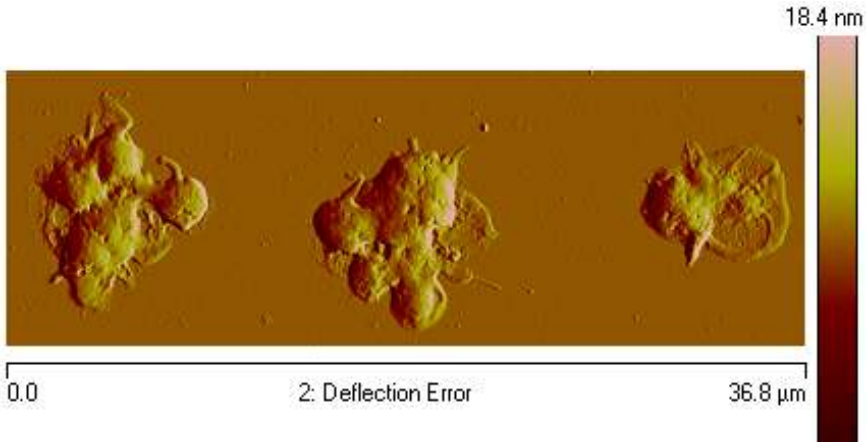

(a)

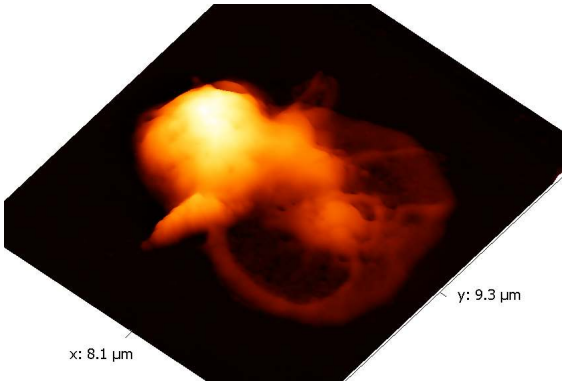

(b)

Figure 5.44: Platelets from WB captured on 6 μm anti-CD42b pattern showing a spot with only 1-2 platelets and with spread morphology. a) AFM deflection error image and b)3D surface plot of the right anti-CD42b spot. Imaged in contact mode in air on dried platelets with tip speed 12 μm/s.

In the next section (5.4.4) is discussed a numerical comparison of the effects that the two different surfaces have on immobilized platelets.

5.4.4 Data comparison

Platelets on fibrinogen micro-printed surfaces adhere in a different way compared to how they adhere on anti-CD42b. As explained in section 5.3.2 fibrinogen is a molecule included in the activation chain process whereas anti-CD42b targets a receptor which is not involved in activation.

A numerical analysis was performed on the platelets confined in the 6 μm spots, which have a high occupancy and a low number of platelets per spot.

One of the most evident differences is that platelets adhere to anti-CD42b clustering in globular groups, while on fibrinogen there are only a few platelets spread almost flat. For each of the spots the number of platelets present can be supposed by looking at the "bumps" in the 3D surface plot. This is a fast and easy way to estimate, but cannot be the basis of a numerical analysis. A more reliable way is to calculate the volume of each spot, and build a histogram of volume frequency.

For each of the spots a 2D height image was plotted and processed to set a height-threshold under which the glass surface and the fibrinogen/anti-CD42b layer are located and over which the whole platelet group is located. The volume is then calculated for only the part of the data over the threshold, i.e. only for a platelet group. The minimum group volume observed was ≈ 1.6 μm^3, found for platelets immobilized on the fibrinogen pattern. This value was related to a platelet group assumed to be composed of one single platelet. Taking into consideration this minimum value, a volume frequency histogram was created with step separation of 2 μm^3. Groups of platelets with volume between 1 and 2 μm^3 are likely to contain one platelet only, groups with volume between 3 and 4 μm^3 could be composed of 2 platelets, etc.. but no precise assumption on the platelet number per spot can be actually made. The volume of a platelet varies from platelet to platelet.

The volume frequency histograms for the two surfaces are presented in figure 5.45. The histograms comparison support what was seen visually in the 2D surface plots: on fibrinogen micro-patterns platelets adhere in groups of fewer platelets (= smaller volumes) compared to the platelet groups immobilized on anti-CD42b spots.

Besides calculating the volume, the total surface area of the group over the protein layer, the projected area of the group (i.e. the area of the surface occupied

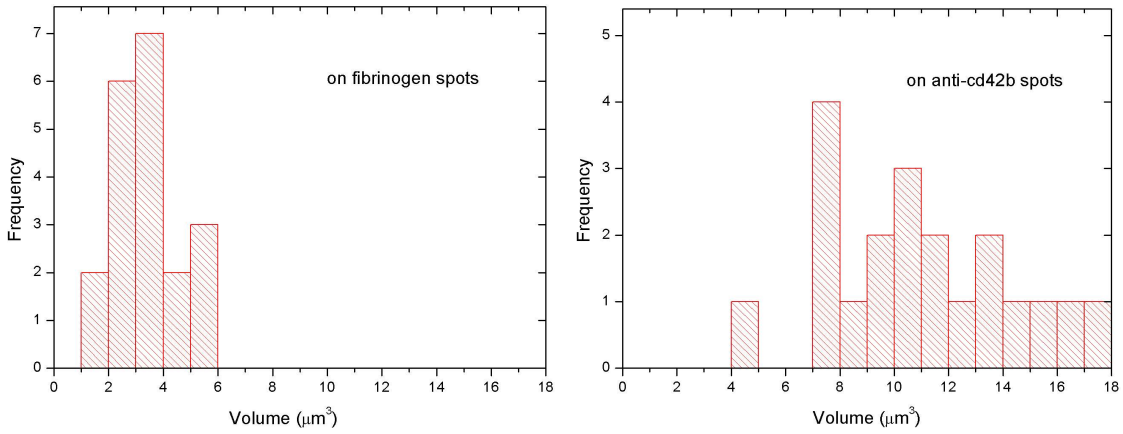

(a) (b)

Figure 5.45: Volume frequency histogram for platelets immobilized on 6 μm spots a) of fibrinogen and b) of anti-CD42b. On anti-CD42b spots platelets adhere in groups of high volume (= more platelets per spot) compared to fibrinogen surfaces where small volumes groups are found.

by the platelets group) and the surface area of the parts of the group exceeding half height of the group itself (defined later on as "surface area at half height") are also calculated for each group of platelets. These data are then averaged over all the analyzed spots. Figure 5.46 summarizes the data obtained.
In 5.46a it can be seen that groups of platelets on 6 μm anti-CD42b spots have an average total surface area higher than platelets immobilized in spots of the same dimensions composed of fibrinogen, being composed of more "bumps" of platelets. Also the projected surface area is higher, meaning that platelets on anti-CD42b patterns expand on average more over the patterned spots. The surface area at half height is, on average, a quarter of the total surface area for platelets on anti-CD42b and one seventh for platelets on fibrinogen. This is quite understandable when considering that groups of platelets on fibrinogen are generally shaped as "fried-eggs", with the main part of the membranes located in the lower part of the group, while instead platelets on anti-CD42b collect in groups maintaining their globular shape.

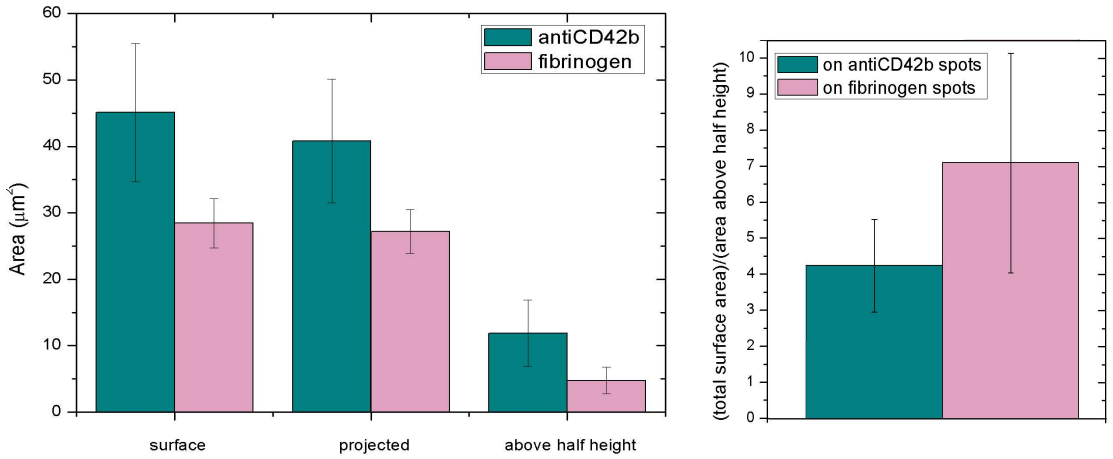

(a) (b)

Figure 5.46: a) Average of total surface area, projected area and surface area at half height for groups of platelets confined on 6 μm spots of fibrinogen or of anti-CD42b. b) Ratio between the average total surface area and the average surface area at half height.

5.4.5 Summary of results

By using AFM it was possible to investigate the different morphologies that platelets assume when immobilized on micro-patterns.

- Platelets adhere on fibrinogen patterns by spreading their membrane flat over the protein in a "fried-egg" style, while they have a globular shape when the pattern is composed of a molecule that does not induce activation (anti-CD42b).
- On 6 μm fibrinogen spots, groups are composed of one or few platelets, while on anti-CD42b spots, groups are always composed of aggregates of more platelets.
- Platelet groups are higher on anti-CD42b patterns, with bigger volumes and with bigger average surface area.

These results show that AFM is a valid tool to discriminate platelet morphology which is related to their activation status.

Chapter 6

Summary and future work

6.1 Overall summary

Silica NPs were synthesized in which are encapsulated NIR664 dye. The NPs have been characterized using DLS, TEM, zeta potential and brightness measurement. Spherical NPs of average diameter 90 ± 15 nm were produced with a good degree of monodispersity. Two different NP-platelet conjugation approaches were tested but much work has still to be done to maximize the efficiency of NP-antibody conjugation and of platelet labelling. The compatibility of the NPs with platelets was investigated using platelet aggregometry test and flow cytometry which indicated that the platelets are not activated in the presence of the NPs. A short study of platelet autofluorescence was carried out to investigate whether there was any correlation between spectral properties with platelet characteristics. Although this investigation is interesting and platelet autofluorescence has not been widely reported in literature, no direct correlation was found between any aspect of the fluorescence and the platelet characteristics. However, this study did establish that, in order to implement the NP-assay, the brightness will need to exceed the platelet autofluorescence, hence the importance of increasing the NP brightness.

Platelet immobilization protocols were tested and characterized through AFM and confocal imaging of fluorescence or autofluorescence signals. The achieved adherence is space controllable by using micro-printed protein patterns which are regular in shape and homogeneous in thickness. Antibody sandwich assays which target the platelet receptor GPIIb-IIIa were efficiently performed on platelets immobilized on glass and on protein patterned surfaces. Studies of platelets in con-

fined micrometer sized areas show the possibility of discerning the platelet activation state with the use of activation specific antibodies or with AFM investigation of platelet morphology.

Together these results show both the development of novel high brightness probes for cell detection and a rapid, highly controllable cell purification technique. Both of these areas have each yielded new insights into the activation state of human platelets and together provide the bases of a novel blood platelet diagnostic platform.

6.2 Future work

- Optimization of NP brightness.
- Development of new protocols for NP-antibody conjugation.
- Optimization of NP-platelet conjugation and elimination of non-specific binding.
- Deeper understanding of the role of different immobilization surfaces on platelets.
- A wider study of morphology and fluorescence signal of platelets on micropatterned surfaces.
- Achievement of controlled confinement of single platelets only.

Bibliography

[1] Andrew Burns, Hooisweng Ow, and Ulrich Wiesner. Fluorescent core-shell silica nanoparticles: towards "lab on a particle" architectures for nanobiotechnology. *Chemical Society Reviews*, 35(11):1028–1042, 2006.

[2] R. P. Haugland. The handbook - a guide to fluorescent probes and labeling technologies 10th edn. Molecular Probes, Eugene, OR, 2005.

[3] Rahul P. Bagwe, Chaoyong Yang, Lisa R. Hilliard, and Weihong Tan. Optimization of dye-doped silica nanoparticles prepared using a reverse microemulsion method. *Langmuir*, 20(19):8336–8342, 2004.

[4] Hooisweng Ow, Daniel R. Larson, Mamta Srivastava, Barbara A. Baird, Watt W. Webb, and Ulrich Wiesner. Bright and stable core-shell fluorescent silica nanoparticles. *Nano Letters*, 5(1):113–117, 2005.

[5] Swadeshmukul Santra, Peng Zhang, Kemin Wang, Rovelyn Tapec, and Weihong Tan. Conjugation of biomolecules with luminophore-doped silica nanoparticles for photostable biomarkers. *Analytical Chemistry*, 73(20):4988–4993, 2001.

[6] Y. F. Zhu, J. S. Lian, and Q. Jiang. Modeling of the melting point, debye temperature, thermal expansion coefficient, and the specific heat of nanostructured materials. *The Journal of Physical Chemistry C*, 113(39):16896–16900, 2009.

[7] Heng Huang, Savas Delikanli, Hao Zeng, Denise M. Ferkey, and Arnd Pralle. Remote control of ion channels and neurons through magnetic-field heating of nanoparticles. *Nature Nanotechnology*, 5(8):602 –606, 2010.

[8] Christoph Alexiou, Roswitha Schmid, Roland Jurgons, Marcus Kremer, Gerhard Wanner, Christian Bergemann, Ernst Huenges, Thomas Nawroth, Wolfgang Arnold, and Fritz Parak. Targeting cancer cells: magnetic nanoparticles as drug carriers. *European Biophysics Journal*, 35:446–450, 2006.

[9] Daniel R. Larson, Warren R. Zipfel, Rebecca M. Williams, Stephen W. Clark, Marcel P. Bruchez, Frank W. Wise, and Watt W. Webb. Water-Soluble Quantum Dots for Multiphoton Fluorescence Imaging in Vivo. *Science*, 300(5624):1434–1436, 2003.

[10] Diane Djoumessi Lekeufack, Arnaud Brioude, Anthony W. Coleman, Philippe Miele, Joel Bellessa, Li De Zeng, and Pierre Stadelmann. Core-shell gold j-aggregate nanoparticles for highly efficient strong coupling applications. *Applied Physics Letters*, 96(25):253107–1–253107–3, 2010.

[11] Ivan H. El-Sayed, Xiaohua Huang, and Mostafa A. El-Sayed. Surface plasmon resonance scattering and absorption of anti-egfr antibody conjugated gold nanoparticles in cancer diagnostics: Applications in oral cancer. *Nano Letters*, 5(5):829–834, 2005.

[12] Thomas J. Webster. *Safety of Nanoparticles - From Manufacturing to Medical Applications*. Springer - Verlag, 2009.

[13] Xiaojun Zhao, Lisa R. Hilliard, Shelly John Mechery, Yanping Wang, Rahul P. Bagwe, Shouguang Jin, and Weihong Tan. A rapid bioassay for single bacterial cell quantitation using bioconjugated nanoparticles. *Proceedings of the National Academy of Sciences*, 101(42):15027–15032, 2004.

[14] Yu-Shen Lin, Chih-Pin Tsai, Hsing-Yi Huang, Chieh-Ti Kuo, Yann Hung, Dong-Ming Huang, Yao-Chang Chen, and Chung-Yuan Mou. Well-ordered mesoporous silica nanoparticles as cell markers. *Chemistry of Materials*, 17(18):4570–4573, 2005.

[15] Indrajit Roy, Tymish Y. Ohulchanskyy, Dhruba J. Bharali, Haridas E. Pudavar, Ruth A. Mistretta, Navjot Kaur, and Paras N. Prasad. Optical tracking of organically modified silica nanoparticles as DNA carriers: A nonviral, nanomedicine approach for gene delivery. *Proceedings of the National Academy of Sciences of the United States of America*, 102(2):279–284, 2005.

[16] Iseult Lynch, Sara Linse, C. Vyvyan Howard, Maciej Stepnik, Konrad Rydzynski, John Hanrahan, Wim de Jong, Dominique Langevin, Joachim Raedler, Wolfgang Parak, Yuri Volkov, Marek Radomski, Robert Thomas, Jacob Klein, Andrew A Barron, Colin Janssen, Fiona M Lyons, Francis Quinn, Bert Swennen, Peter Cuypers, Angela Duffy, and Kenneth A Dawson. Nanointeract: A rational approach to the interaction between nanoscale materials and living matter? *Journal of Physics: Conference Series*, 170(1):012040, 2009.

[17] Tian Xia, Leonar Rome, and Andre Nel. Particles slip cell security. *Nature Materials*, 7:519–520, 2008.

[18] T. Cedervall, M. Foy, I. Lynch, T. Berggard, S. Linse, S. Donnelly, G. Cagney, and K. A. Dawson. Detailed identification of plasma proteins adsorbed on copolymer nanoparticles. *Angewandte Chemie International Edition*, 46(30):5754–5756, 2007.

[19] Marco P. Monopoli, Dorota Walczyk, Abigail Campbell, Giuliano Elia, Iseult Lynch, Francesca Baldelli Bombelli, and Kenneth A. Dawson. Physical-chemical aspects of protein corona: Relevance to in vitro and in vivo biological impacts of nanoparticles. *Journal of the American Chemical Society*, 133(8):2525–2534, 2011.

[20] Sheng-Li Chen, Peng Dong, Guang-Hua Yang, and Jiu-Jin Yang. Kinetics of formation of monodisperse colloidal silica particles through the hydrolysis and condensation of tetraethylorthosilicate. *Industrial and Engineering Chemistry Research*, 35(12):4487–4493, 1996.

[21] K. Osseo-Asare and F. J. Arriagada. Growth kinetics of nanosize silica in a nonionic water-in-oil microemulsion: A reverse micellar pseudophase reaction model. *Journal of Colloid and Interface Science*, 218(1):68 – 76, 1999.

[22] Werner Stober, Arthur Fink, and Ernst Bohn. Controlled growth of monodisperse silica spheres in the micron size range. *Journal of Colloid and Interface Science*, 26(1):62 – 69, 1968.

[23] Jilin Yan, M. Carmen Estévez, Joshua E. Smith, Kemin Wang, Xiaoxiao He, Lin Wang, and Weihong Tan. Dye-doped nanoparticles for bioanalysis. *Nano Today*, 2(3):44 – 50, 2007.

[24] Hirofumi Yamauchi, Tatsuo Ishikawa, and Seiichi Kondo. Surface characterization of ultramicro spherical particles of silica prepared by w/o microemulsion method. *Colloids and Surfaces*, 37:71 – 80, 1989.

[25] M. Ethayaraja, K. Dutta, D. Muthukumaran, and R. Bandyopadhyaya. Nanoparticle formation in water-in-oil microemulsions: experiments, mechanism, and monte carlo simulation. *Langmuir*, 23(6):3418–3423, 2007.

[26] M. de Dios, F. Barroso, C. Tojo, and M.A. Lopez-Quintela. Simulation of the kinetics of nanoparticle formation in microemulsions. *Journal of Colloid and Interface Science*, 333(2):741 – 748, 2009.

[27] Hong Wu, Qisheng Huo, Susan Varnum, Jun Wang, Guodong Liu, Zimin Nie, Jun Liu, and Yuehe Lin. Dye-doped silica nanoparticle labels/protein microarray for detection of protein biomarkers. *Analyst*, 133:1550–1555, 2008.

[28] J. Godoy-Navajas, MP. Aguilar-Caballos, and A. Gómez-Hens. Synthesis and characterization of oxazine-doped silica nanoparticles for their potential use as stable fluorescent reagents. *Journal of Fluorescence*, 20(1):171–180, 2010.

[29] Robert Nooney, Ciara McCahey, Ondrej Stranik, Xavier Le Guevel, Colette McDonagh, and Brian MacCraith. Experimental and theoretical studies of the optimisation of fluorescence from near-infrared dye-doped silica nanoparticles. *Analytical and Bioanalytical Chemistry*, 393:1143–1149, 2009.

[30] Lin Wang, Wenjun Zhao, and Weihong Tan. Bioconjugated silica nanoparticles: Development and applications. *Nano Research*, 1:99–115, 2008.

[31] Peter M. Price, James H. Clark, and Duncan J. Macquarrie. Modified silicas for clean technology. *Journal of the Chemical Society, Dalton Transactions*, 1(2):101–110, 2000.

[32] Claire Harrison and Samuel Machin. *Thrombocytopenia (reduced platelet count)*. Online resource, http://www.netdoctor.co.uk/diseases/facts/ thrombocytopenia.htm, September 2006.

[33] Lisa K. Jennings. Role of platelets in atherothrombosis. *The American Journal of Cardiology*, 103(3, Supplement 1):4A – 10A, 2009.

[34] J. Yip, Y. Shen, M. C. Berndt, and R. K. Andrews. Primary Platelet Adhesion Receptors . *Australian Biochemist*, 35(2):4–8, 2004.

[35] C. Bauters. Atherothrombosis: the same process for different arterial territories? *Annales de cardiologie et d'angeiologie*, 51:177–180, 2002.

[36] Andrew D. Blann, Martin J. Landray, and Gregory Y. H. Lip. ABC of antithrombotic therapy: An overview of antithrombotic therapy. *British Medical Journal*, 325(7367):762–765, 2002.

[37] S. Carr, A.. Farb, WH. Pearce, et al. Atherosclerotic plaque rupture in symptomatic carotid artery stenosis . *Journal of Vascular Surgery*, 23:755–765, 1996.

[38] R. Corti and JJ. Badimon. Biologic aspects of vulnerable plaque . *Current Opinion in Cardiology*, 17:616–625, 2002.

[39] L. Marquardt, A. Ruf, U. Mansmann, et al. Course of platelet activation markers after ischemic stroke. *Stroke*, 33:2570–2574, 2002.

[40] M. Di Napoli and F. Papa. Inflammation, hemostatic markers, and antithrombotic agents in relation to long-term risk of new cardiovascular events in first-ever ischemic stroke patients. *Stroke*, 33:1763–1771, 2002.

[41] LA. Harker. Therapeutic inhibition of platelet function in stroke. *Cerebrovascular Diseases*, 8(5):8–18, 1998.

[42] Lawrence F. Brass. Thrombus formation: stability matters . *Blood*, 108:2883–2884, 2006.

[43] Bruce Furie and Barbara C. Furie. Role of platelet p-selectin and microparticle psgl-1 in thrombus formation. *Trends in Molecular Medicine*, 10(4):171 – 178, 2004.

[44] J.R. Lakowicz. *Principles of Fluorescence Spectroscopy*. Springer, New York, third edition, 2006.

[45] R. Rigler, U. Mets, J. Windengren, and P. Kask. Fluorescence correlation spectroscopy with high count rate and low background: analysis of translational diffusion. *European Biophysics Journal*, 22:169 – 175, 1993.

[46] D.M. Sheppard, C.J.R.and Shotton. *Confocal Laser Scanning Microscopy.* Springer-Verlag New York Inc., New York, 1997.

[47] Denis Semwogerere and Eric R. Weeks. *Encyclopedia of Biomaterials and Biomedical Engineering.* Taylor & Francis, London, 2005.

[48] Bernadette F. Rodak, George A. Fritsma, and Kathryn Doig. *Hematology: clinical principles and applications.* Saunders, Philadelphia, third edition, 2007.

[49] David R. Baselt. *The tip-sample interaction in atomic force microscopy and its implications for biological applications.* PhD thesis, California Institute of Technology, 1993.

[50] Engineering & Physical Sciences at University of Central Lancashire Insitute of Computing. *The principles of Atomic Force Microscopy.* Online resource, http://www.uclan.ac.uk/schools/computing_engineering_ physical/jost/files/AFM.pdf.

[51] Ricardo Garcia and Ruben Perez. Dynamic atomic force microscopy methods. *Surface Science Reports*, 47(6-8):197 – 301, 2002.

[52] John A. Kiernan. Formaldehyde, formalin, paraformaldehyde and glutaraldehyde: What they are and what they do. *Microscopy Today*, 00(1):8–12, 2000.

[53] JS Collins and TH Goldsmith. Spectral properties of fluorescence induced by glutaraldehyde fixation. *Journal of Histochemistry & Cytochemistry*, 29(3):411–414, 1981.

[54] Rahul P. Bagwe, Lisa R. Hilliard, and Weihong Tan. Surface modification of silica nanoparticles to reduce aggregation and nonspecific binding. *Langmuir*, 22(9):4357–4362, 2006.

[55] M. Martini, M. Montagna, M. Ou, O. Tillement, S. Roux, and P. Perriat. How to measure quantum yields in scattering media: Application to the quantum yield measurement of fluorescein molecules encapsulated in sub-100 nm silica particles. *Journal of Applied Physics*, 106(9):094304 –094304–9, 2009.

[56] L. Basabe-Desmonts, S. Ramstrom, G. Meade, S. O'Neill, A. Riaz, L. P. Lee, A. J. Ricco, and D. Kenny. Single-step separation of platelets from whole

blood coupled with digital quantification by interfacial platelet cytometry (ipc). *Langmuir*, 26(18):14700–14706, 2010.

[57] Douglas J. Taatjes, Anthony S. Quinn, Richard J. Jenny, Paul Hale, Edwin G. Bovill, and Jan McDonagh. Tertiary structure of the hepatic cell protein fibrinogen in fluid revealed by atomic force microscopy. *Cell Biology International*, 21(11):715 – 726, 1997.

List of Abbreviations

ADP = adenosine diphosphate
AFM = atomic force microscopy
APTES = amino-propyltriethoxysilane
APTMS = (3-aminopropyl)-trimethoxysilane
BCA = bicinchoninic acid
BSA = bovine serum albumine
CD41 = cluster of differentiation 41
CD42b = cluster of differentiation 42b
CD62P = cluster of differentiation 62P
D = diffusion coefficient
DLS = dynamic light scattering
DNA = deoxyribonucleic acid
EDC = 1-Ethyl-3-[3-dimethylaminopropyl]-carbodiimide hydrochloride
FAD = flavin adenine dinucleotide
FITC = fluorescein isothiocyanate
FL1 = fluorescence channel number 1
FL2 = fluorescence channel number 2
FMN = flavin mononucleotide
FS = forward scattering
GP = glycoprotein
HEA = Health Education Authority
HEPES = (4-(2-hydroxyethyl)-1-piperazineethanesulfonic acid)
IgG = immunoglobulin G
K_a = acid dissociation constant
LOD = limit of detection

MES = 2-(N-morpholino)ethanesulfonic acid
MPTES = (3-Mercaptopropyl)triethoxysilane
MRI = magnetic resonance imaging
NADPH = nicotinamide adenine dinucleotide phosphate
NIR664 = 4,5-Benzo-5'-(iodoacetaminomethyl)-1',3,3,3',3'-pentamethyl-1 -(4-sulfobutyl)indodicarbocyanine
NP = nanoparticle
PAC-1 = 2-(4-benzylpiperazin-1-yl)-N-[(2-hydroxy-3-prop-2-enyl-phenyl) methylideneamino]acetamide
PBS = phosphate buffered saline
PDI = polydispersity index
PDMS = polydimethylsiloxane
PE = R-phycoerythrin
PFA = paraformaldehyde
PMT = photomultiplier tube
PPP = platelet poor plasma
PRP = platelet rich plasma
RCSI = Royal College of Surgeons in Ireland
RGB = red green blue
ROI = region of interest
S_0 = ground state
S_1 = first singlet excited state
S_2 = first singlet excited state
SS = side scattering
Sulfo-NHS = N-hydroxysulfosuccinimide
T_1 = first triplet excited state
TEM = transmission electron microscopy
TEOS = tetraethyl orthosilicate
THPMP = 3-trihydroxysilyl)propyl methylphosphonate
TRAP = thrombin receptor-activated peptide
UV = ultravioled
vWF = von Willebrand factor
WB = whole blood

List of Figures

List of Tables